ADDIS ABABA UNIVERSITY

ADDIS ABABA INSTITUTE OF TECHNOLOGY

SCHOOL OF GRADUATE STUDIES

Beyond Alternate Load Path Method: Progressive Collapse Analysis Accounting Initial Condition and Damage

A Thesis Submitted to the School of Graduate Studies in Partial Fulfillment of the Requirements for the Degree of Master of Science in Civil Engineering (Structures)

By

Benyam Melkeneh

Adviser Dr.-Ing Bedilu Habte

May 2024

Addis Ababa

A Thesis

Submitted in Partial Fulfillment of the Requirements for the Degree of Master of Science

The undersigned have examined the thesis entitled '**Beyond Alternate Load Path Method: Progressive Collapse Analysis Accounting Initial Condition and Damage**' presented by;

Benyam Melkeneh GSR/6970/15

(May 2024)

Candidate for the degree of **Master of Science** and hereby certify that it is worthy of acceptance.

Dr.-Ing Bedilu Habte		
Advisor	Signature	Date
Internal Examiner	Signature	Date
External Examiner	Signature	Date
Chair person	Signature	Date

UNDERTAKING

I certify that research work titled “Beyond Alternate Load Path Method: Progressive Collapse Analysis Accounting Initial Condition and Damage” is my own work. The work has not been presented elsewhere for assessment. Where material has been used from other sources it has been properly acknowledged / referred.

Benyam Melkeneh 

ACKNOWLEDGEMENT

Completing this thesis has been a remarkable journey, and I am grateful to the many people who provided support and encouragement along the way.

First and foremost, I would like to express my sincere gratitude to my thesis supervisor, Dr.-Ing Bedilu Habte. Your invaluable guidance, insightful feedback, and continuous support throughout this project were instrumental in its success. I especially appreciate your patience and willingness to explain complex concepts in a clear and concise manner.

I would also like to extend my heartfelt gratitude to Dr. Girum Solomon at George Mason University. His unwavering support from the beginning of this research and his expertise in blast analysis were invaluable in refining my research and strengthening my arguments.

Finally, I would like to thank the members of my thesis committee, Dr. Esayas G. Yohannes and Dr. Abrham Gebre, for their time and valuable suggestions.

Thank you all.

TABLE OF CONTENTS

LIST OF TABLES

LIST OF FIGURES

ACRONYMS AND ABBREVATIONS

APM – Alternate Load Path Method

DoD – Department of Defense

UFC – Unified Facility Criteria

GSA – General Service Administration

MPH – Moment Plastic Hinge

MAPH – Moment-Axial Plastic Hinge

TNT – Trinitrotoluene

ANFO – 94% ammonium nitrate and 6% fuel oil

DIF – Dynamic Increase Factor

SDOF – Single Degree Of Freedom

CFD – Computational Fluid Dynamics

P_s – Incident peak static overpressure

z – Scaled distance

R – Stand-off distance

W – Charge mass of TNT

t_d – Positive phase of blast duration

b – Waveform parameter

P_o – ambient air pressure

P_r – Reflected pressure

t_a – Arrival time

$P(t)$ – Pressure time history

f_{cu} – Characteristic cubical compressive strength of concrete

$f_{ck}(f'_c)/f_{cd}$ – Characteristic cylindrical compressive strength of concrete (nominal/design)

f'_{dc} – Dynamic cylindrical compressive strength of concrete

f_{ctm} – Mean value of axial tensile strength of concrete

E_{cm} – Secant modulus of elasticity of concrete

f_{ctm} – Mean value of axial tensile strength of concrete

ε_{c1} – Compressive strain in the concrete at the peak stress

ε_{c2} – Strain at reaching the maximum strength in the concrete

$\varepsilon_{cu1,2}$ – Ultimate compressive strain in the concrete

$f_{yk}(f_y)$ – Characteristic yield strength of reinforcement

f_{dy} – Dynamic yield strength of reinforcement

$f_t(f_u)$ – Characteristic tensile strength of reinforcement

f_{du} – Dynamic tensile strength of reinforcement

ε_{uk} – Characteristic strain of reinforcement at maximum load

E_s – Modulus of elasticity of rebar

b_o – Width of confined core (to centerline of the hoops)

h_o – Depth of confined core (to centerline of the hoops)

μ_ϕ – Required value of the curvature ductility factor

v_d – Normalized design axial force

ε_{yd} – Design value of tension steel strain at yield

α – Confinement effectiveness factor

$A_{sv,x}/A_{sv,y}$ – Confinement reinforcement area in the X and Y direction

ω_{wd} – Mechanical volumetric ratio of confining hoops within the critical region

h/D – Depth of column

b – Width of column

d – Effective depth of column

K_{LM} – Transformation factor

k_I/k_{gt} – Elastic stiffness of the member

k_{II} – Elastoplastic stiffness of the member

k_{III} – Plastic stiffness of the member

k_y – Yield stiffness of the member

x – Displacement of the member

$\dot{x}$ – Velocity of the member

$\ddot{x}$ – Acceleration of the member

P_a/N – Axial load of the member

L – Length of the member

M – Mass of the member

u_{cr} – Threshold of elastic displacement (cracked displacement)

u_y – Threshold of elastoplastic displacement (yield displacement)

u_u – Ultimate displacement

u_{eq} – Equivalent displacement

M_{cr} – Cracking moment

M_y – Yield moment

I_{gt} – Uncracked gross moment of inertia

I_{cr} – Cracked moment of inertia

$\bar{x}$ – Depth from the neutral axis to the tension end

A_g – Gross moment of inertia

R_{cr} – Cracked restoring force

R_y – Yield restoring force

μ_e – Factor to account for reduction in resisting moment

ω – Mechanical reinforcement ratio of the section

A_{st} – Area of steel of the flexural reinforcement

ζ – Distribution coefficient

a_I/a_{II} – Uncracked and cracked portion of the displacement

θ – Effective support rotation

x_m – Midspan deflection

μ – Ductility ratio

τ_e – Elastic shear resistance

τ_m – Maximum shear resistance

ρ_{vt} – Longitudinal reinforcement ratio

τ_y – Yield shear resistance

R_{DSi} – Increased shear resistance accounting axial load

γ_v – Average shear strain

D_{sm} – Maximum shear slip at the support

P_{re} – Residual axial load capacity

P_c – Residual axial load capacity of concrete

P_s – Residual axial load capacity of steel

ϕ_{max} – Curvature at maximum drift

ϕ_y – Curvature at yield

ϕ_p – Plastic curvature

θ_p – Plastic rotation

L_p – Plastic hinge length

d_b – Diameter of the reinforcement

Δ_p – Plastic displacement

P_N – Nominal axial load carrying capacity

A_{core} – Uncrushed concrete core

Z_p – Plastic section modulus

s – Transverse reinforcements spacing

D_m – Damage degree

$f_{c,dmg}$ – Damaged concrete's compressive strength

E_{dmg} – Damaged Young's modulus of concrete

ABSTRACT

This thesis investigates progressive collapse analysis accounting initial conditions and damage. A method proposed by Shi et al., is considered with modification on the calculation of the residual axial load carrying capacity. The research aimed to demonstrate the overestimation of the potential for progressive collapse using the Alternate Load Path Method (APM) analysis. The methodology involved: conventional design of a 3-story moment-resisting frame, selection of a single charge weight, selection of 12 blast locations, calculation of reflected blast pressure at two points per column (center for flexure and end for direct shear), SDOF analysis of each column based on the angle of incidence, computation of residual axial load carrying capacity and initial displacement and velocity, and finally, progressive collapse analysis using these initial conditions. The key findings revealed that APM analysis overestimates the building's capacity. Compared to the benchmark analysis (blast-structure interaction), APM analysis either predicted partial collapse or no collapse at all. In contrast, APM with initial conditions and damage showed a similar trend to the benchmark analysis. However, for blast locations where no columns failed under direct blast loading, APM with initial conditions resulted in a progressive collapse occurring later than the benchmark analysis, with smaller transverse displacements, comparatively, over time. Nevertheless, progressive collapse was still triggered, with vertical displacement and velocity showing similar trends at the final stage. These findings suggest that using APM alone is inaccurate for investigating the potential for progressive collapse from blast loads. However, incorporating initial velocity and damage of all columns into the APM analysis yields results comparable to the blast-structure interaction method.

CHAPTER 1 INTRODUCTION

1.1 Design Approach to Progressive Collapse

Most buildings are analyzed and designed for lateral action induced by earthquake and/or wind, natural disasters. Especially, here in Ethiopia the provision of the revised building code led the focus of many structural engineers towards design for seismic resistance. However, man-made disaster is being overlooked. It has become mundane to hear and see several ammunitions and bombs being confiscated by the Federal Police. The amplified domestic and neighboring threats have elevated the probability of government entities being targeted by explosives. Accordingly, there should be a paradigm shift in what constitute and govern the design of new buildings and assessment of existing buildings, especially governmental and essential structures.

All over the world, increased terrorist attacks have concerned structural engineers and building code developers to take a step back and assess the effect of blast on the performance of buildings. Similar to earthquake, blast-induced damage requires a specific hazard level and performance level. The hazard level for blast is categorized by local intensity and the performance level is the vulnerability to that damage from partial collapse or total collapse.

This research examined the effect of standoff distance on the progressive collapse of buildings. Widely used method to assess the initial local failure is the “Direct Design Approach”. This includes the Alternate Load Path Method (APM), which requires that the structure should be able to withstand the loss of a structural element without collapsing, and the damage should be limited to the immediate area of the lost element and the other method is the Specific Local Resistance (SLR) method, which requires that the building, or sections of the building, should exhibit the necessary strength to withstand a predetermined load or threat. The APM being the most popular of the two.

The idea behind APM is to remove the column damaged by the blast load and analyze the building, if progressive collapse is imminent [1]. It's important to acknowledge that the analysis, in a way, remains threat-independent. This means that a single column or other vertical load-bearing element is hypothetically removed without any damage to

surrounding elements. While this doesn't accurately represent a real-world blast scenario where damage would be more dispersed and potentially affect multiple columns, it serves as a valuable method for incorporating additional redundancy and ductility into the design to prevent progressive collapse. Hence, it does not take into account the effect of the removal on other columns in the vicinity exposed and damaged due to the blast. Subsequently, APM overestimates the capacity of the structure to resist collapse after the blast has taken place [2]. Therefore, zero initial stress condition for calculating progressive collapse will result in erroneous outcome.

The aim of the thesis is to investigate the vulnerability to progressive collapse of an idealized buildings subjected to blast load. This is accomplished by subjecting peripheral columns to surface blast load at different standoff distances and examining the structure under non-zero initial stress condition and velocity, which is a realistic scenario.

1.2 Scope

The outcome of the research is aimed to show the drawbacks of APM method for assessing the performance of moment resisting frame to progressive collapse under blast load and provide alternate method of analysis by incorporating initial velocity and damage.

For purpose of this study, representative three story reinforced concrete moment resisting frame located in seismic zone 3 and designed to meet the requirements set out in ES EN 2015 is subjected to a single charge weight at different standoff distances. Three different analysis is carried out for each standoff distances: blast-structure interaction, APM and APM with initial condition and damage.

The following are the limitations of the research:

- The impact of ground shock from blast loads is not factored into this study.
- The study focuses solely on surface blasts (or near surface blast), which are explosions that occur on the surface or near surface of the ground.
- The impact of post-blast thermal loading, resulting from a fire ignited by the explosion, has not been evaluated in this investigation.
- The impact of non-structural components on progressive collapse is not considered in this study.

- This study only considers the effects of blast waves in unconfined spaces. This means that the study does not consider the effects of blast waves that are reflected by walls or other structures.

1.3 Objectives

The objective of the research is to investigate the vulnerability of moment frame building for progressive collapse caused by surface blast load at the ground floor level from different standoff distances. This entails:

- The assessment of structural columns for localized damage from breach, flexural and direct shear failure and leading to either instability or global failure.
- The effect of non-zero initial condition and damage of non-critical columns. It is clear that if a blast can damage several columns, neighboring columns will experience comparatively lesser damage but damage nonetheless. Subsequently, the progressive collapse analysis has to be carried out based on the removal of damaged columns (reduced stiffness and strength of the adjacent columns).

1.4 Research Strategy

The progressive collapse analysis is carried in two stages: blast analysis of structural columns followed by collapse analysis based on the damage and initial conditions of these columns. The strategy follows conventional design with blast load analysis, capacity assessment, damage assessment and finally progressive collapse analysis.

In the initial design stage, a 3-story 2bay by 2bay moment resisting frame building is analyzed and designed for conventional gravity and lateral load (earthquake and wind). This step involves acquiring the structural geometry and element size with the reinforcement detail. Selection of explosive type, charge weight and array of standoff distances is done at this stage. Based on these data, the peak overpressure, positive phase duration and time of arrival is calculated. The reflected pressure history is then calculated at each column by considering the orientation of the threat on the ground to each column.

The second stage is capacity assessment which involves the column damage modes and limit states, namely, breach, flexural and direct shear failure modes. Breach resistance

is calculated first based on empirical formulas, followed by either flexural or direct shear resistance. Both flexural and shear resistance are computed using generalized-single-degree-of-freedom. The ductility ratio and end rotations are computed for flexure, whereas, shear slip at the ends is computed for shear resistance.

The third stage is damage assessment, entails comparing the demand to the response limit. Flexural damage is evaluated at mid-span as the lateral translation is allowed at this location. The shear damage is computed at the ends, as shear slip occurs at this location. The damage level (material strength and stiffness degradation) is also assessed at this stage. Initially, the occurrence of breach is assessed first for each column by comparing the reflected pressure of each column to the capacity of that column. If the column's has breached and then it is no longer considered a functional part of the frame's system. In cases where breaching does not occur, the column's ability to withstand flexural and shear forces is assessed by comparing the response with the limits.

The final stage is global response, progressive collapse analysis is performed for the damaged structure and the resulting consequence is evaluated. A comprehensive assessment of the structure's collapse behavior is conducted using LS-DYNA for each stand-off distance. Three distinct analyses are carried out: a benchmark analysis simulating blast-structure interaction, an APM analysis assuming the removal of the critically damaged column, and a damage-propagation analysis using APM but considering initial velocity and damage. The output of these analyses, including vertical displacement, transverse displacement, and vertical velocity, is evaluated to compare the structure's performance under varying loading conditions.

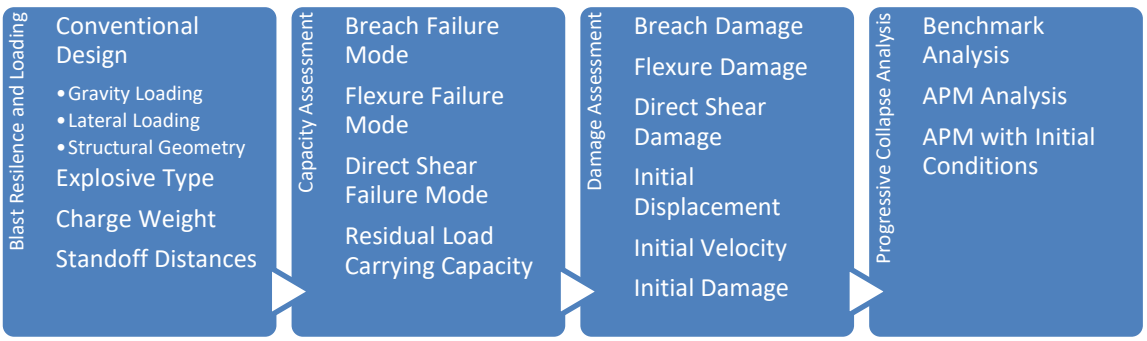

Figure 1-1: Research Strategy

CHAPTER 2 Literature Review

Numerous researches have been conducted on the effect of blast load on structures especially after the destruction of the World Trade Center [3, 4, 5, 6, 7, 8, 9]. Most of them showing similar trends on collapse analysis. The analysis commences with damage assessment of individual vertical structural members leading to the progressive collapse analysis based on the performance levels of these members.

The primary progressive collapse analysis methods for building structure are direct simulation method and alternate load path method (APM). The direct simulation method as the name suggests is a three-dimensional model taking into account the building structure, air, explosive, non-structural elements, wave propagation and geometric & material nonlinearity. Hence, this method is supposed to provide the most accurate prediction of the collapse mechanism. The alternate load path method on the other hand, supported by US General Service Administration (GSA) [10] and US Department of Defense (DoD) [1], considers redundancy in load path. Instead of simulating every component of the system, the APM considers gravity analysis of the structure by removing critically damaged vertical load carrying members.

Yanchao Shi et al. [11] proposed a new method for progressive collapse analysis by taking into account non-zero initial condition, which this research is based on. Three story two bay RC moment resisting frame is analyzed by numerical simulations; blast-structure simulation (the bench mark), GSA's procedure and the author proposed new method. The bench mark analysis demonstrated collapse by instigation of localized failure of the column in direct contact with the blast load followed by failure of neighboring columns. For the latter two methods, performance level of the damaged column need to be determined prior to performing progressive collapse analysis. Based on individual member assessment, the ground level column was deemed completely damaged (no resistance for gravity load) and removed for collapse analysis. GSA's nonlinear dynamic analysis considering the removal of the ground level column showed redistribution of load to far end columns leading to overestimation of the structural capacity, resulting in the absence of a trigger for progressive collapse. However, based on the author proposed new method, that considers non-zero initial condition and damage of the neighboring columns prior to

collapse analysis in addition to the removal of the critical column, resulted in a total collapse, similar to the bench mark analysis [11].

Matthew J. Gombeda et al. [12] provided explicit threat-dependent framework for evaluating column damage. Three capacity assessments are considered for potential modes of failure for columns directly exposed to blast loading. If breach failure occurs the column is removed for the collapse analysis, otherwise for flexure or shear failure the pressure-impulse capacity is checked and assessed compared to the reflected pressure-impulse stress. The analysis showed that multiple columns suffered breach under high blast load at small standoff distance. Significant damages to building frame can occur even in the case where no columns are removed resulting in compromised structural integrity [12].

Based on demand to capacity ratio, progressive collapse potential was assessed by Y.A. Al-Salloum et al. [13]. The unique feature of this paper is the consideration of an actual 22 story apartment building with a 500Kg TNT equivalent blast load placed at the ground floor level. After detonation, the hoops of the columns ruptured which led to loss of confinement and eventually loss of load bearing capacity of the columns [13]; finally, leading to a partial collapse of the building. The analysis method followed GSA's procedure by removing the damaged column for progressive collapse analysis. Similar research is conducted by Abdulaziz K. [14], where an RC frame is subjected to blast load at 3m, 5m, 7m and 10m standoff distance. Critical column is removed and nonlinear analysis is conducted to assess the potential for progressive collapse utilizing UFC 2005 guidelines. At standoff distance less than 7m, progressive collapse is triggered due to an increased number of plastic hinges [14].

Most researches show that the response of structural elements to blast load is subjected to the ductility ratio and end rotations, for flexure and end slip for shear [6, 15, 1, 12, 11, 16]. A structure's ability to withstand blast forces stems from a combination of its material properties, both elastic and inelastic, and its inertial resistance, determined by its mass. Designing solely for peak blast pressures is likely impractical or excessively costly. Acceptable structural performance for blast, and progressive collapse is primarily concerned with hazard mitigation and casualty prevention. Since inelastic behavior is allowed in elements subjected to these loads, performance is typically deformation-

controlled [17]. This means that a certain amount of allowable rotation or ductility (based on minimizing debris) is specified for each structural member type for blast loads.

Incorporating structural design improvements to mitigate the effects of blast and progressive collapse typically incurs an additional cost of no more than 5% for the design and construction of a new facility [17]. This holds true regardless of the type of materials used, be it concrete, steel, masonry, or any other. However, this percentage could increase significantly for buildings or facilities classified as "critical," where specialized hardening measures are deemed necessary.

Javeed [18] discussed the practice in blast and progressive collapse of RC structures by taking into account several building code standards and concluded that the realm of blast-resistant design and progressive collapse mitigation is not as extensively understood or implemented as it should be. The unique characteristics of blast loading induce a material response that deviates from the behavior observed under conventional loads, such as earthquakes. Under blast loading, the capacity for ductility is restricted, which can lead to brittle failure of structural members. These localized failures can potentially trigger progressive collapse if there are no alternative load paths with sufficient strength and ductility to redistribute the gravity load. It is crucial to recognize that the redundancy, strength, and detailing provisions designed to counter the effects of earthquakes may not be suitable or adequate for blast protection [18].

Xu Jun-Xiang and et al. [19] proposed a two-step approach to progressive collapse analysis of building structures under blast loading. The first step involves identifying the damaged elements using a coupled Lagrangian-Eulerian method and assigning a damage index to each element, with 0 indicating no damage and 1 indicating failure. Based on the extent of damage, the failed elements are conceptually removed from the structure. The second step involves computing the potential for progressive collapse of the remaining structure under gravity loading. If the structure reaches an equilibrium position without exceeding the capacity of any elements, then progressive collapse is not expected to occur. However, if the strain in any element exceeds its capacity, progressive collapse can ensue. The initiation and propagation of progressive collapse under blast loads is often triggered by failures at beam-column connections. Strengthening these critical structural connections can effectively mitigate the risk of collapse due to abnormal loading [19].

Jennifer Righman McConnell and Houston Brown [20] evaluated progressive collapse using alternate load path analyses for designing blast resistance steel columns. They highly stressed the ineffectiveness of APM for small charges at near-end and large charges at far-end blast load. A localized blast impact, even if it doesn't cause a complete column failure, could have broader consequences [20], thus highlighting the inability of APM to predict progressive collapse. The blast load could affect nearby structural members and connections, reducing their capacity to handle the redistributed loads in the damaged structure.

M. Sasani [21] showed the effect of catenary action in beams to mitigate progressive collapse both analytically and experimentally. He conducted two span beam supported by three columns, followed by the removal of the middle column. The experiment showed that a sudden decline in the resisting force is observed twice during the loading test, coinciding with the fracture of the two bottom reinforcing bars on the right side of the RC beam center stub. This was mainly due to the incorporation of transverse reinforcement, in accordance with "ACI integrity requirements", permitted the top continuous reinforcement to adopt a catenary or cable-like response without damaging the concrete cover on top of the reinforcement [21]. In addition to the above experiment, an actual 11 story RC structures was evaluated to show the overestimation of moment plastic hinge (MPH) model over moment-axial plastic hinge (MAPH). The measured permanent vertical deflection at the removed columns under MPH was 81mm, under MAPH was 46mm and the actual experimental deflection was 43mm. The structural model with moment-plastic hinges (MPHs) exhibits a notable overestimation of the permanent vertical displacements of the structure in relation to experimental results. Consequently, it is inferred that the structural model utilizing MPHs, which neglects axial deformations of beams, fails to accurately capture the actual structural response [21].

S. Jeyarajan et al. [22] conducted blast induced progressive collapse analysis of a 10-story steel-concrete composite building. They highlighted two thoughts concerning the response of the structure to blast: the effect of strain rate and the non-conservative assessment of APM. The analysis showed that considering strain rate effects, frames experience diminished deflections, both vertical and lateral, as opposed to frames without strain rate effects [22]. Furthermore, frames incorporating strain rate effects encounter increased force demands relative to frames without strain rate effects. The building was

subjected to 500Kg TNT at 20m standoff distance, the comparison between APM and the nonlinear dynamic analysis showed that alternate path (AP) analysis, which neglects lateral loads, yields a lower estimate of lateral deflection resulting from the removal of three columns compared to a nonlinear dynamic analysis [22]. Subsequently, under predicting the building response compared to the real response. They concluded that capturing the true behavior of buildings subjected to high blast loads necessitates the application of scenario-based nonlinear dynamic analyses.

Mohamed Ahmed Gala et al. [8] proposed a two-stage nonlinear dynamic analysis for progressive collapse analysis of steel-concrete composite building. Similar to Shi et al. the first stage involves determining the damage of individual columns followed by nonlinear dynamic analysis of APM. The prevalent failure criteria for evaluating steel column damage under blast loading—stability, yielding, and fracture—fail to accurately reflect the true severity of damage sustained by these columns [8]. Hence, suggesting that the criterion to evaluate damage of columns is best represented by the conditions stated by Shi et al. The analysis revealed that the stability-based criteria overpredicted the stand-off failure limit, leading to an overestimation of the number of columns susceptible to progressive collapse. These findings underscore the significance of considering the column's primary role as a vertical load-bearing element, suggesting that damage criteria should be anchored in its axial capacity and overall structural behavior.

Progressive collapse resistance of RC beam-slab substructures made with rubberized concrete was conducted by Ibrahim M. H. Alshaik et al. [4] An important output of the research is that the inclusion of slab in the analysis of collapse mechanism improved the frame’s stiffness, ductility and integrity. The collapse mechanism is broken down into three stages: an elastic phase, compressive arch/membrane action (CAA/CMA) and tensile catenary/membrane action (TCA/TMA). The first phase, characterized by uncracked concrete, represented the elastic stage. Upon cracking, the CAA/CMA mechanism became active. Identifying the point where the horizontal reaction force flips from negative (compression due to CAA/CMA) to positive (tension due to TCA/TMA) reveals the beginning of the catenary stage. All specimens reached their maximum capacity before the TCA/TMA mechanism activated. The TCA and TMA forces (the catenary effect), acting in the longitudinal rebars of the beams and slabs, played a crucial role in resisting progressive collapse [4]. They concluded that the inclusion of the slab's

mechanical properties significantly impacted the specimens' performance. On average, those with slabs exhibited a 33% increase in capacity compared to their slab less counterparts. Moreover, slabs facilitated a remarkable increase in the specimens' energy absorption capacity, indicating greater ductility. This implies that the inclusion of slab increased the resistance to progressive collapse during the crucial stages of compressive arching and catenary action [4].

Mohamed Foda El-Shahat [23] conducted nonlinear static progressive collapse analysis of RC building frames with different seismic design levels. As expected buildings designed for earthquake resistance showed a higher potential for mitigating progressive collapse, moreover, structures designed for Seismic Zone 3 exhibit reduced susceptibility to progressive collapse [23]. In addition, slab thickness plays an important role in the formulation of plastic hinges. The influence of slab thickness on plastic hinge formation and beam failure is substantial. Notably, a 160 mm slab exhibits the minimum number of plastic hinges and failed beam elements, highlighting its superior performance in mitigating structural collapse. Additionally, the membrane action of the slab significantly contributes to bridging the void left by removed columns, facilitating efficient load distribution to neighboring structural components [23].

A simplified RC frame blast analysis methodology incorporating the Reinforcement Contact technique using Ansys Workbench was introduced and its accuracy rigorously examined by Han-Soo Kim et al. [24]. A paramount investigation from this numerical simulation is that the model's collapse resistance benefited from the implementation of continuous bottom bars and closely spaced stirrups, yet these measures ultimately fell short of achieving the desired level of resilience against progressive collapse under the specified blast scenario [24].

Another two stage analysis is proposed by Yousef Al-Salloum et al. [3] in order to alleviate the problem of assessing the appropriate criteria for deciding column removal in subsequent progressive collapse analysis. Local column failure is described by the inability to resist its gravitational load [3]. This takes into account the shear failure surface, strain-rate effects and the volumetric damage of the concrete component. The subsequent progressive collapse analysis showed that the loss of column resistance in the blast zone

shifted gravity loads onto the floor slab, inducing flexural stresses which exceeded the slab's flexural capacity resulting in partial collapse.

Several methods for analyzing progressive collapse in structures after explosions have limitations [3, 13, 20, 23]. Most of the methods considered two-stage analysis; calculating the damage of columns followed by gravity load analysis for progressive collapse. However, they overlooked the initial damage and initial conditions for the progressive collapse analysis (that is the output of the blast loading phase) – the outputs of the forced vibration phase are used as initial conditions for the free vibration phase. These initial conditions are the initial velocities and damage.

This method is articulated by Shi et al. [11], they presented an improvised method for collapse analysis considering the initial damage and velocity, however, requires rigorous FEAs calculation of the residual axial-load carrying capacity for individual columns. Additionally, only a single standoff distance was considered, which may not reflect real-world scenarios. It also only considers columns that completely fail during the blast, neglecting those with permanent deformation that can still bear some load. The initial damage is considered by Matthew [12], who provided a threat dependent blast scenario which leaps ahead of APM, but lacks details on how the damage translate to material degradation, in addition, zero initial condition is taken into account. Methods based on the APM like those by Al-Salloum [13] and Abdulaziz [14] remove damaged columns without considering neighboring column damage or initial conditions, potentially overestimating collapse risk. Javeed [18] highlighted the importance of this research, stating that unless there are alternative load paths with sufficient strength and ductility to redistribute the gravity load, progressive collapse is imminent. Here, the important word is ‘sufficient strength and ductility’, hence, if the non-critical columns are damaged but still bear load after the blast loading, they may succumb to failure after the loss of the critical column. Therefore, deeming columns as undamaged may overpredict the potential of the building to collapse. Xu Jun-Xiang and et al. [19] followed the two-step process and neglected the damage and stress condition of the non-critical columns. Jennifer Righman McConnell and Houston Brown [20] even though considering only the initial damage of the neighboring columns stressed that APM is ineffective for small blasts at near field and large blasts at far field. This is another aspect of this research, the impact of standoff distance. These papers utilized a single standoff distance to assess the potential for

progressive collapse, however, the threat from blast is unpredictable and hence the structural response should reflect probable locations of explosions. This also has an effect on the damage of both critical and non-critical columns, in addition to the conditions of the non-critical columns.

Addressing these limitations is the focus of this research. Investigating the impact of non-zero initial velocity and varying degrees of initial damage through stress-strain profile of columns at different standoff distances to improve progressive collapse analysis.

CHAPTER 3 CONVENTIONAL DESIGN AND BLAST LOADING

3.1 Resilience

When talking about structural resilience, it is mainly associated with structural robustness. That is the building must not exhibit an unreasonable susceptibility to the effects of accidental events. In particular, it should be designed to avoid situations where damage to limited areas or the failure of individual elements can trigger a disproportionate or progressive collapse. In the context of progressive collapse analysis, ensuring robustness primarily involves designing structures with alternative load paths capable of redistributing gravity loads after localized failures. This can be achieved through mandatory tie connections or by utilizing structural systems with demonstrated bridging capabilities under blast scenarios.

A fundamental requirement is for a structure to be firmly interconnected, allowing it to leverage its entire mass and withstand localized damage without extensive collapse. This necessitates designing elements and their connections with tensile capacity and ductility, leading to a preference for reinforced concrete or steel-framed buildings. A well-tied framed building provides numerous alternative pathways for transferring loads to the ground. Analogous to static load design, engineers should employ limit state design techniques for progressive collapse analysis, encompassing both ultimate limit state (ULS) and serviceability limit state (SLS) approaches. ULS prioritizes the preservation of life safety by preventing overall collapse, even if the frame sustains severe damage and becomes unfit for further use. SLS, conversely, focuses on maintaining post-event functionality, often through controlled deflection exceeding the elastic limit, defined by limits expressed as ductility ratios or element end rotations. This is pertinent especially when a nearby column fails, significant rotations occur at the beam-column connections. To prevent the structure from collapsing, the rotational ductility capacity of these connections must be greater than the imposed demand.

3.2 Blast Loading

Blast loading is described by the explosion it creates which is a rapid chemical reaction that generates temporary pressure waves in the air, known as blast waves. For an explosive device detonated at ground level, the resulting pressure wave propagates as a hemispherical wavefront away from the source until encountering obstructions. The peak overpressure (the pressure exceeding atmospheric pressure) and its duration exhibit spatial dependence, varying with distance from the device. The magnitude of these parameters is further influenced by the specific explosive materials and the construction of the bomb. Traditionally, bomb size is expressed in terms of an equivalent weight of TNT.

Explosions can be categorized as physical, nuclear or chemical events. The research focuses on chemical explosions. A chemical explosion is characterized by the rapid oxidation of fuel elements (carbon and hydrogen atoms) present within the explosive compound. This reaction is self-contained, meaning it requires no oxygen from the surrounding air to occur, as the necessary oxygen is already incorporated within the compound itself. When explosive materials decompose at a rate much slower than the speed of sound within the material, the resulting combustion process is called deflagration. Heat liberated by the reaction propagates deflagration, with the flow of the reaction products moving in the opposite direction of decomposition. Detonation, on the other hand, is a highly intense shock wave generated by sufficient stimulation, which can be achieved with most explosives. Consequently, the research focuses on the effect of blast due to detonation.

3.2.1 Explosive Classification

Explosives are typically classified based on their sensitivity to detonation. Primary explosives readily detonate with simple ignition sources like sparks, flames, or impact. Examples include mercury fulminate, found in firearm percussion caps. Secondary explosives require stronger stimuli to detonate, like TNT and RDX (cyclonite), often used in military shells and cartridges as the main explosive charge.

The question becomes what type of explosive is eminently used during an explosion incident. Because it's hard to get military grade explosives like Semtex in most countries, terrorist groups often are limited to homemade bombs called IEDs (Improvised Explosive Devices) instead. These bombs contain homemade explosives, often made from

materials like fertilizer and hydrogen peroxide. While less potent than military explosives, large quantities of these improvised materials can cause significant damage to structures, similar to military-grade explosives.

Therefore, based on affordability and readily-available production process ANFO (94% ammonium nitrate and 6% fuel oil) is selected as the explosive. Table 3-2 shows the different explosive types. A 345 Kg ANFO is selected as the blast load which translates to 300Kg of TNT (see table 3-2 for conversion). This selection is based on availability, ease of transportation (a closed van is able to carry such a weight (table 3-1)) and able to knock-off a column from a building (achieved after some iteration).

Table 3-1 Charge weight based on type of vehicle [7]

Vehicle	Charge (Kg)
Compact car trunk	115
Trunk of a large car	230
Closed van	680
Closed truck	2,270
Truck with a trailer	13,610
Truck with two trailers	27,220

The mechanics of blast wave in air under high explosive starts when a concentrated high explosive detonates. The initial reaction produces extremely hot gas products (detonation products) with pressures ranging from 10 to 30 GPa and temperatures reaching approximately 3000 to 4000°C. These gases rapidly expand, violently pushing away the surrounding air. This expulsion creates a compressed air layer known as the blast wave, which encapsulates the hot gas products. The compressed air layer, the blast wave, carries the majority of the energy released by the explosion in the form of pressure energy. Once full detonation occurs, the total system energy stabilizes. As the blast wave travels further from the explosion source, its pressure decreases due to energy dissipation. The momentum of the expanding gas induces a negative pressure phase at the wave's tail, falling below atmospheric pressure. This negative phase creates a suction effect, decelerating surrounding gas molecules and reversing their flow back towards the explosion center until equilibrium is restored. Hence, that is why debris are found outside the building. The process can be represented by a pressure-time history as shown in figure 3-1.

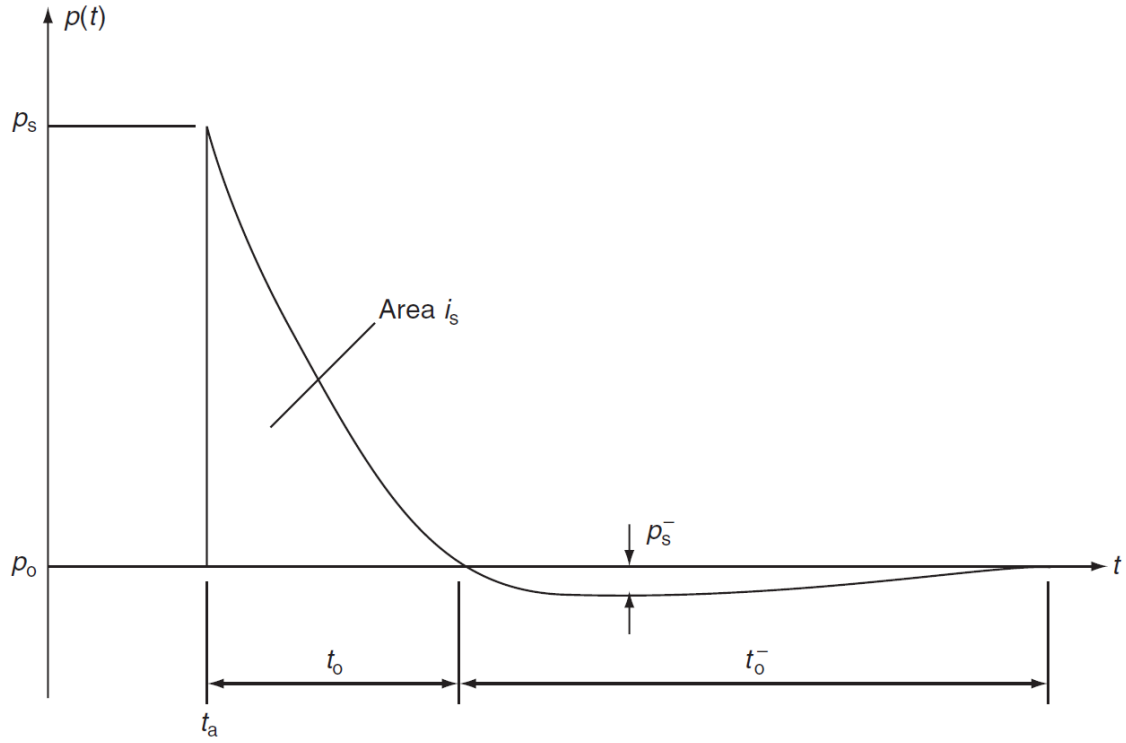

Figure 3-1 Typical pressure—time history for blast wave in free air [25]

3.2.2 Blast-Structure Interaction

Energy transfer from a blast wave to a structure occurs primarily via pressure energy, which acts in all directions. This incident or side-on pressure represents the dominant mode of energy transfer.

The interaction of a blast wave with a solid surface involves both reflection and diffraction, the relative prominence of each depending on the geometry and size of the surface. Reflection facilitates energy transfer between the wave and the object. A classic example is the normal incidence of a blast wave on the facade of an infinitely large building during a surface explosion. Upon encountering the building, the incident wave undergoes reflection, creating a zone of heightened air compression localized near the structure. The surface exerts a force on each air molecule, imparting an equal and opposite momentum. This momentum change results in a local pressure increase above the incident pressure that would occur at the same location in the absence of the structure. This phenomenon is referred to as reflected pressure. The pressure time history on structures and other elements exposed to blast is shown in figure 3-3.

There are several proposed empirical relationship for computing the incident, reflected pressure and positive time duration. The widely applied and accepted numerical equations resulting in an acceptable predictions are Kingery-Bulmash, Graham-Kinney, Henrych and Sadovskii. While other relationships deviate from this curves as the basis of this relationships was nuclear not chemical reaction [26]. The next paragraphs goes through these relations.

Kingery-Bulmash provide a general polynomial equation for all parameters; time of arrival, incident pressure, reflected pressure, positive phase duration and incident impulse by only changing the coefficients. The polynomial equation is given by;

$$\boldsymbol{Function} = e^{(A+B*\ln Z+C*(\ln Z)^2+D*(\ln Z)^3+E*(\ln Z)^4+F*(\ln Z)^5+G*(\ln Z)^6)} \quad \textbf{(3-1)}$$

For the function 3-1, the coefficients A to G are varied to obtain the different parameters, and these coefficients are simplified and presented by Michael and et al. [27]. Z is the scaled distance (equation 3-2).

$$z = \frac{R}{W^{\frac{1}{3}}} \quad \textbf{(3-2)}$$

R is the stand-off distance from the center of a spherical charge in meters. W is the charge mass in Kg of TNT. The charge weight for different explosive classifications based on TNT equivalence is presented by W.E. Baker et al. [5].

Kinney and Graham provided different equations for each parameter. The peak overpressure is given by [28];

$$P_s = P_o \frac{808 * \left[1 + \left(\frac{Z}{4.5}\right)^2\right]}{\sqrt{\left[1 + \left(\frac{Z}{0.048}\right)^2\right]\left[1 + \left(\frac{Z}{0.32}\right)^2\right]\left[1 + \left(\frac{Z}{1.35}\right)^2\right]}} \quad \textbf{(3-3)}$$

Where P_o is the ambient air pressure and Z is the scaled distance which is a function of the stand-off distance and charge weight.

Henrych proposed the following equations for computing the peak positive over pressure [29] ;

$$P_{pos} = \frac{14.072}{Z} + \frac{5.540}{Z^2} - \frac{0.357}{Z^3} + \frac{0.00625}{Z^4} bar(0.05 < Z < 0.3) \quad \textbf{(3-4a)}$$

$$P_{pos} = \frac{6.194}{Z} - \frac{0.326}{Z^2} + \frac{2.132}{Z^3} bar(3 \leq Z \leq 1) \quad \textbf{(3-4b)}$$

$$P_{pos} = \frac{0.662}{Z} + \frac{4.05}{Z^2} + \frac{3.228}{Z^3} bar(1 \leq Z \leq 10) \quad \textbf{(3-4c)}$$

Sadovskiy also presented the following equation [30];

$$P_{pos} = 0.085\frac{W^{1/3}}{R} + 0.3\left(\frac{W^{1/3}}{R}\right)^2 + 0.8\left(\frac{W^{1/3}}{R}\right)^3 Mpa \quad \textbf{(3-5)}$$

All these equations are compared with an experimental result and the better suited equations considering different parameters is utilized (see section 3.2.3).

Table 3-2 Conversion factors (TNT Equivalence) for some high explosives [5]

Explosive	Mass Specific Energy, $(E/M)_x$ (kJ/kg)	TNT Equivalence, $(E/M)_x/(E/M)_{TNT}$	Density, Mg/m^3
Amatol 80/20 (80% ammonium nitrate, 20% TNT)	2630	0.586	1.60
Baratol (barium nitrate, TNT, aluminum)	4750	1.051	2.32
Compound B (60% RDX, 40% TNT)	3190	1.148	1.69
RDX (Cyclonite)	5360	1.185	1.65
Ammonium picrate	3360	0.740	1.53
HMX	5680	1.256	1.90
Lead Azide	1540	0.340	3.80
Lead Styphnate	1910	0.423	2.90
Mercury fulminate	1790	0.395	4.43
Nitroglycerine (liquid)	6700	1.481	1.59
Nitroguanidine	3020	0.668	1.62
Octol, 70/30 (70% HMX, 30% TNT)	4500	0.994	3.80
PETX	5800	1.282	1.77

Pentolite 50/50 (50% PETN, 50% TNT)	5110	1.129	1.66
Picric Acid	4180	0.926	1.71
Silver Azide	1890	0.419	5.10
Tetryl	4520	1.000	1.73
TNT	4520	1.000	1.60
Torpex (42% RDX, 40% TNT, 18% Al)	7540	1.667	1.76
Tritonal (80% TNT, 20% Al)	7410	1.639	1.72
C-4 (91% RDX, 9% plasticizer)	4870	1.078	1.58
PBX 9404 (94% HMX, 3% nitro-cellulose, 3% 1.078plastic binder)	5770	1.277	1.844
Blasting Gelatin (91% nitro-glycerin, 7.9 % nitrocellulose, 0.9% antacid, 0.2% water)	4520	1.000	1.30
60% Straight Nitroglycerin Dynamite	2710	0.600	1.30
ANFO (94% ammonium nitrate, 6% fuel oil)	3932	0.870	1.00
Semtex	5660	1.250	1.53

This table is better organized in chart and presented in figure 3-2.

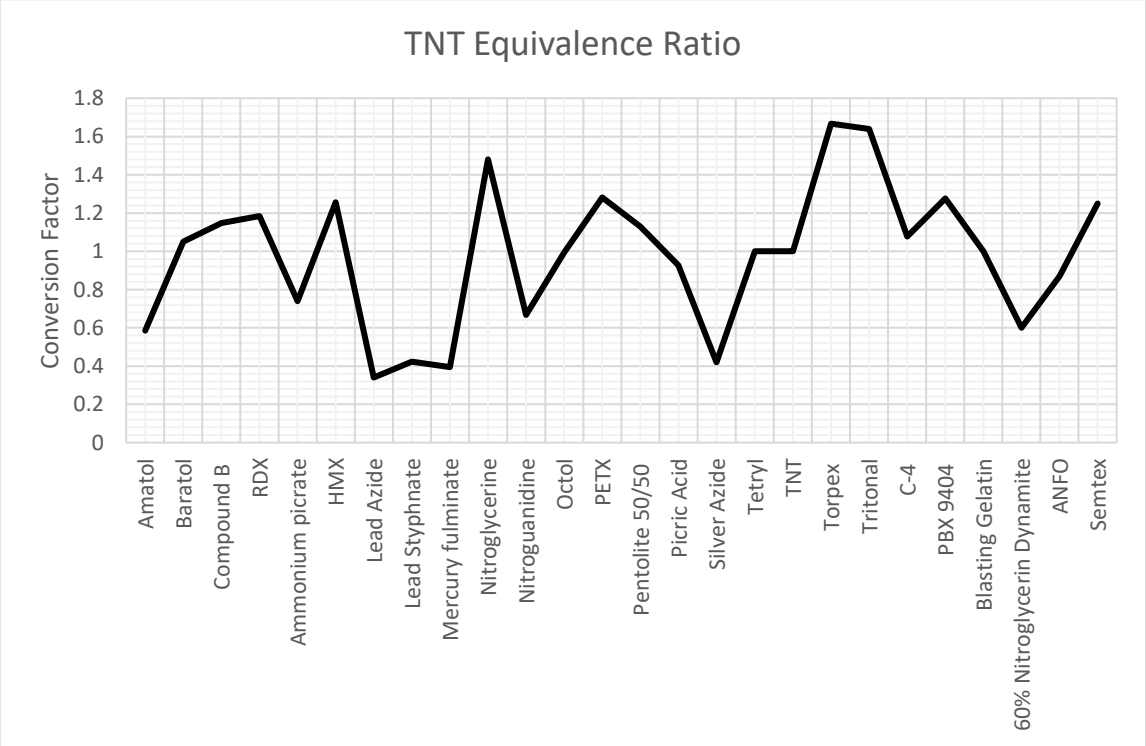

Figure 3-2 TNT equivalence conversion factor

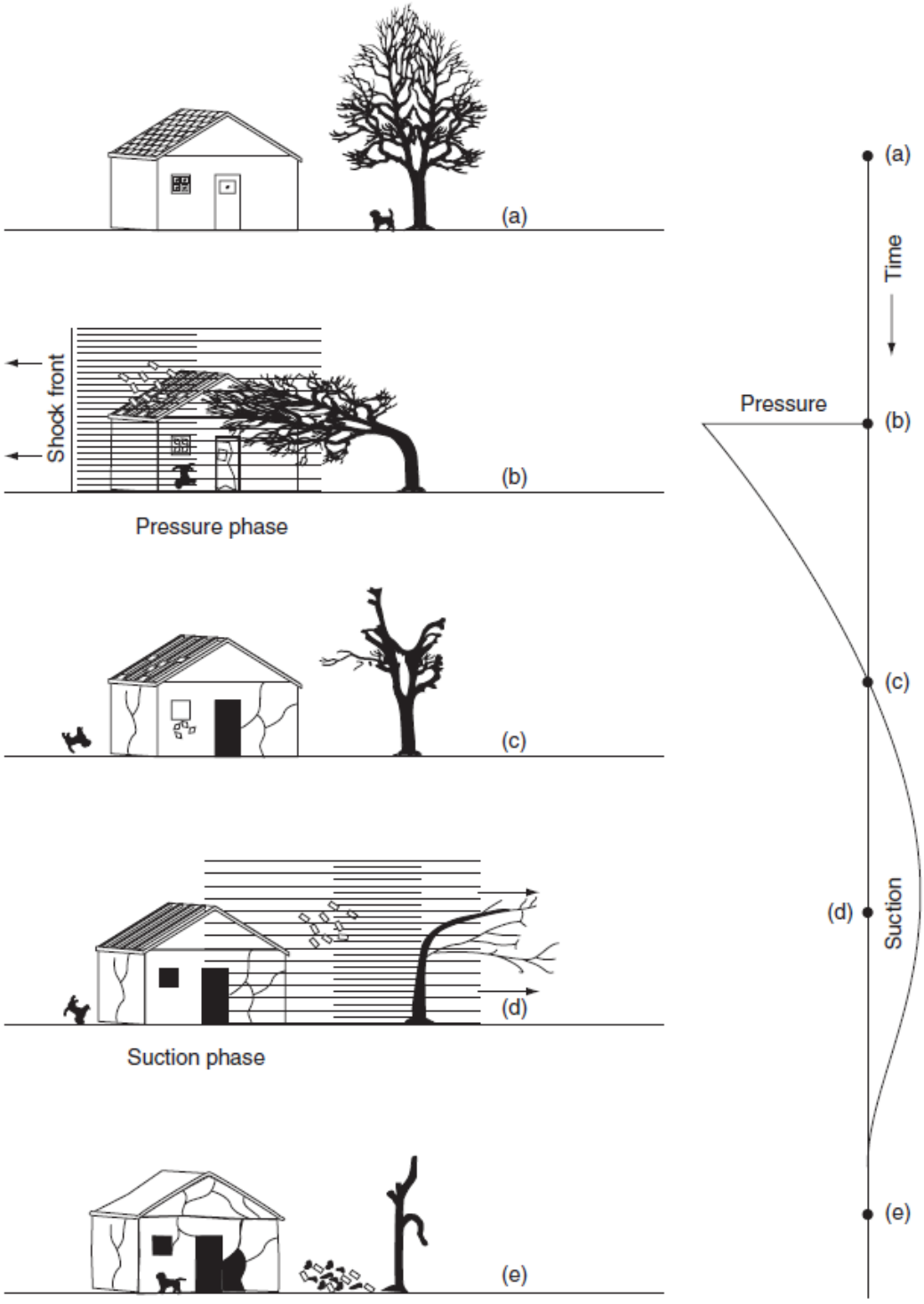

Figure 3-3 Elements subjected to blast loading [25]

3.2.3 Blast pressure-time history

The pressure-time history of a blast wave relative to the arrival time may be described by an exponential function proposed by Friedlander [28].

$$P(t) = P_r * \left[1 - \frac{t - t_a}{t_d}\right] * e^{\left\{-\frac{b(t-t_a)}{t_d}\right\}} \quad \textbf{(3-6)}$$

From formula 3-6, the parameter b is the waveform parameter. The parameter b is important for the extent of negative phase in the exponential distribution and the impulse of the blast wave. t_d is the positive duration of the blast load and t_a is the arrival time of the blast wave. The positive duration of the blast load according to Kingery-Bulmash is computed using the same equation as 3-1 but under different coefficients presented in [27].

For chemical explosion the positive duration according to Kinney and Graham is given as [28];

$$\frac{t_d}{W^{\frac{1}{3}}} = \frac{980\left[1 + \left(\frac{z}{0.54}\right)^{10}\right]}{\left[1 + \left(\frac{z}{0.02}\right)^{3}\right]\left[1 + \left(\frac{z}{0.74}\right)^{6}\right]\sqrt{\left[1 + \left(\frac{z}{6.9}\right)^{2}\right]}} \quad \textbf{(3-7)}$$

As per Henrych [29] the positive duration is given as;

$$t_{pos} = e^{(-2.75 + 0.27 \log W^{1/3})} \quad \textbf{(3-8)}$$

Sadovskiy [30] presented the following positive duration;

$$t_{pos} = 1.2\sqrt[6]{W}\sqrt{R} \quad \textbf{(3-9)}$$

An exponential pressure time history is considered as the exciting force instead of a triangular pulse (b = 0), as it predicts the blast pressure relatively accurate. Figure 3-4 shows the normalized pressure history for different values of waveform parameters. As the decay coefficient increases the negative phase diminishes. The wave decay parameter for the Kingery-Bulmash blast pressure is presented by Vasilis et al. [31] using the following equation;

$$\boldsymbol{Y = C_0 + C_0U + C_2U^2 + \ldots + C_nU^n \ with\ U = K_0 + K_1T} \quad \textbf{(3-10)}$$

In equation 3-10, C_0 to C_n and K_0 and K_1 are constants presented by Vasilis. T is the common logarithm of the scaled distance (Z).

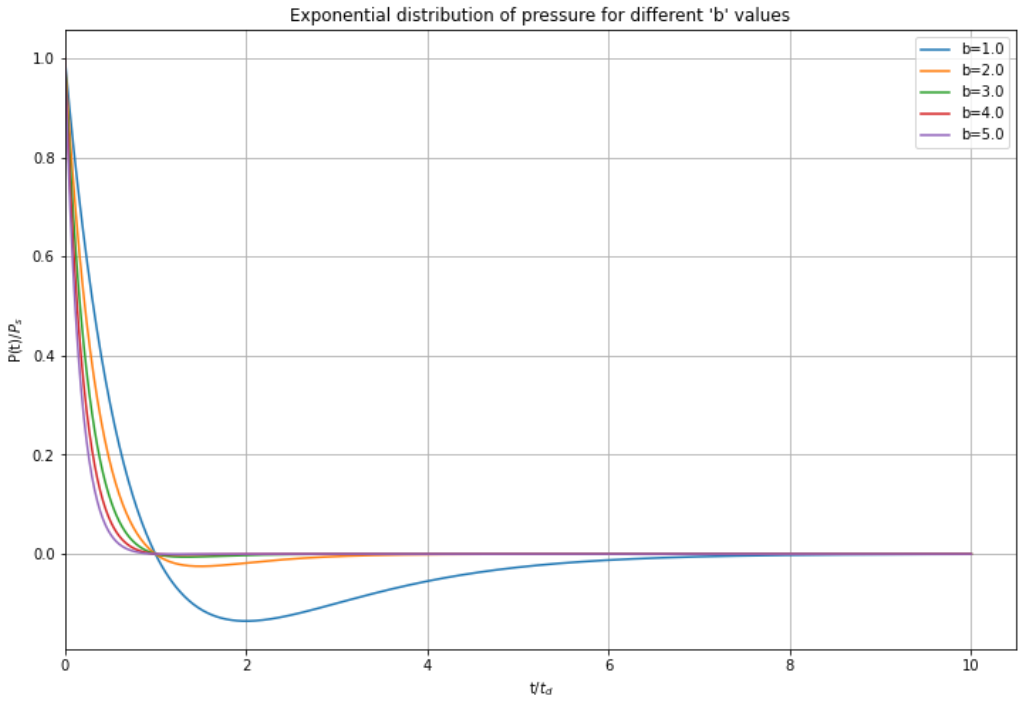

Figure 3-4 Exponential pressure history distribution for different waveform parameters

The reflected pressure is proposed by Rankine and Hugoniot , under the assumption that air behaves as a real gas with specific heat ratio, in terms of peak overpressure. The peak dynamic reflected pressure is given by;

$$\boldsymbol{P_r = 2P_s\left[\frac{7P_o + 4P_s}{7P_o + P_s}\right]} \quad \textbf{(3-11)}$$

In equation 3-11, P_o is the ambient air pressure and P_s is the incident peak static overpressure. This equation is for Kinney-Graham, Henrych and Sadovskiy, as Kingery-Bulmash utilizes the polynomial equation of 3-1 under different coefficients.

Graphs 3.5 to 3-9 show the output of the above equations in relation to an experimental results. Based on these findings a better approximation is provided by Kingery-Bulmash and Kinney-Graham. Considering that Kingery-Bulmash provides all the necessary

parameters for computing the pressure time history compared to Kinney-Graham, it is the chosen empirical equation. Furthermore, Kingery-Bulmash is the basis for computing blast pressure as per UFC [15] and DOD [1], and also, utilized by the United Nations Safe Guards for assessing bomb threats.

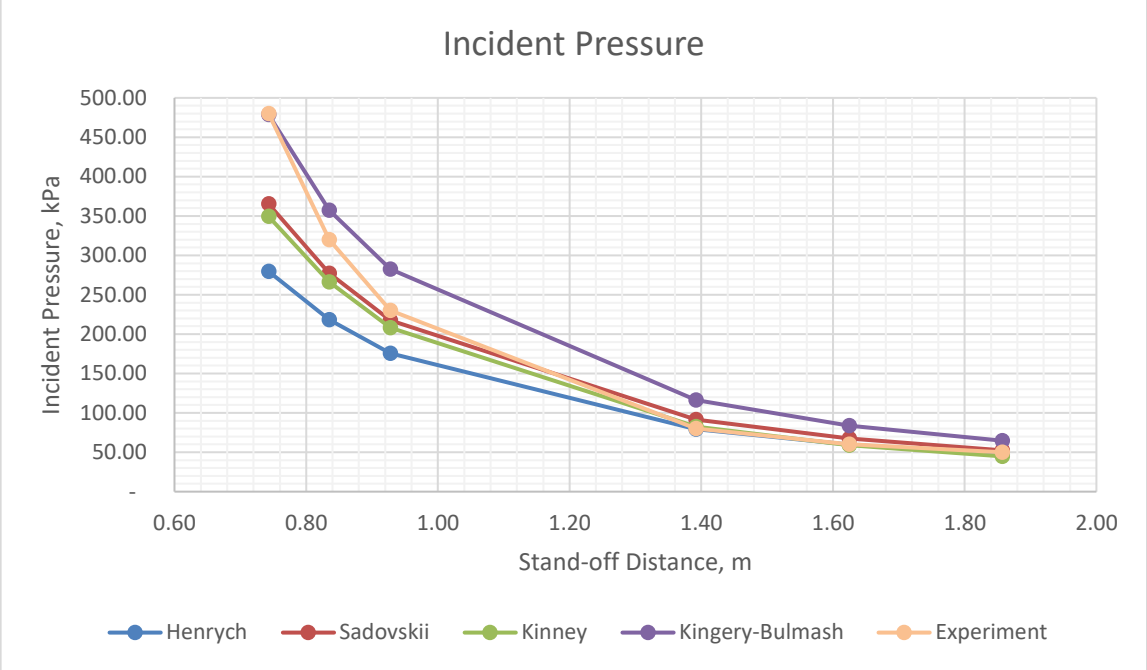

Figure 3-5: Incident pressure considering different equations and experimental result

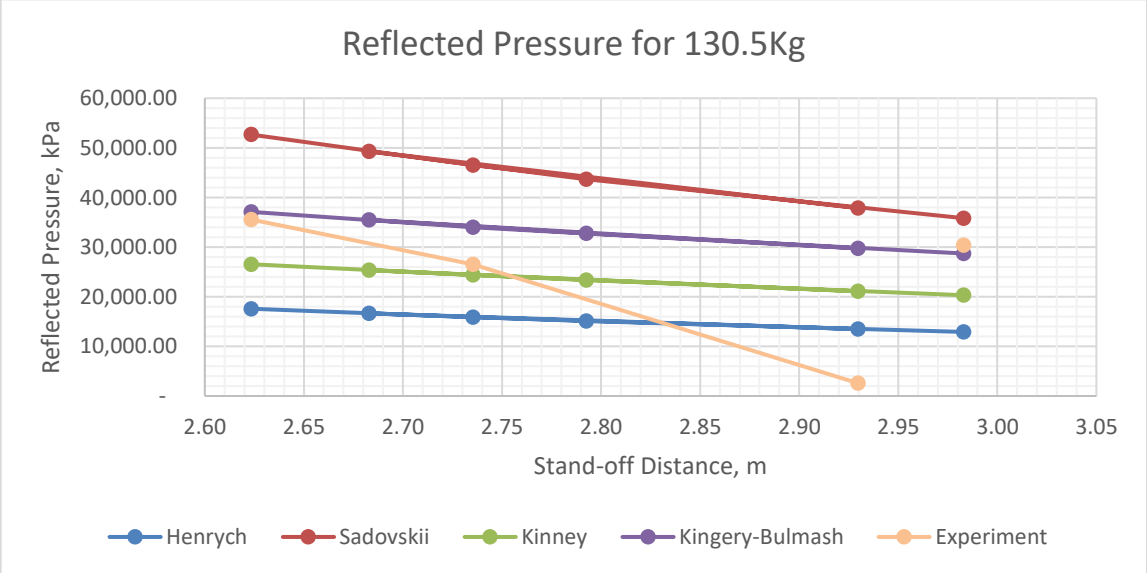

Figure 3-6: Reflected pressure considering different equations and experimental result

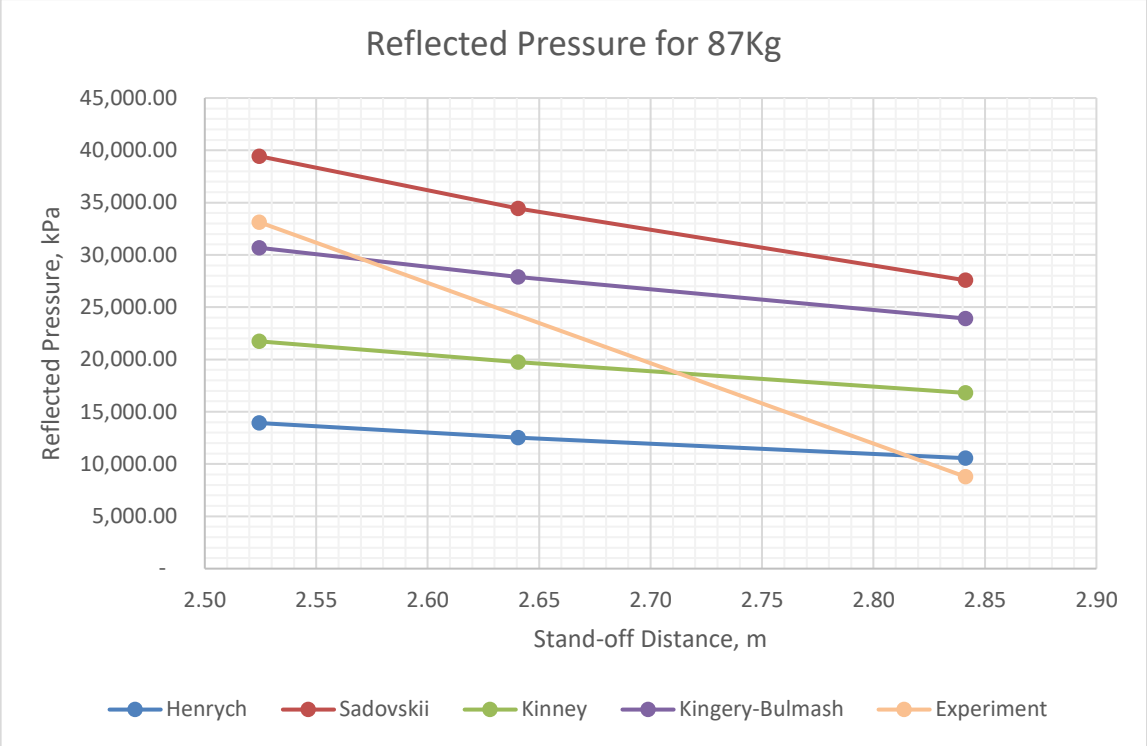

Figure 3-7: Reflected pressure considering different equations and experimental result

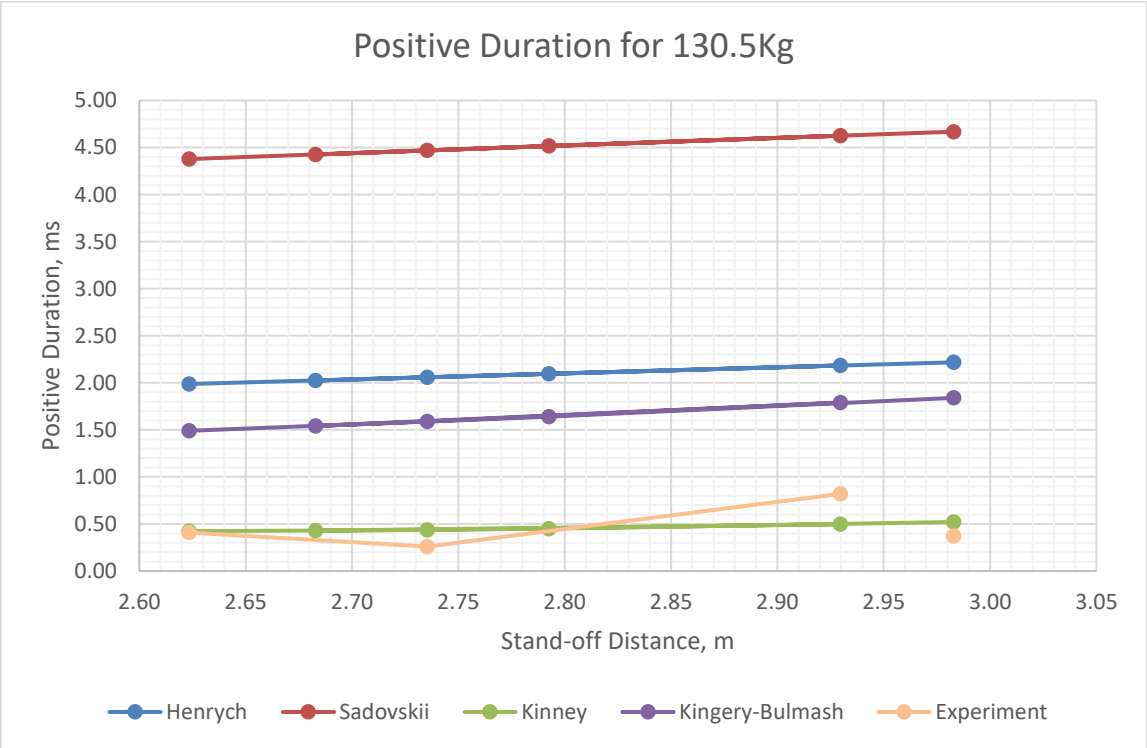

Figure 3-8: Positive duration considering different equations and experimental result

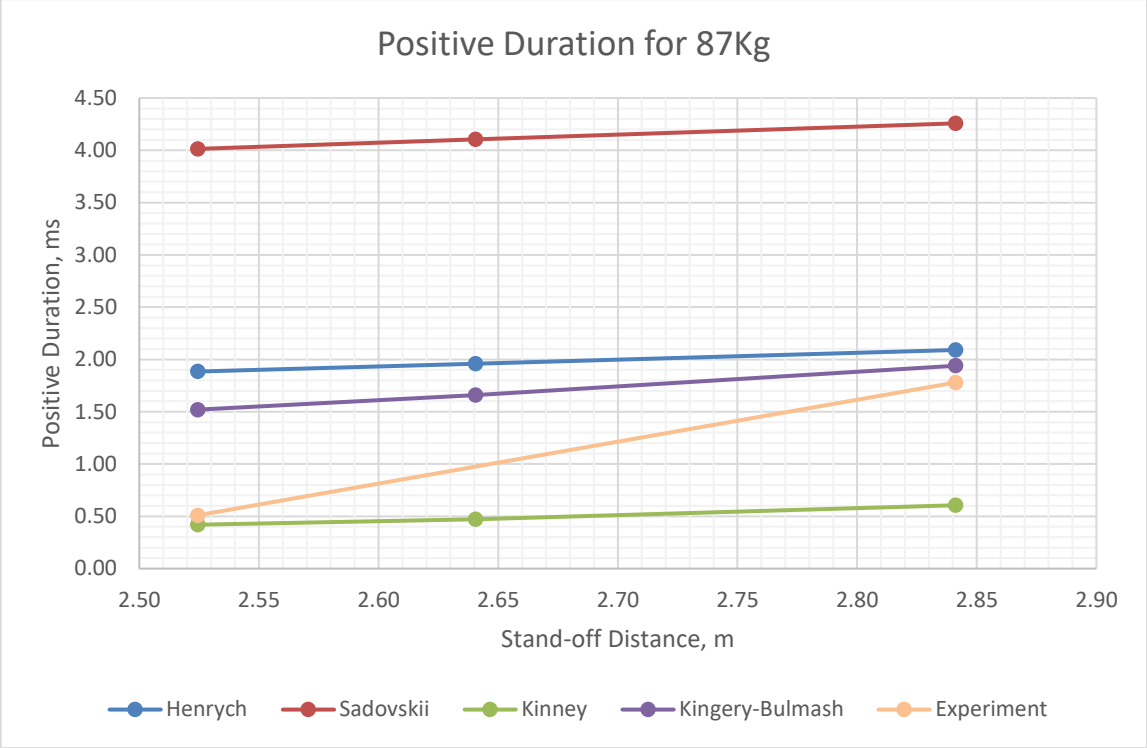

Figure 3-9: Positive duration considering different equations and experimental result

3.2.4 Selection of building dimension and blast location

The blast load (charge weight) is previously selected (section 3.2.1) based on ease of accessibility and effect on the structural elements, the next stage is to select the standoff distance and building geometry.

The standoff distance of the blast is separated into a rectangular array as shown in figure 3-11. The nearest location is placed 4m from the face of the perimeter column and divided in plan by 1.5m grid spacing parallel to the depth of the building up to 8.5m and by 3 m throughout the width of the building, totaling 12 blast locations (without considering symmetry). The first three blast locations are situated at a height of 0.5m above the ground in account of the blast carrying vehicle and to induce direct shear failure and the remaining locations are placed at 1.5m above the ground floor to induce flexural failure.

The reflected pressure-time history (considering peak overpressure, positive time duration, time of arrival and wave decay parameter) obtained based on Kingery-Bulmash equations are calculated at the ends and middle of the story columns as shown in figure 3-10.

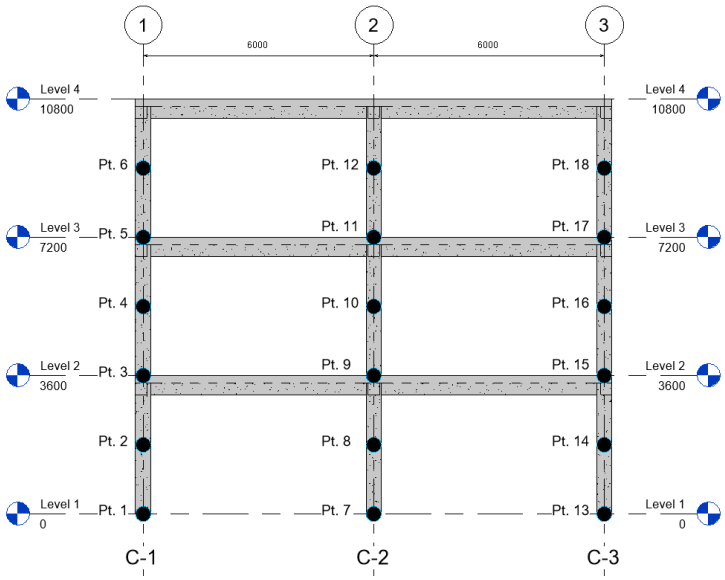

Figure 3-10 Column-pressure positions

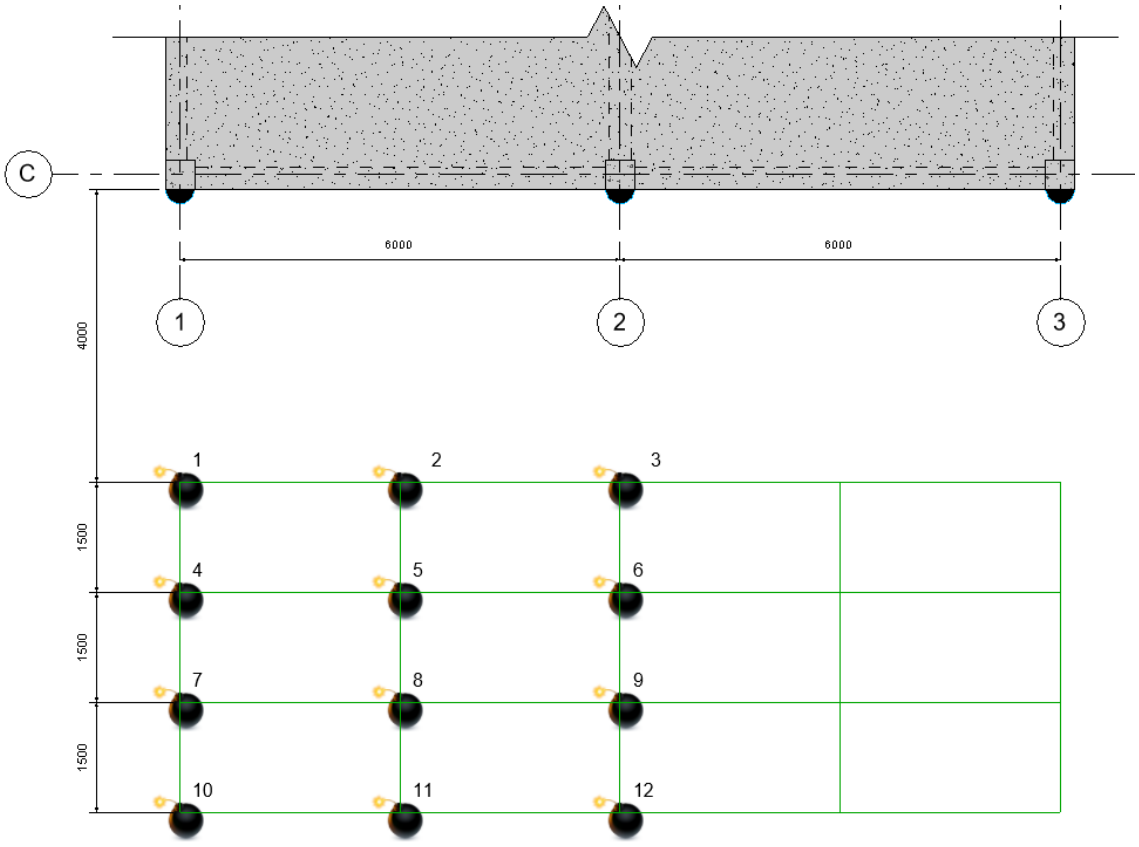

Figure 3-11 Blast locations

Based on these blast locations, pressure positions and pressure equations 3-1 to 3-5, the reflected pressure history is calculated and presented in figures 3-12 and 3-13.

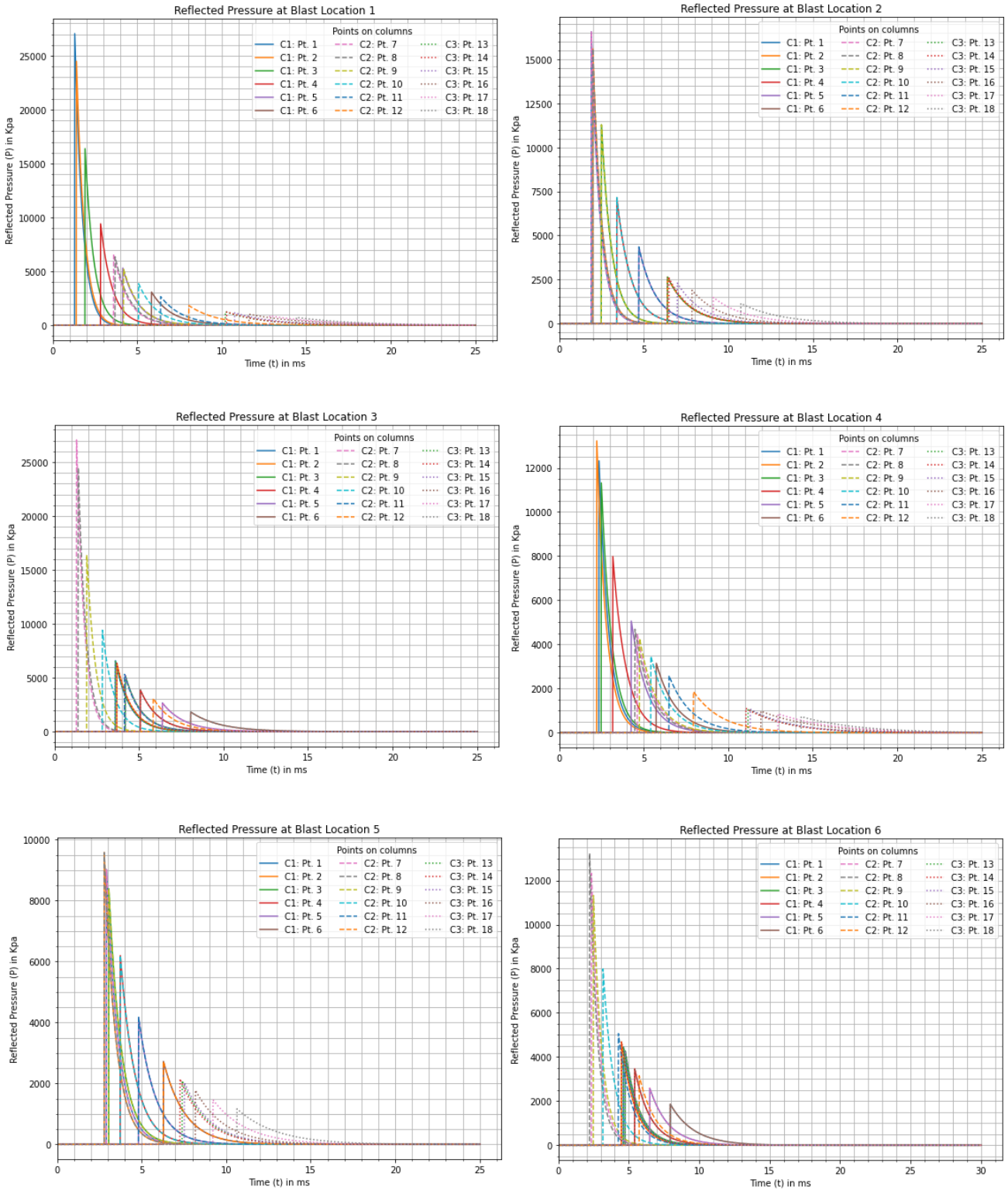

Figure 3-12 Reflected pressure at blast locations 1 to 6

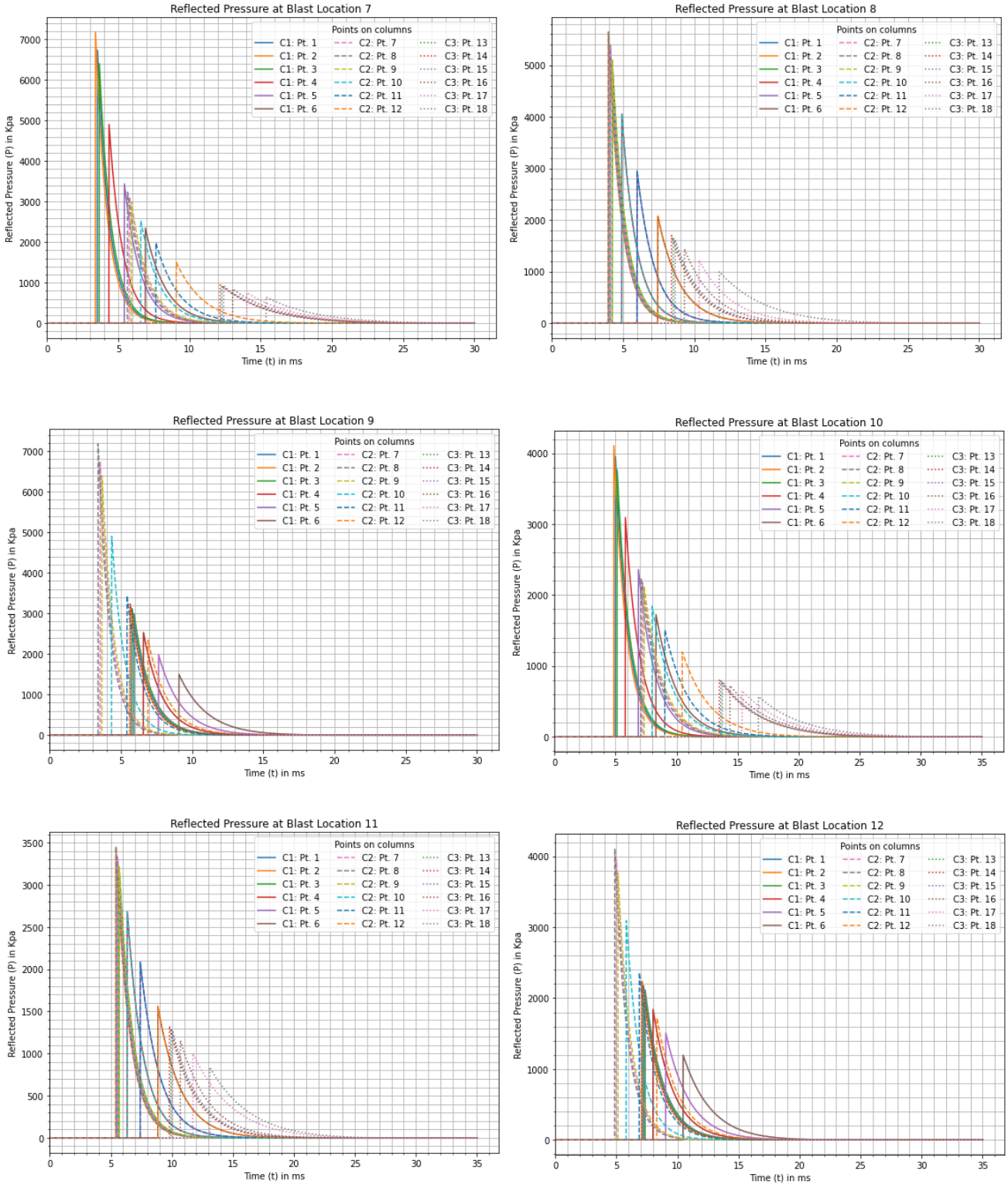

Figure 3-13 Reflected pressure at blast locations 7 to 12

3.3 Conventional design

The building considered for progressive collapse analysis is 2 bays by 2 bay square building with 6m grid spacing. The structural configurations and material properties are as follows:

- Perimeter columns – 400mmx400mm
- Interior column – 500mmx500mm
- Floor beams – 500mmx300mm (Depth x Width)
- Floor slabs – thickness 200mm
- Concrete grade C25/30
    - Characteristic cubical compressive strength, $f_{cu} = 30Mpa$
    - Characteristic cylindrical compressive strength, $f_{ck} = 25Mpa$
    - Secant modulus of elasticity of concrete, $E_{cm} = 31Gpa$
    - Mean value of axial tensile strength, $f_{ctm} = 2.6Mpa$
    - Compressive strain in the concrete at the peak stress, $\varepsilon_{c1} = 2.1‰$
    - Strain at reaching the maximum strength, $\varepsilon_{c2} = 2.0‰$
    - Ultimate compressive strain in the concrete, $\varepsilon_{cu1,2} = 3.5‰$
- Rebar grade S400
    - Characteristic yield strength of reinforcement, $f_{yk} = 400Mpa$
    - Characteristic tensile strength of reinforcement, $f_t = 600Mpa$
    - Rebar class B
    - Characteristic strain of reinforcement at maximum load, $\varepsilon_{uk} = 20‰$
    - Modulus of elasticity of rebar, $E_s = 200Gpa$

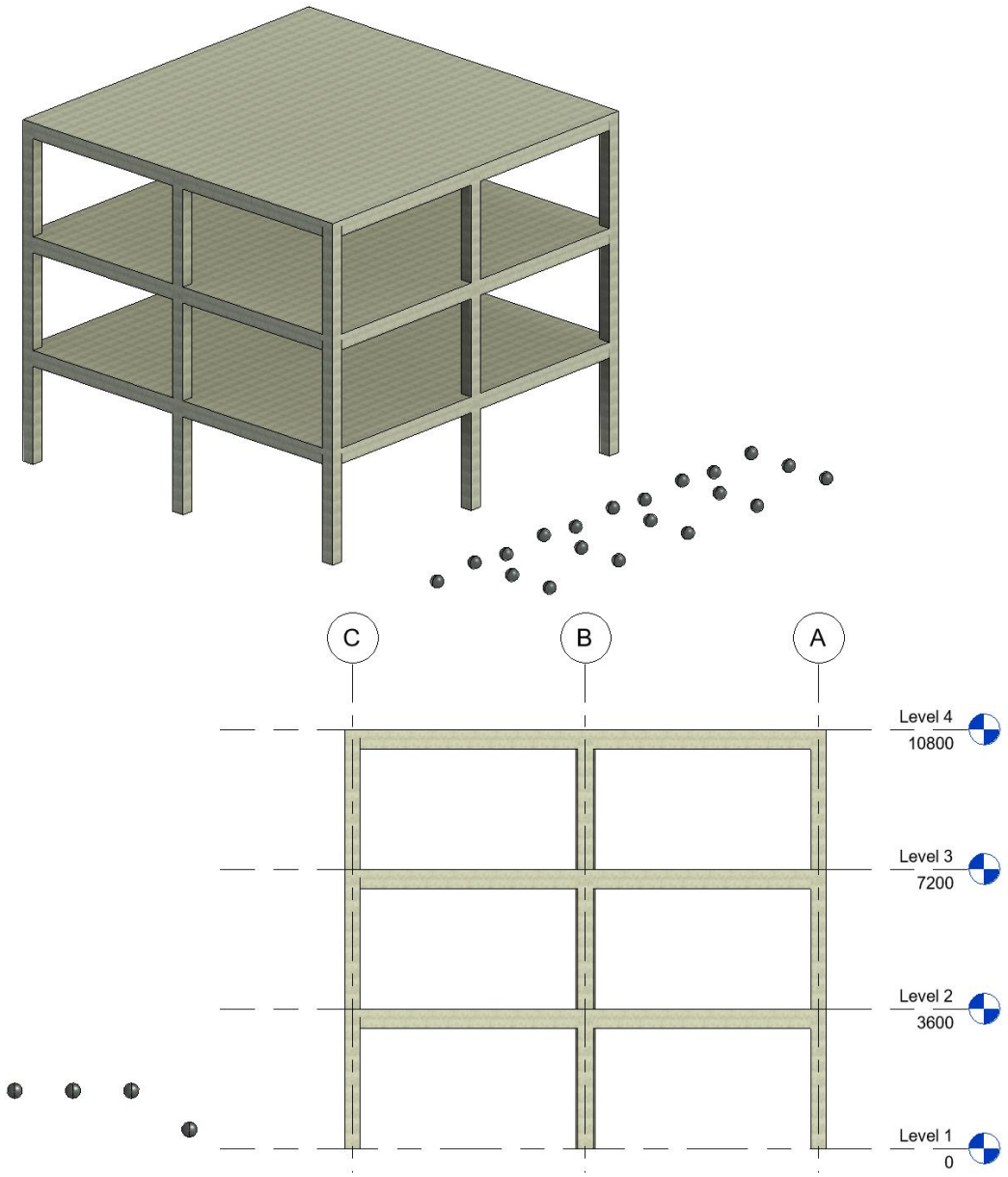

Figure 3-14 Structural model of the building including blast location

The conventional design followed these standard codes: ES EN 1990, 1991-1-4, 1992-1-1 and 1998-1-1. The gravity loads considered are;

- Total dead load including partition (excluding self-weight) is 4.5kN/m^2 for all floors.
- Total live load is 3kN/m^2 for all floors.
- Wind load:
    - Basic wind speed: 35m/s
    - Terrain category: IV

- Air density: 0.94kg/m^3

- Seismic action:
  - Peak ground acceleration: 0.1g
  - Spectrum type:1
  - Ground type: B
  - Behavior factor: 3.9
- Global imperfection:
  - Basic value of inclination: 1/200

Based on these inputs and previous section and material property, the structure is analyzed and designed considering a rigid base at the ground floor. The analysis and design followed the codes specified above. As the main objective of this paper is to investigate the effect of blast on progressive collapse, the gravity and lateral load analysis will not be shown here. However, the perimeter column confinement is displayed here based on the output of the structural analysis;

Behavior Factor	3.9
N_{ed} (kN)	698.2
Depth (mm)	400
Width (mm)	400
F_{cd} (MPa)	14.17
F_{yd} (MPa)	347.83
Concrete Cover (mm)	30
Diameter of stirrup (mm)	8
b_o (mm)	330
h_o (mm)	330
Stirrup transverse spacing (mm)	120

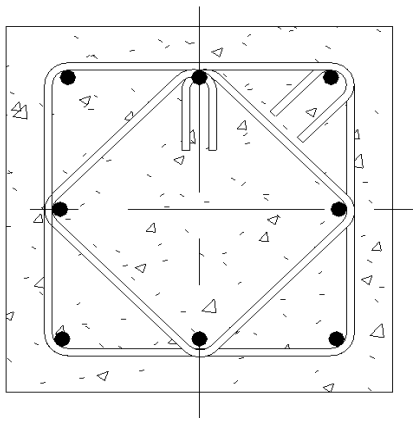

C/C distance between laterally restrained longitudinal bars, b_i (mm)	152.00

Number of legs in the X-direction	3
Number of legs in the Y-direction	3
Diameter of longitudinal bar, ∅ (mm)	16
μ_ϕ	6.80
V_d	0.31
ε_{yd} (%)	0.17
α	0.50
$A_{sv,x}$ (mm^2)	150.80
$A_{sv,y}$ (mm^2)	150.80
ω_{wd}	0.19
$30 * \mu * V_d * \varepsilon_{yd} * (b_c/b_o) - 0.035$	0.09
$\alpha * \omega_{wd}$	0.09

Chapter 4 SDOF Assessment of Columns

Assuming damage in beams is preserved by the rigid floor diaphragm, capacity assessment is done for columns. When analyzing structures under blast loads, often the main interest lies in their final condition after the blast, not the detailed trajectory of their deformation over time. To understand this response, we start with a simplified "single-degree-of-freedom" (SDOF) model, where the entire structure's behavior is condensed into one point. The principles of analyzing this SDOF system can be applied to model plastic behavior and specific structural elements that can be approximated as SDOF systems. By defining such an equivalent SDOF system, the overall structural response can be described by a single dynamic equation of motion. The use of SDOF is recommended in design manuals such as UFC-3-340-02 [15]. This equation includes an inertia term based on the structure's mass and a stiffness term based on its geometry and material properties, both acting in opposition to the applied blast load.

Before commencing on the capacity assessment of columns, the dynamic properties of reinforced concrete under high strain rates needs to be investigated. This includes the dynamic properties of both concrete and rebar.

4.1 Material properties at high strain-rate

Explosions generate incredibly high strain rates (10^2 to 10^4 s^{-1} whereas static loads in contrast generate strain rates at 10^{-6} to 10^{-5} s^{-1}), dramatically changing how structures respond to the force. This rapid deformation alters the expected damage mechanisms in various structural components. Notably, in reinforced concrete structures subjected to blast effects, both the concrete and steel reinforcing bars can exhibit a significant increase in strength due to the influence of strain rate on their mechanical properties.

The influence of strain rate on the strength of concrete and steel is commonly expressed through the dynamic increase factor (DIF), defined as the ratio between the material's dynamic strength (measured under blast loading) and its static strength (obtained under slow, controlled loading) at a particular strain rate.

4.1.1 Dynamic properties of concrete

The mechanical response of concrete under dynamic loading exhibits distinct characteristics compared to static conditions. While the dynamic stiffness remains comparable to the static value, the sustained stresses achievable for specific durations under dynamic scenarios can significantly exceed the static compressive strength, demonstrating the enhanced load-bearing capacity of concrete under rapid deformation.

4.1.2 Dynamic properties of rebar

In addition to examining the dynamic behavior of concrete under blast loads, there is significant strength enhancement of steel reinforcing bars subjected to high strain rates. For reinforced concrete elements the Dynamic Increase Factor (DIF) is presented in UFC [15] and presented in table 4-1.

Table 4-1 DIF for design of reinforced concrete elements

Type of Stress	**Far Design Range**			**Close-In Design Range**		
	Reinforcing		Concrete	Reinforcing		Concrete
	f_{dy}/f_y	f_{du}/f_u	f'_{dc}/f'_c	f_{dy}/f_y	f_{du}/f_u	f'_{dc}/f'_c
Bending	1.17	1.05	1.19	1.23	1.05	1.25
Diagonal Tension	1.00	-	1.00	1.10	1.00	1.00
Direct Shear	1.10	1.00	1.10	1.10	1.00	1.10
Bond	1.17	1.05	1.00	1.23	1.05	1.00
Compression	1.10	-	1.12	1.13	-	1.16

4.2 Capacity Assessment

Capacity assessment involves the damage modes and limit states of the columns which are breach, flexure and direct shear failure modes. Breach failure mode is calculated using empirical formula presented in Blast Effects on Buildings [25]. Whereas flexure and shear failure modes are calculated using SDOF approach.

4.2.1 Breach failure mode

Breach of a concrete column is a critical failure condition characterized by the complete loss of concrete material across the entire thickness of a column cross-section. The significant concentrated pressures necessary to breach a reinforced concrete element result in this failure mode being frequently associated with the intense demands of close-

in explosions (near-field). The following equations lead to the determination of the minimum standoff distance at which breach occurs according to David Cormie et al. [25]:

$$\frac{h}{W} = 0.03Z^{-0.62} \quad \textbf{(4-1)}$$

And the minimum distance where no damage should occur is given by;

$$\frac{h}{W} = 0.07Z^{-0.62} \quad \textbf{(4-2)}$$

The occurrence of scabbing in reinforced concrete components happens when there is tension failure perpendicular to the exposed surface, often leading to significant deflections. This phenomenon becomes particularly pronounced when the angle of support rotation surpasses 4 degrees. Concrete damage is most severe in the covers, experiencing the highest strains and lacking confinement as visible in Zhang's experiment.

Figure 4-1: Occurrence of scabbing [32]

Based on this empirical formula, none of the column at any story level and standoff distance are exposed to breach. The minimum depth of column that would result in breach is 84mm.

4.2.2 Flexural failure mode

Flexural performance evaluation employs standardized resistance functions defined in DoD [1] and a simplified single-degree-of-freedom (SDOF) analysis framework. Each column is represented as a mass-spring system with a single translational degree of freedom in the horizontal direction parallel to the exciting force. R(x) denotes the SDOF system's resistance as a function of displacement (x), M represents the equivalent mass of

the system, and P(t) signifies the laterally applied reflective pressure load as a function of time and P_a represents the axial load as presented in equation 4-3.

The analysis takes into account the axial load acting on the column, which varies based on its position in the structure. This axial load, a compressive stress, typically increases the column's moment capacity by offsetting some of the tension induced in the reinforcing steel due to bending. Additionally, it delays the onset of cracking in the concrete. However, the interaction between the axial load (P) and the lateral deflection at the midspan (Δ) caused by bending generates an additional moment called the P-Δ moment, which must be factored in for accurate analysis.

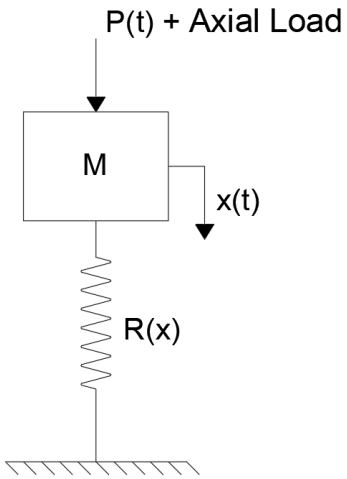

Figure 4-2 Equivalent SDOF with axial load

The equation of motion for the column is defined as [33];

$$\boldsymbol{K_{LM}M\ddot{x} + c\dot{x} + kx = P(t) + \frac{8 * P_a}{L}x} \quad \textbf{(4-3)}$$

The axial load is that represents the static load, according to GSA [10] guidelines is represented by dead load plus 25% of the live load. From equation 4-3, K_{LM} is the transformation factor, it is the ratio of the load to the mass transformation factor.

The common SDOF model considers damping effects even though the short duration of the blast event is insignificant compared to the column's natural vibration period, which governs its inherent damping behavior. So, how is energy dissipated? Energy is dissipated by plastic deformation rather than structural damping [34].

4.2.2.1 Resistance function

The modeling of columns in continuous frames typically involves the selection of appropriate boundary conditions, with the three most common options being fixed-fixed (both ends rigidly restrained against rotation and translation), fixed-simple (one end fixed and the other allowed to rotate but not translate), and simple-simple (both ends allowed to rotate and translate). Here, fixed-fixed boundary condition is utilized. The SDOF analysis followed a fixed end column with a uniformly distributed load as it depicts the building under study.

The resistance followed three stages: elastic, elastoplastic and plastic. The elastic stage is where the concrete retains its tensile strength. The elastoplastic stage follows the elastic stage until the reinforcements reaches its yield strength. Finally, at the plastic stage plastic hinges is formed at the mid span when the ultimate deflection is reached.

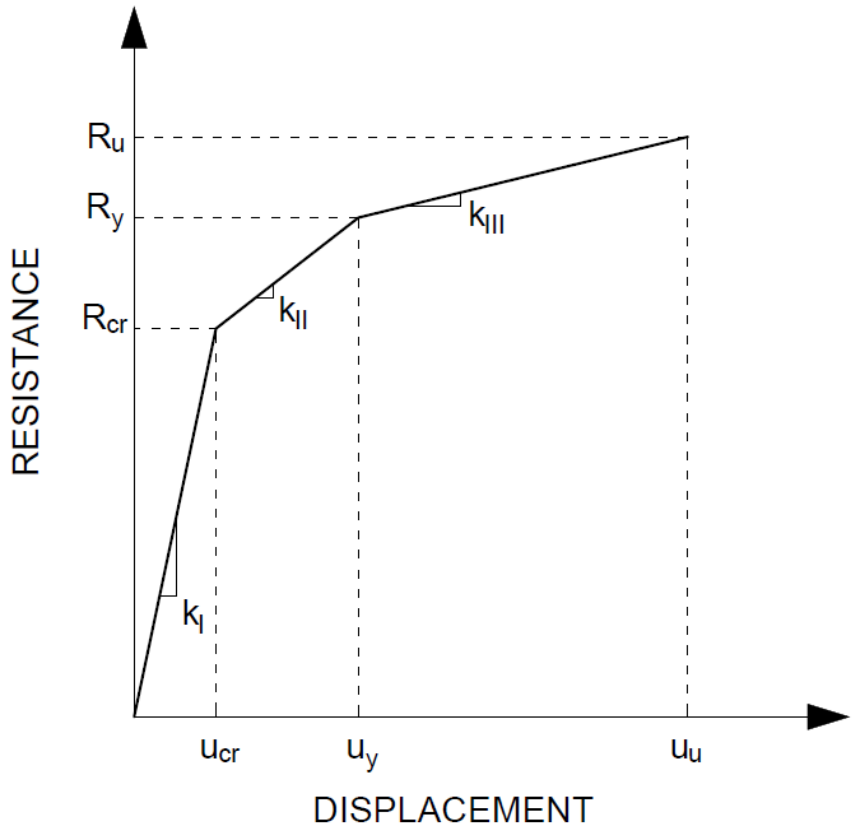

Figure 4-3 Elastic-Elastoplastic-plastic resistance-displacement graph [6]

Simplified resistance function is proposed by Carvalho [6] and summarized here. The cracking moment considering axial load, as it decreases the tension in the reinforcement and is given by;

$$\boldsymbol{M_{cr} = \frac{I_{gt}}{\bar{x}} * \left(f_{ctm} - \frac{N}{A_g} \right)} \quad \textbf{(4-4)}$$

In equation 4-4, I_{gt} is the uncracked gross moment of inertia, $\bar{x}$ is the depth from the neutral axis to the tension end, f_{ctm} is the mean tensile strength of concrete, N is the column's axial load and A_g is the gross cross-sectional area of concrete. The displacement at the end of the elastic zone is;

$$\boldsymbol{u_{cr} = \frac{R_{cr}}{k_{gt}} = \frac{12 * M_{cr}}{L} * \frac{L^3}{384 E I_{gt}}} \quad \textbf{(4-5)}$$

After the concrete cracks, the elastoplastic stage follows, this stage is limited by the yielding of the tensile reinforcement. The yield moment is given by;

$$\boldsymbol{M_y = \mu_e b d^2 f_{ck}} \quad \textbf{(4-6)}$$

The factor μ_e in equation 4-6 is to account for reduction in resisting moment due to cracking. It is given by;

$$\boldsymbol{\mu_e = \omega(1 - \omega)} \quad \textbf{(4-7)}$$

Where ω is the mechanical reinforcement ratio of the section, it is given by;

$$\boldsymbol{\omega = \frac{A_{st} * f_y}{b d f_{ck}}} \quad \textbf{(4-8)}$$

To account tension stiffening, intermediate state between cracked and uncracked concrete, the yield displacement is calculated in two portions (cracked and uncracked);

$$u_y = \zeta a_{II} + (1 - \zeta) a_I \quad \textbf{(4-9)}$$

In equation 4-9, the distribution coefficient ζ is given by;

$$\zeta = 1 - \left(\frac{M_{cr}}{M_y}\right)^2 \quad \textbf{(4-10)}$$

The uncracked portion (a_I) of the displacement equation (4-9) is calculated by;

$$a_I = R_y * k_{gt} = \frac{16 * M_y}{L} * \frac{5L^3}{384EI_{gt}} \quad \textbf{(4-11)}$$

The cracked portion (a_{II}) of the displacement equation (4-9) is calculated by;

$$a_{II} = R_y * k_y = \frac{16 * M_y}{L} * \frac{5L^3}{384EI_{cr}} \quad \textbf{(4-12)}$$

The final stage is the plastic stage – post yield stage, where the reinforcement has yielded and is reaching the ultimate capacity before rupture, strain hardening. Similar steps followed in the elastoplastic stage are carried out at this stage. When calculating the mechanical reinforcement ratio, instead of the yield strength the ultimate strength is taken into account. Instead of the yield moment the ultimate moment is computed using the above mechanical reinforcement ratio. The uncracked portion remains the same, however, the cracked portion differs from elastoplastic stage. The cracked moment of inertia that takes into account the modular ratio of reinforcement to concrete, now is revised by the new modulus of elasticity of rebar. The new modulus of elasticity of rebar is computed using the ultimate tensile strength and characteristic strain of reinforcement at maximum load (section 3.3), strain hardening.

Solving a nonlinear system using the above resistance function results in unrealistic response or numerical error. Therefore, the trilinear resistance function is converted to a bilinear resistance curve as proposed by Carvalho [6]. The equivalent stiffness and displacement are calculated by:

$$u_{eq} = u_{cr} + u_y\left(1 - \frac{R_{cr}}{R_y}\right) \text{ and } k_{eq} = \frac{R_y}{u_y} \quad \textbf{(4-13)}$$

When converting from trilinear to bilinear, equation 4-13 guarantees the area under the resistance displacement graph remains the same.

Note: As blast load is considered as accidental, all materials are analyzed using their nominal strength (no factor of safety).

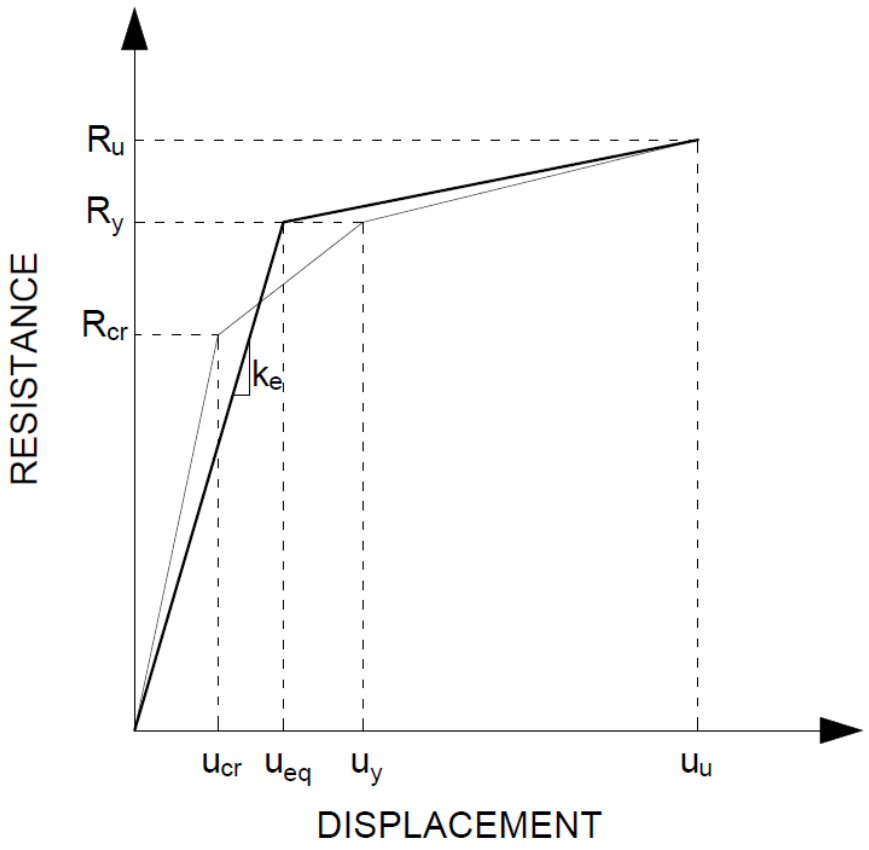

Figure 4-4 Bilinear resistance-displacement curve [6]

After the resistance is computed the final stage is solving the nonlinear dynamic analysis. This is solved using the widely used Newmark's Beta method (average acceleration) as described in Dynamics of Structures: Theory and Applications to Earthquake Engineering by Anil K. Chopra [35].

4.2.2.2 Damping function

The contribution of structural damping to overall energy dissipation is minimal compared to plastic deformations [34] as stated earlier. Nevertheless, damping effect is

incorporated and the damping coefficient (c) is calculated using formula 4-14, given a known damping ratio;

$$\boldsymbol{c = 2 * \xi * K_M * M * \sqrt{\frac{k}{K_{LM} * M}}} \quad \textbf{(4-14)}$$

In equation 4-14, ξ is the damping ratio (Conrad's blast simulations [36] yielded various results, with a 5% value appearing to be the most reliable), K_M is the mass transformation factor, M is the total mass and k is the stiffness.

4.2.3 Direct shear failure mode

Direct shear resistance of the column can be attributed to its initial dynamic rigid body motion, observed before the onset of flexural response. This rigid body behavior results in a localized concentration of shear stresses near the supports.

4.2.3.1 Resistance function

Accurately modeling the direct shear resistance of RC structures remains a challenge, leading to a reliance on empirical approaches. The resistance-slip model, pioneered by Krauthammer et al. (1986) [37], represents a significant step in this direction. The stress-strain curve of a material can be divided into five distinct stages:

- OA (elastic response): Linear relationship between stress and strain, material returns to its original shape after stress removal.
- AB (hardening): Stress increases at a faster rate than strain, material exhibits strain hardening.
- BC (plastic flow): Nonlinear relationship between stress and strain, permanent deformation occurs.
- CD (softening): Stress decreases with increasing strain, material experiences damage and softening.
- DE (final yielding): Material ruptures and fails completely.

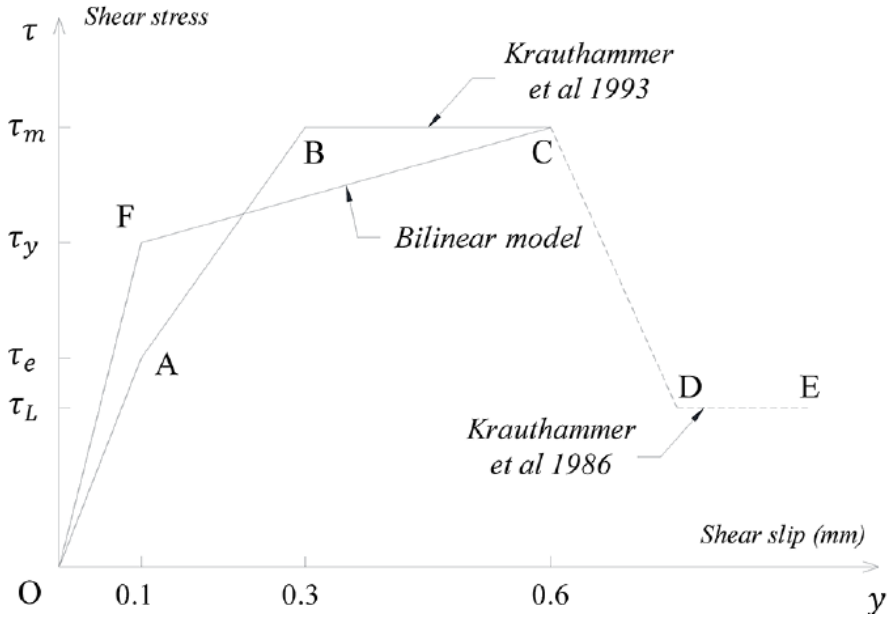

Figure 4-5 Direst shear resistance-slip curve [38]

The elastic shear resistance (OA and OF) and the maximum shear resistance is proposed by Krauthammer et al. [37]. Similar to the flexural resistance the shear resistance is converted to a bilinear model (figure 4-5) using the energy balance method proposed by Cui et al [38]. The elastic shear resistance limits up to 0.1mm is given by in psi;

$$\boldsymbol{\tau_e = 165 + 0.157 f'_c \leq \frac{\tau_m}{2}} \quad \textbf{(4-15)}$$

The maximum shear resistance limits up to a maximum shear slip of 0.6mm is calculated by;

$$\boldsymbol{\tau_m = 8\sqrt{f'_c} + 0.8\rho_{vt} f_y \leq 0.35 f'_c} \quad \textbf{(4-16)}$$

Based on the energy balance method the yield shear resistance is proposed by Cui et al [38];

$$\boldsymbol{\tau_y = \frac{\tau_e + \tau_m}{2}} \quad \textbf{(4-17)}$$

In equation 4-16 to 4-17 ρ_{vt} is the longitudinal reinforcement ratio, f'_c is the concrete compressive strength in psi and f_y the yield strength of reinforcement in psi. Considering the two supports and axial load (increases shear resistance), the revised shear resistance is given by Matthew [12];

$$\boldsymbol{R_{DSi} = \left(1 + \frac{P_u}{2000A_c}\right)\tau_i} \quad \textbf{(4-18)}$$

From equation 4-18, P_u is the factored axial load during the blast loading (DL + 0.25LL) and A_c is the gross cross-sectional area.

4.2.4 Residual axial load carrying capacity

The initial damage entails whether the damaged column can sustain some degree of load carrying capacity. This is an important concept when performing progressive collapse analysis as it dictates whether the given column can bear the existing axial load. A rigorous method is proposed by Shi et al. [39]. This research, however, followed another simplified method for calculating the residual axial-load carrying capacity based on the stress-strain profile of each column. This practical method, based on mechanics for RC bridge columns, is proposed by Gordon Warn and Mehmet Unal [40]. The residual axial capacity is a combination of the resistance of the concrete and rebar and given by;

$$\boldsymbol{P_{re} = P_c + P_s} \quad \textbf{(4-19)}$$

In equation 4-19, P_c and P_s are the residual axial load capacity of concrete and rebar, respectively.

Gordon Warn and Mehmet Unal, based on inelastic deformation, proposed the curvature at maximum drift as the sum of yield and plastic curvature.

$$\boldsymbol{\phi_{max} = \phi_y + \phi_p} \quad \textbf{(4-20)}$$

Priestly et al. [41] give the yield curvature as;

$$\boldsymbol{\phi_y = \frac{\lambda \varepsilon_y}{D}} \quad \textbf{(4-21)}$$

λ in equation 4-21 is taken as 2.14 for rectangular columns as per Berry et al. [42] and D is the depth of the column. The plastic curvature is calculated by;

$$\boldsymbol{\phi_p = \frac{\theta_p}{L_p}} \quad \textbf{(4-22)}$$

Where L_p is the plastic hinge length, calculated based on Pauley and Priestely as;

$$\boldsymbol{L_p = 0.08 * L + 0.15 * f_y d_b \geq 0.3 f_y d_b} \quad \textbf{(4-23)}$$

In equation 4-23, L is length of column. f_y is yield strength of reinforcement and the diameter of the reinforcement is d_b. The plastic rotation is given by;

$$\boldsymbol{\theta_p = \frac{\Delta_p}{\left(L - \frac{L_p}{2}\right)}} \quad \textbf{(4-24)}$$

Where Δ_p is the plastic displacement. The plastic displacement can be obtained by subtracting the yield displacement from the maximum displacement.

The nominal axial load carrying capacity as per ACI,

$$\boldsymbol{P_N = 0.85 * f_{ck} * A_c + f_{yk} * A_{st}} \quad \textbf{(4-25)}$$

In equation 4-25, f_{ck} is the cylindrical compressive strength of concrete, A_c is the net area of concrete, f_{yk} is the yield strength of reinforcement and A_{st} is the area of reinforcement.

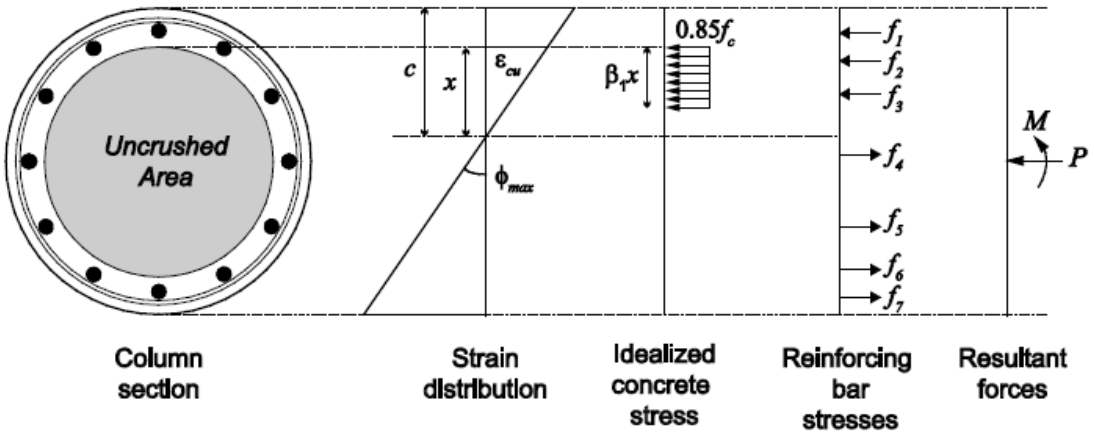

Figure 4-6: Uncrushed concrete depth based on strain [40]

Following the determination of the concrete's crushing depth via sectional analysis, the residual axial load capacity within the concrete portion of the column section can be determined. If the crushing depth is confined to the cover region, indicating no core region deterioration, the complete area of the confined concrete region is employed in residual axial load capacity calculations. This assumption stems from the anticipated spalling of the concrete cover prior to axial failure. Under this scenario, the residual axial load capacity of concrete adheres to the following equation:

$$\boldsymbol{P_{c,1} = 0.85 * f_{cc}(A_{core} - A_{st})} \quad \textbf{(4-26)}$$

Where A_{core} is the uncrushed concrete core, computed as;

$$\boldsymbol{A_{core} = (D - crushed\ depth) * b} \quad \textbf{(4-27)}$$

The crushed depth is computed as per the strain distribution and maximum curvature as shown in figure 4-6.

Once the axial load carrying capacity of the concrete is calculated the axial load capacity of the reinforcement is followed. The axial load carrying capacity of the reinforcement is based on the minimum capacity of either the plastic resistance or buckling resistance. In both cases the reinforcement is treated as a beam spanning between two transverse reinforcements.

The plastic capacity is given by;

$$P_{s,p} = \frac{8 * Z_p * f_{yk}}{s} \quad \textbf{(4-28)}$$

Where Z_p is the plastic section modulus of the rebar and s is the stirrup spacing. The buckling force is given by;

$$P_{s,b} = \frac{\pi^2 EI}{s^2} \quad \textbf{(4-29)}$$

In formula 4-29, EI is the flexural stiffness of the reinforcement bar (note the calculations are performed for a single reinforcement and finally multiplied by the number of rebars). The capacity of the reinforcement is the minimum of $P_{s,p}$ and $P_{s,b}$.

The total residual axial load carrying capacity is then given by;

$$P_{re} = P_c + P_s \quad \textbf{(4-30)}$$

And the damage degree is given by [39];

$$D_m = 1 - \frac{P_{re}}{P_N} \quad \textbf{(4-31)}$$

4.3 Damage Assessment

4.3.1 Flexural response limits

The evaluation of the flexural limit states of the columns employed response criteria established in U.S. Army Corps of Engineers publications [16]. These criteria focus on two key parameters: ductility (μ) and effective support rotation (θ). Ductility is defined as a dimensionless ratio, representing the ability of the column to deform beyond its initial elastic limit before failure. It is calculated as the ratio of the blast-induced midspan deflection to the yield displacement at midspan, where the steel reinforcement begins to yield. Furthermore, the midspan deflection can be normalized by the member length to obtain the effective support rotation (θ), which approximates the rotation at the base of the column and is calculated using equation 4-32.

$$\boldsymbol{\theta = \tan^{-1}\frac{2 * x_m}{L}} \quad \textbf{(4-32)}$$

$$\boldsymbol{\mu = \frac{Midspan\ deflection}{deflection\ at\ elastic\ limit} = \frac{x_m}{x_e}} \quad \textbf{(4-33)}$$

In equations 4-32 and 4-33, x_m is the midspan lateral deflection and L is the height of the column.

The damage levels are constrained by four response limits presented by ASCE/SEI-11 standard [43] and presented in table 4-2. Table 4-3 shows the corresponding description of the damage presented in U.S. Army Corps of Engineers [16].

Table 4-2 Flexural response limits for RC elements [43] [16]

Member		**B1**		**B2**		**B3**		**B4**	
		μ	θ	μ	θ	μ	θ	μ	θ
Flexure	No shear reinforcing/ without tension membrane	1	-	-	2^0	-	5^0	-	10^0
	With compression face steel reinforcement and shear reinforcing/without tension membrane	1	-	-	4^0	-	6^0	-	10^0
	With tension membrane (L/h>=5)	1	-	-	6^0	-	12^0	-	20^0
Combined Flexure and Compression	No shear reinforcing/ without tension membrane	1	-	-	2^0	-	2^0	-	2^0
	With compression face steel reinforcement and shear reinforcing/without tension membrane	1	-	-	4^0	-	4^0	-	4^0
Compression	Walls & Seismic Columns	0.9	-	1	-	2	-	3	-
	Non-Seismic Columns	0.7	-	0.8	-	0.9	-	1	-
Tension or Combined Flexure and Tension		No response limits							

The level of protection for building components of table 4-3 is directly taken from U.S. Army Corps of Engineers Protective Design Center Technical Report Single Degree of Freedom Structural Response Limits for Antiterrorism Design.

Table 4-3 Summary of building level of protection – component response relationship [16]

Descriptions of potential overall structural damage	**Description of component damage**		
	Primary Components [1]	**Secondary Components [2]**	**Non-Structural Components [3]**
Severe Damage - Progressive collapse likely. Space in and around damaged area is unusable.	Hazardous [4] (B3 – B4)	Blowout [5] (>B4)	Blowout [5] (>B4)
Heavy Damage - Onset of structural collapse. Progressive collapse is unlikely. Space in and around damaged area is unusable.	Heavy [6] (B2 – B3)	Hazardous [4] (B3 – B4)	Hazardous [4] (B3 – B4)
Unrepairable Damage – Progressive collapse will not occur. Space in and around damaged area is unusable.	Moderate [7] (B1 – B2)	Heavy [6] (B2 – B3)	Heavy [6] (B2 – B3)
Repairable Damage - Space in and around damaged area can be used and is fully functional after cleanup and repairs.	Superficial [8] (<B1)	Moderate [7] (B1 – B2)	Moderate [7] (B1 – B2)
Superficial Damage - No permanent deformations. The facility is immediately operable.	Superficial [8] (<B1)	Superficial [8] (<B1)	Superficial [8] (<B1)

1. Members whose loss would affect a number of other components supported by that member and whose loss could potentially affect the overall structural stability of the building in the area of loss.
2. Structural component supported by a primary framing component.
3. Components whose loss would have little effect on the overall structural stability of the building in the area of loss.
4. Component has failed, and debris velocities range from insignificant to very significant.
5. Component is overwhelmed by the blast load causing debris with significant velocities.
6. Component has not failed, but it has significant permanent deflections causing it to be unrepairable.

7. Component has some permanent deflection. It is generally repairable, if necessary, although replacement may be more economical and aesthetic.
8. Component has no visible permanent damage.

4.3.2 Direct shear response limits

The shear response limits are defined by limiting the shear strain considering the shear slip. Here, the deflection is the shear slip, determined for each shear resistance limits.

Like flexural response, SDOF analysis is computed for evaluating shear slip using the proposed resistance function. The response (shear slip) from the SDOF is used to evaluate the shear stain as follows [38];

$$\boldsymbol{\gamma_v = \frac{D_{sm}}{\delta h}} \quad \textbf{(4-34)}$$

D_{sm} is the maximum shear slip at the support, δ is defined as 0.866 and h is the thickness of the column.

Table 4-4 Direct shear response limits [38]

Damage level	Average shear strain (%)
Minor damage	$1 \leq Strain \leq 2$
Moderate damage	$2 < Strain \leq 3$
Severe damage	$3 < Strain$

4.3.3 Initial Damage

The damage degree is translated in the model of the members through material strength and stiffness degradation as proposed by Shi et al. [11]. Therefore, the damaged concrete's compressive strength and Young's modulus is calculated by;

$$\boldsymbol{f_{c,dmg} = f'_c(1 - D_m)\ and\ E_{dmg} = E(1 - D_m)} \quad \textbf{(4-35)}$$

4.4 Validation of SDOF system

In order to make sure the above method of analysis for blast response considering single-degree-of-response is reliable, the output is compared with experimental results.

Two different experimental results from two different sources are considered; Experimental study on scaling of RC beams under close-in blast loading by Zhang et al. [32] and Near-Field explosion effects on reinforced concrete columns: An experimental investigation by Farouk Siba [9]. Zhang et al. experiment involved spherical air burst on a beam with dimension 100x100x1100 mm. The standoff distance was fixed at 0.4m and the charge weight was varied. The prevailing failure mode was flexural with scabbing of the covers at higher charge weight. The deflection was measured by long needles placed inside a fine sand, see figure 4-7. The scaled distance varied from 0.57 to 0.40 m/kg$^{1/3}$.

The output of the spherical air burst test result and the SDOF is shown in table 4-5, Δ_{max} is the maximum displacement, μ is the ductility ratio, θ is the end rotation and γ is the average shear strain. As table 4-5 demonstrates the SDOF gives a reliable result regarding the response of the structure especially at higher charge weights. What is considered as an acceptable margin of error? There isn't a single published source outlining a universally accepted range for error between experimental and numerical results in engineering, several resources discuss common practices and considerations in addition to conference discussions [38, 44]. According to Yehya et al. [44] the maximum allowed margin of error is 9.25% and as per Cui et al. [38] the accepted margin of error vary from -11.2% to 58.3%. The calculated errors in this research vary from 34.22% to 3.58%. Considering only sample B2-1 has an error of 34.22% with an increase in displacement of only 3mm, the SDOF is regarded as acceptable. More significantly, the prevailing failure modes, flexural failure, is well represented as indicated by the ductility ratio and rotation compared to the shear slip and average shear strain.

Table 4-5: Comparison of test and SDOF results of reinforced concrete beams

Beam	**Scaled distance (m/kg$^{1/3}$)**	**Test central deflection (mm)**	**SDOF analysis**						
			Flexure				Shear		Damage degree
			Δ_{max} (mm)	Error (%)	μ	$\theta(°)$	Δ_{max} (mm)	$\gamma(\%)$	
B2-1	0.57	9	12.08	34.22	1.51	1.26	0.39	0.45	0.137
B2-2	0.50	25	20.25	-19.00	2.54	2.11	0.68	0.78	0.190
B2-3	0.44	35	33.00	-5.71	4.13	3.43	1.22	1.41	0.226
B2-4	0.40	40	41.43	3.58	5.19	4.31	1.59	1.84	0.238

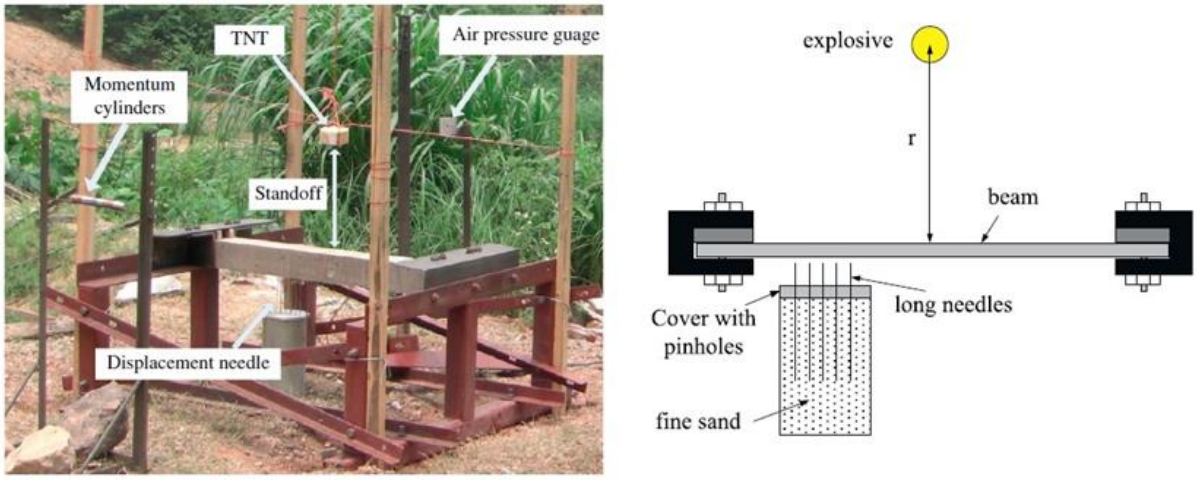

Figure 4-7: Picture of Zhang et al. test setup and illustration [32]

Zhang et al. experiment was dominated by flexural mode because the blast was spherical air burst and located at the center of the beam. The flexural and shear responses for the tests based on SDOF analysis is shown in figures 4-8 and 4-9. The next experimental output considered is Farouk's, this experiment closely resembles this research as it is a hemispherical surface air burst located close to the surface. As the bomb is in close contact to the base rather than the middle height, shear failure was prevailing in most cases in addition to some flexural cracks. The column has a dimension of 300x300x3000 subjected to a charge weight of 82 Kg and 123 kg TNT equivalent of ANFO at different standoff distance. Most of the gauges were deemed unreliable due to damage, however, the SDOF analysis showed that the shear is the prevailing failure mode. The ductility ratio is 2.30 and the end rotation is 2.40^0. Whereas the shear slip is 12.40mm and the average shear strain is 4.77% (which is significantly higher than the severe damage response limit of 3%).

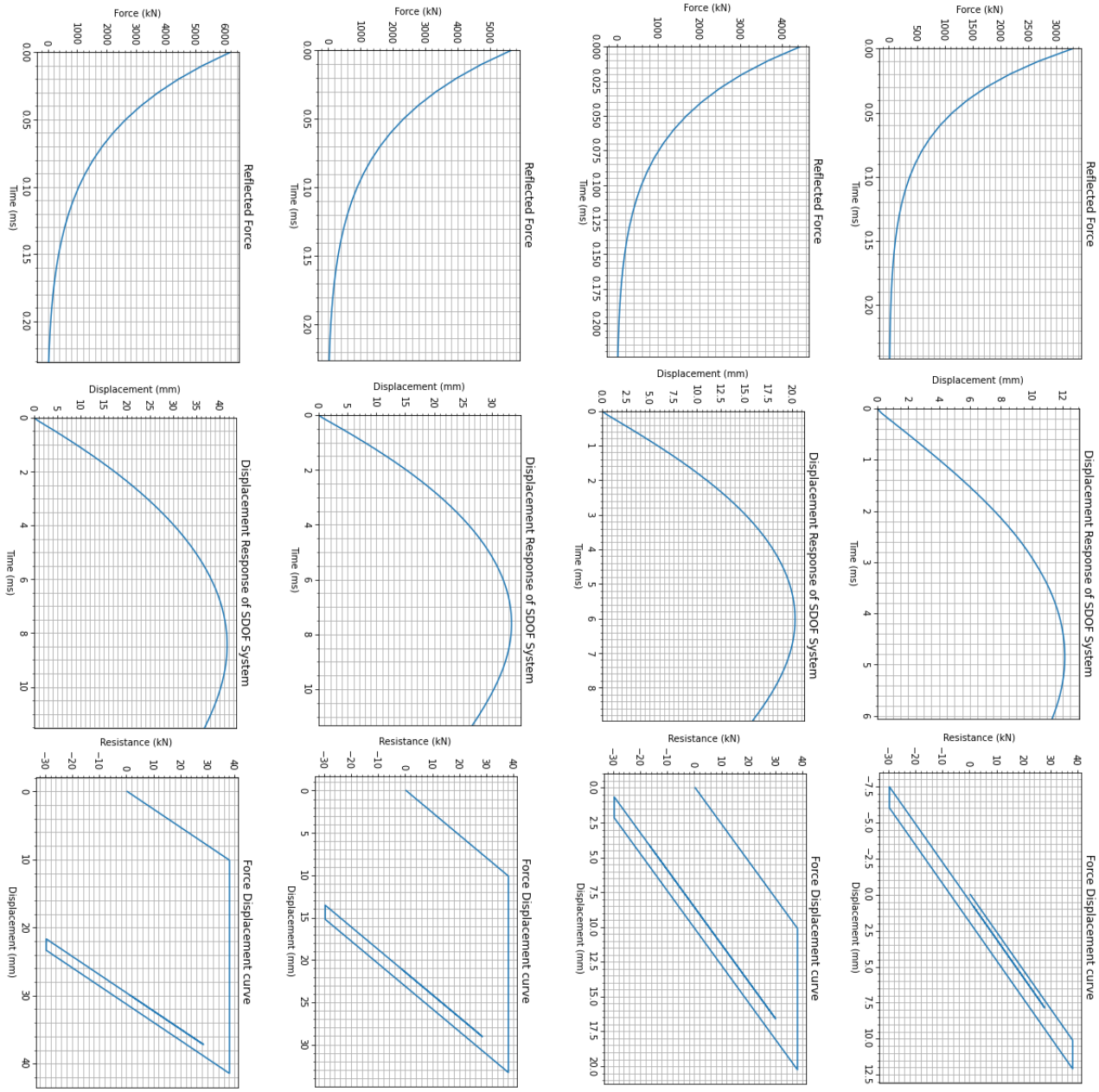

Figure 4-8: Flexural response for beams B2-1 to B2-4

The flexural and shear responses of Farouk's experiment are shown in figure 4-10, including the reflected force and the force displacement curve.

Figure 4-9: Farouk's test setup [9]

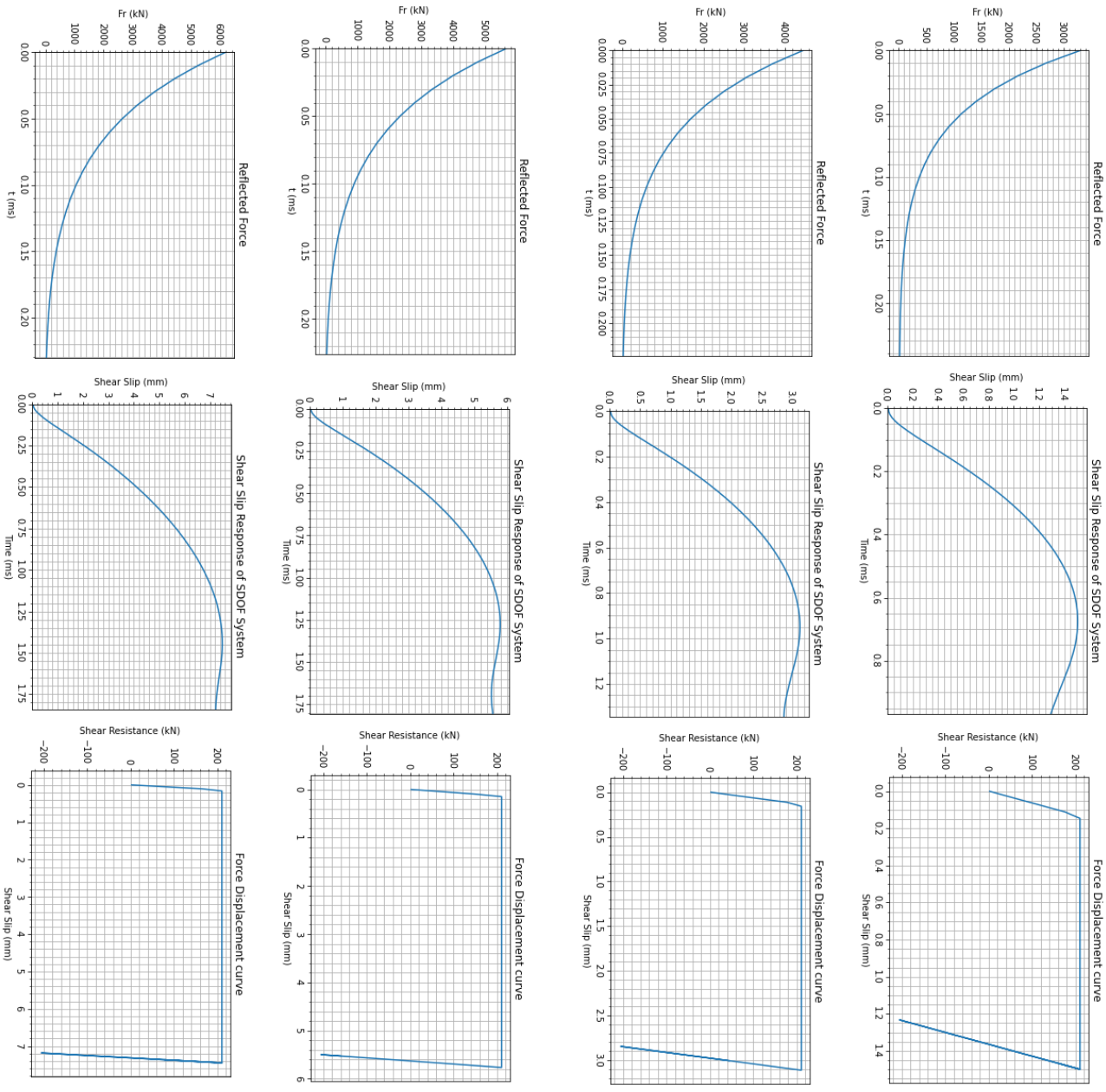

Figure 4-10: Shear response for beams B2-1 to B2-4

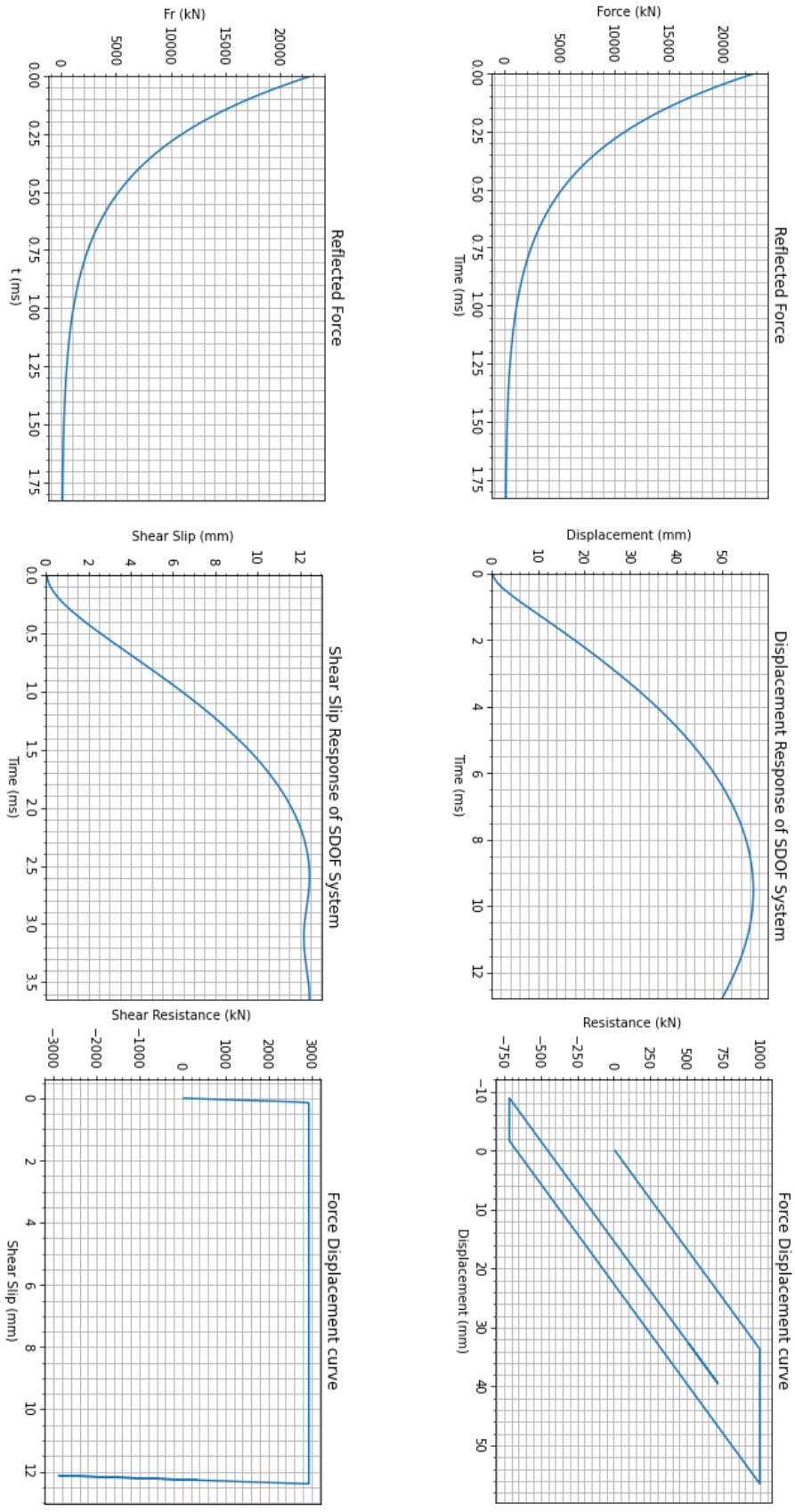

Figure 4-11: Shear and flexural response for RC column of Farouk's experiment

4.5 Response of the building's vertical elements

For this research the responses (flexural and direct shear) for each column based on the selected charge weight (discussed in section 3.2.1) and standoff distance (discussed in section 3.2.4) are shown in figures 4-12 to 4-23.

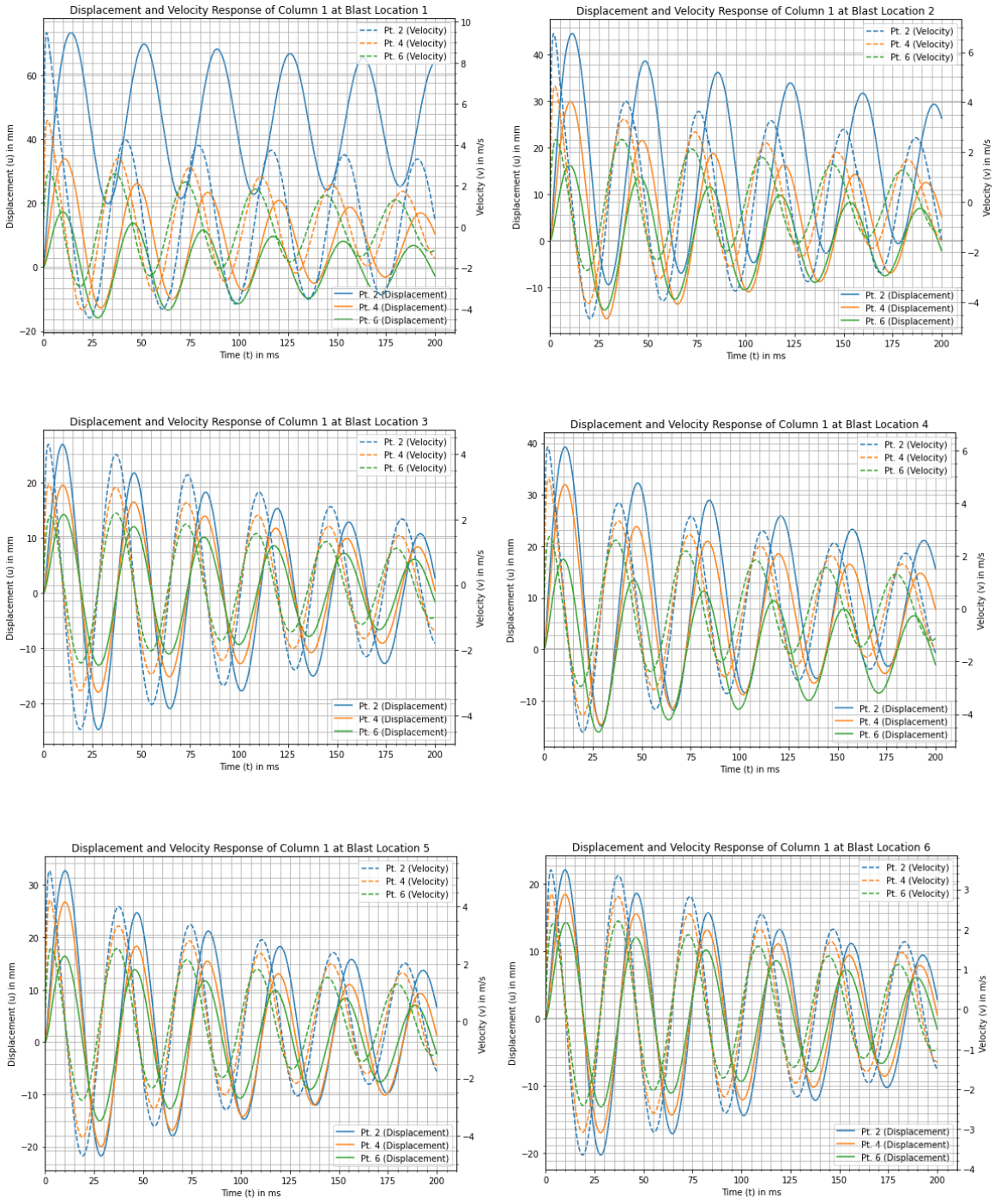

Figure 4-12: Flexural response of column 1 at blast locations 1 to 6

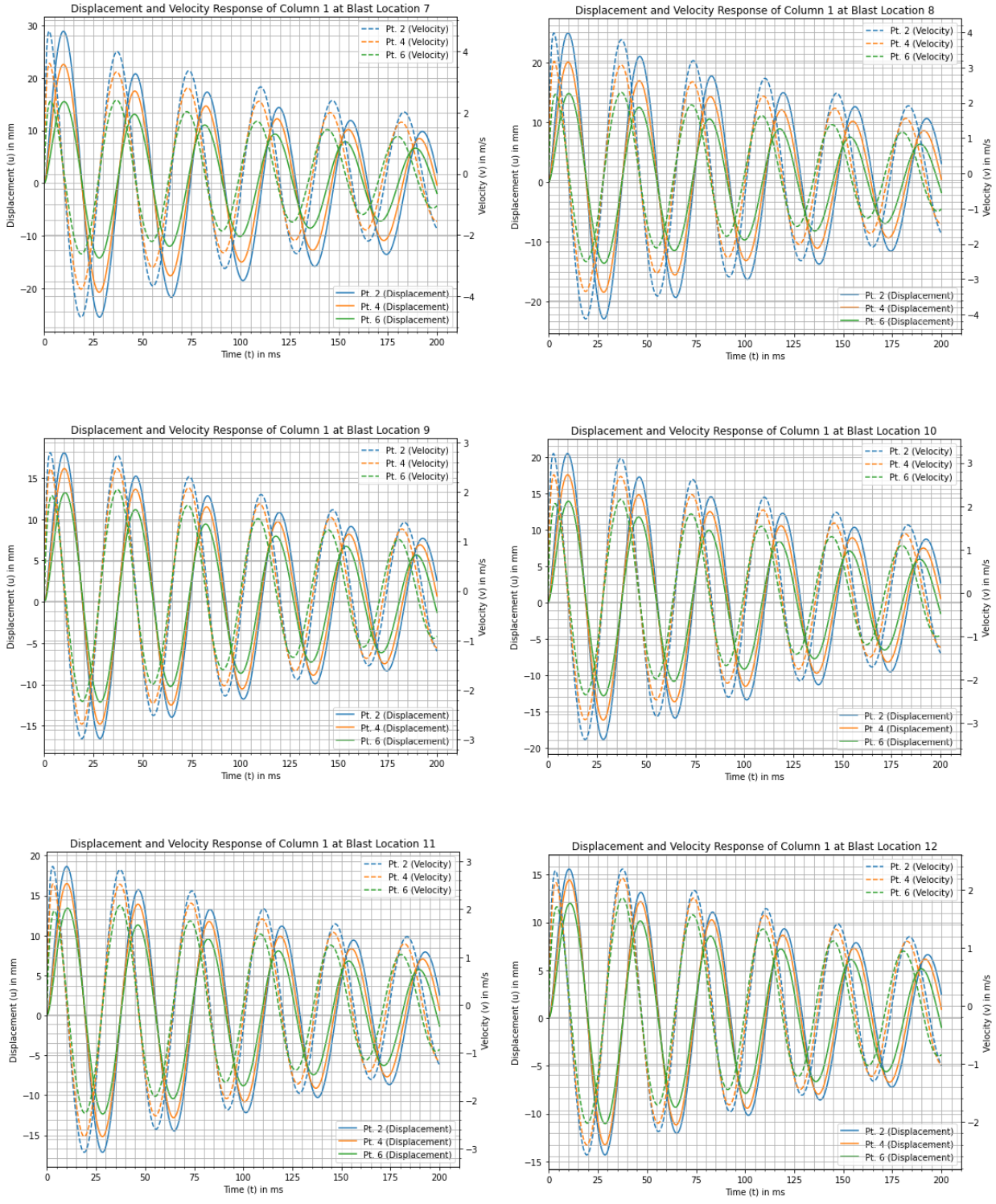

Figure 4-13: Flexural response of column 1 at blast locations 7 to 12

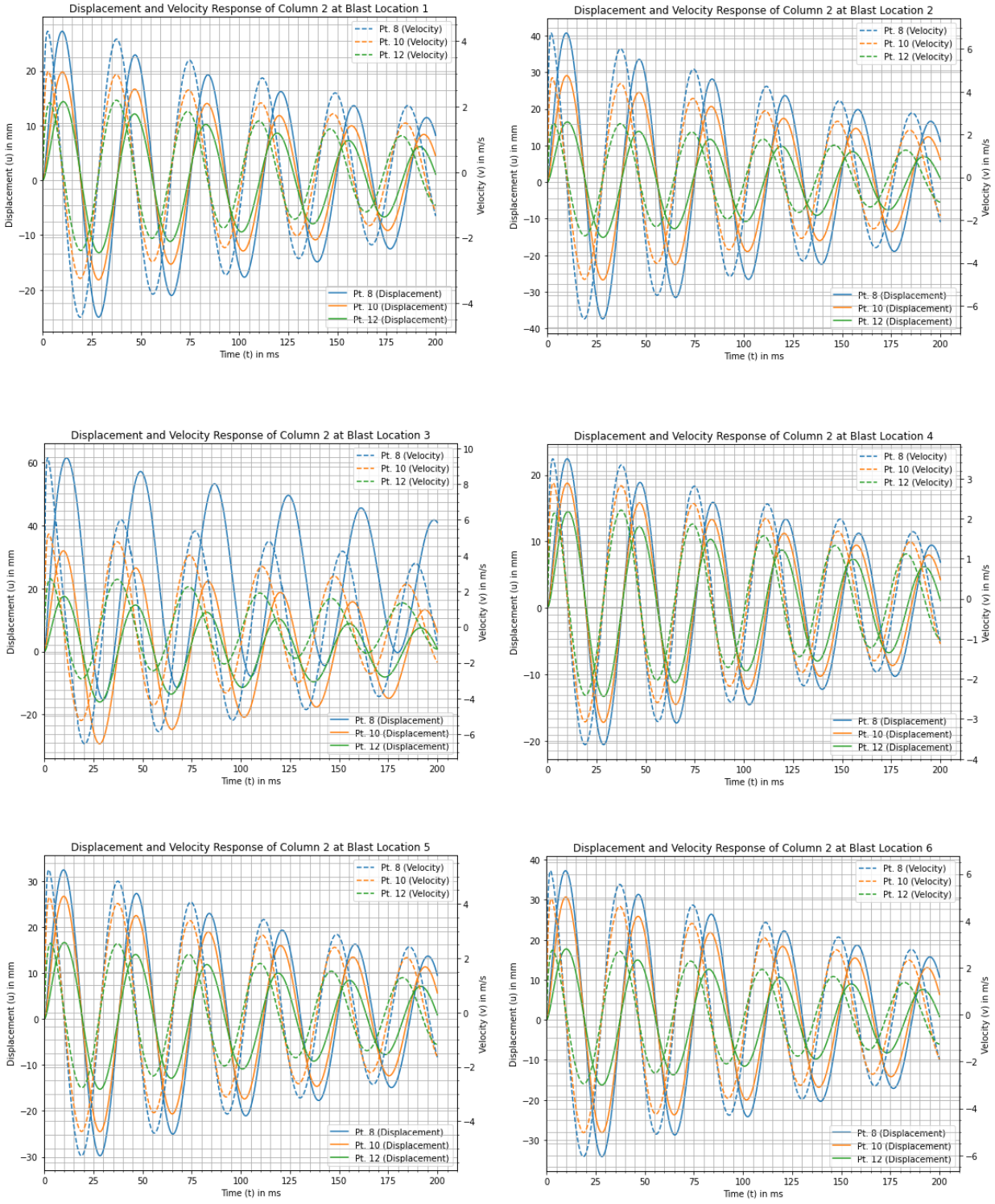

Figure 4-14: Flexural response of column 2 at blast locations 1 to 6

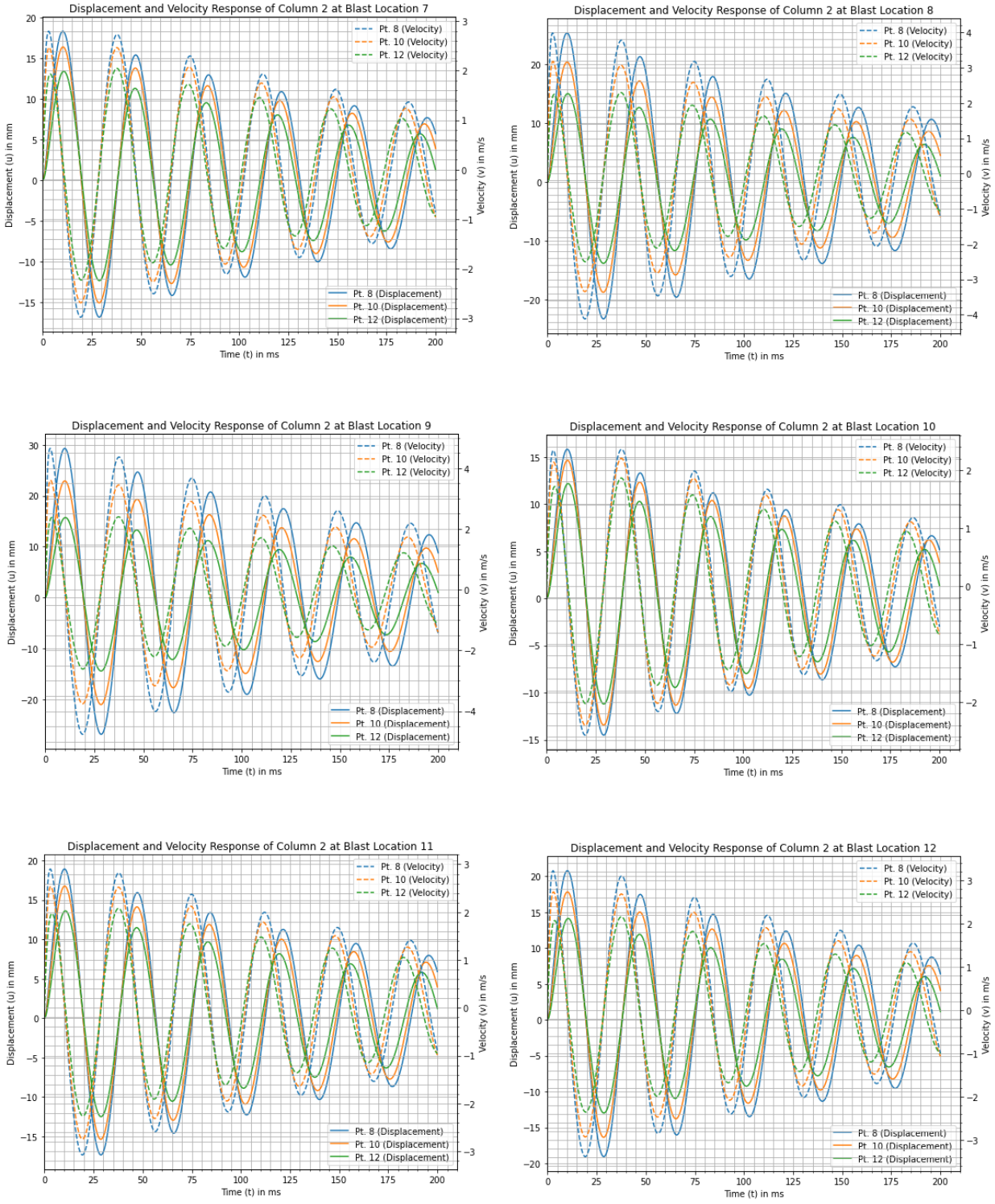

Figure 4-15: Flexural response of column 2 at blast locations 7 to 12

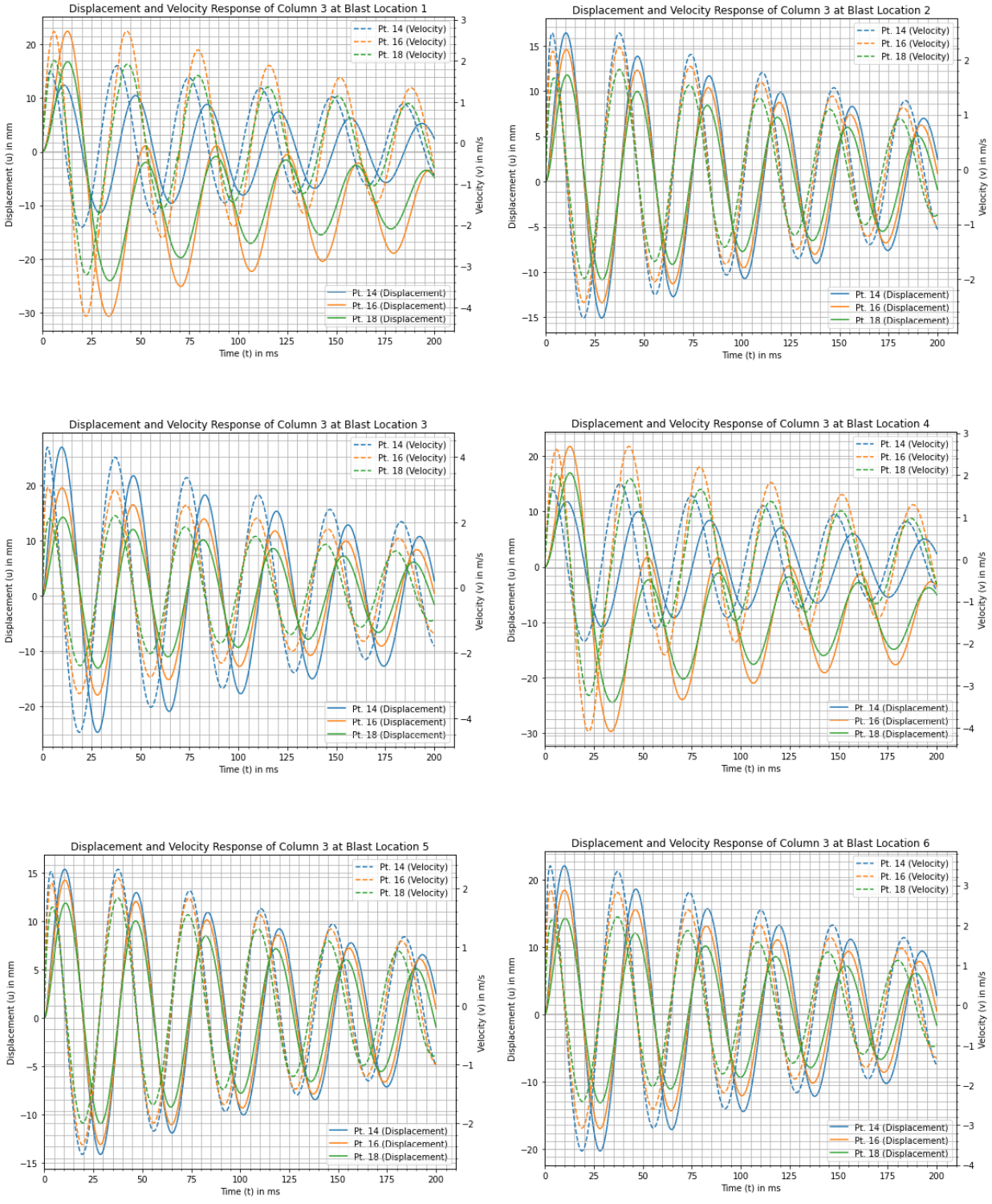

Figure 4-16: Flexural response of column 3 at blast locations 1 to 6

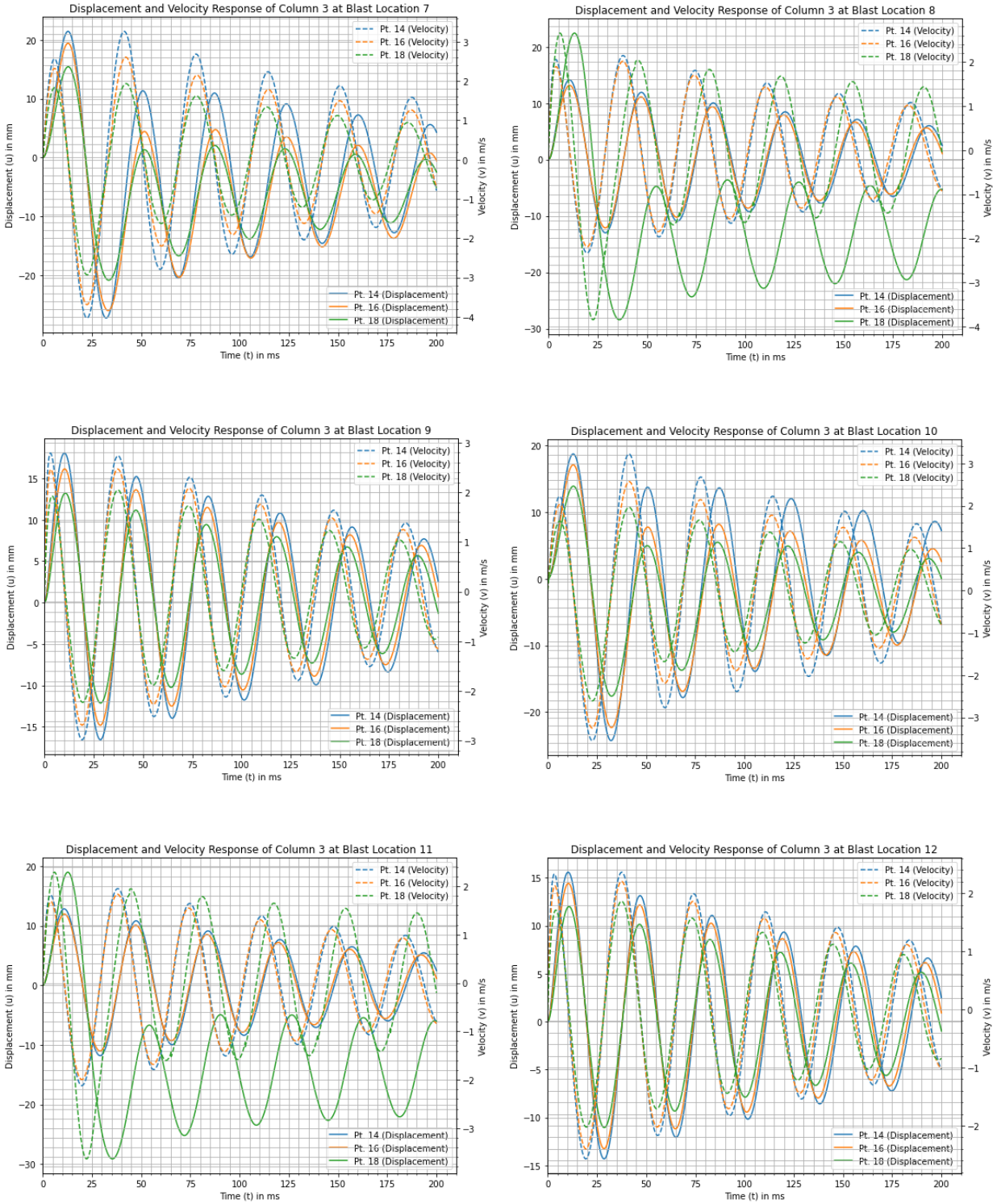

Figure 4-17: Flexural response of column 3 at blast locations 7 to 12

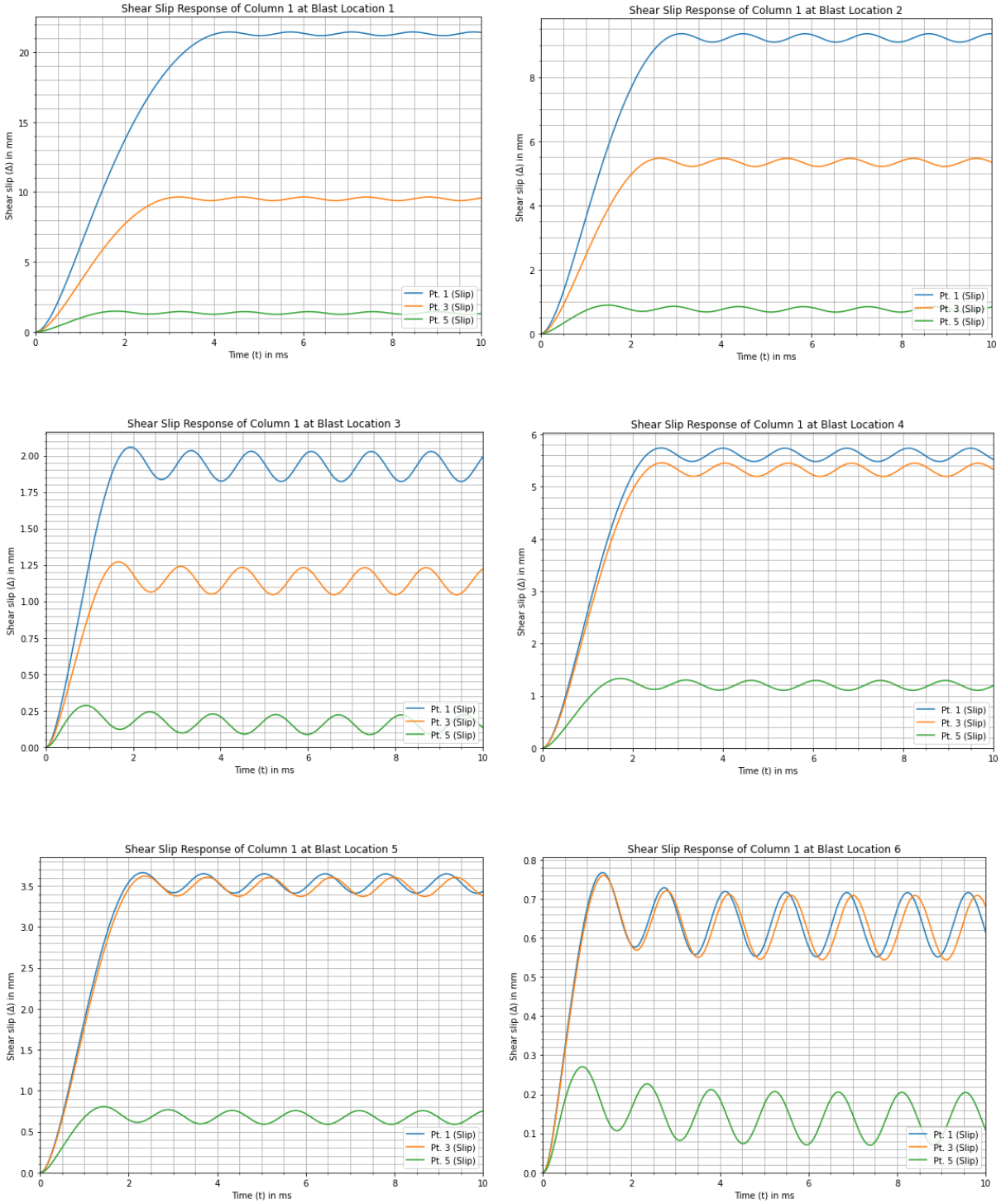

Figure 4-18: Direct shear response of column 1 at blast locations 1 to 6

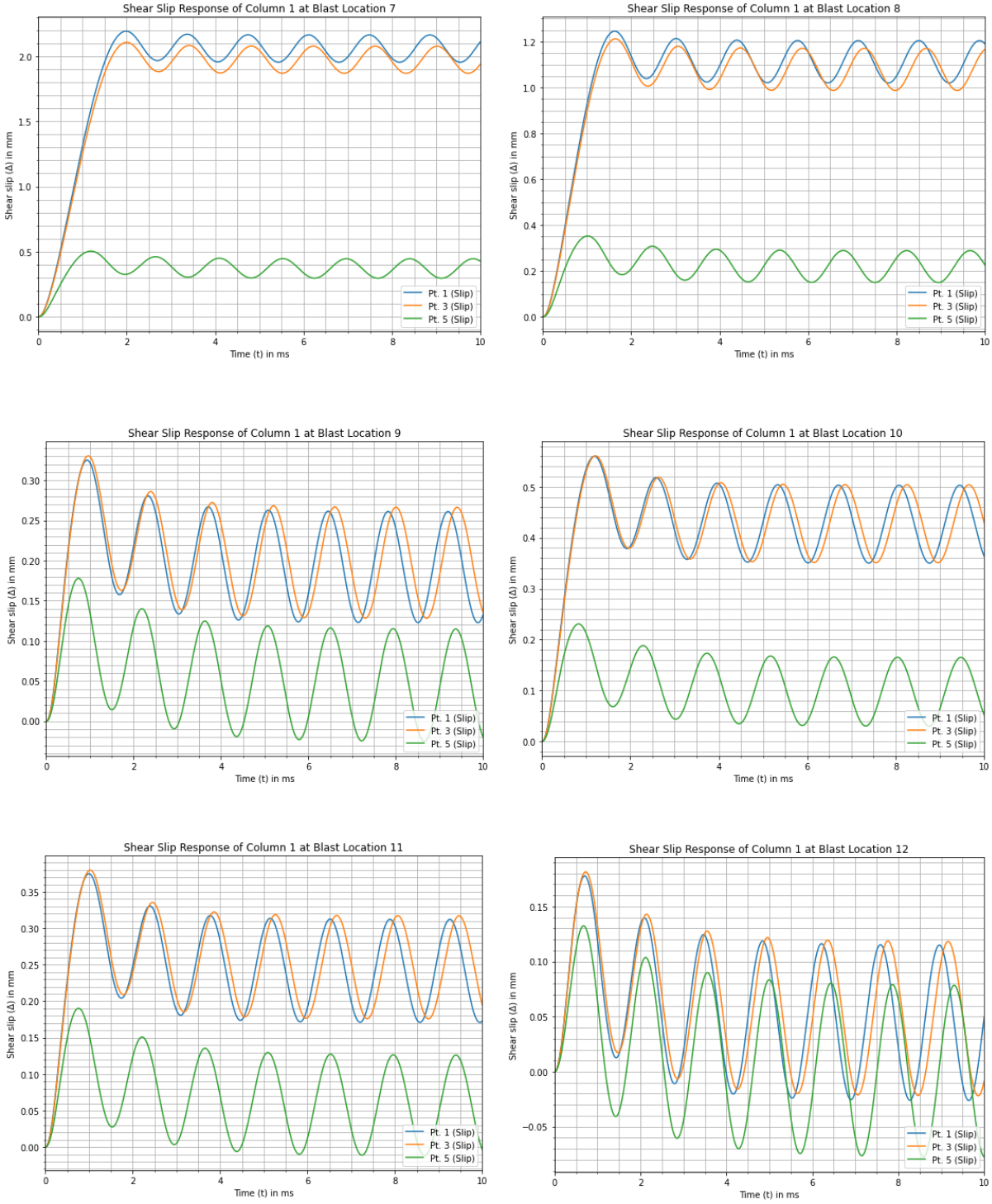

Figure 4-19: Direct shear response of column 1 at blast locations 7 to 12

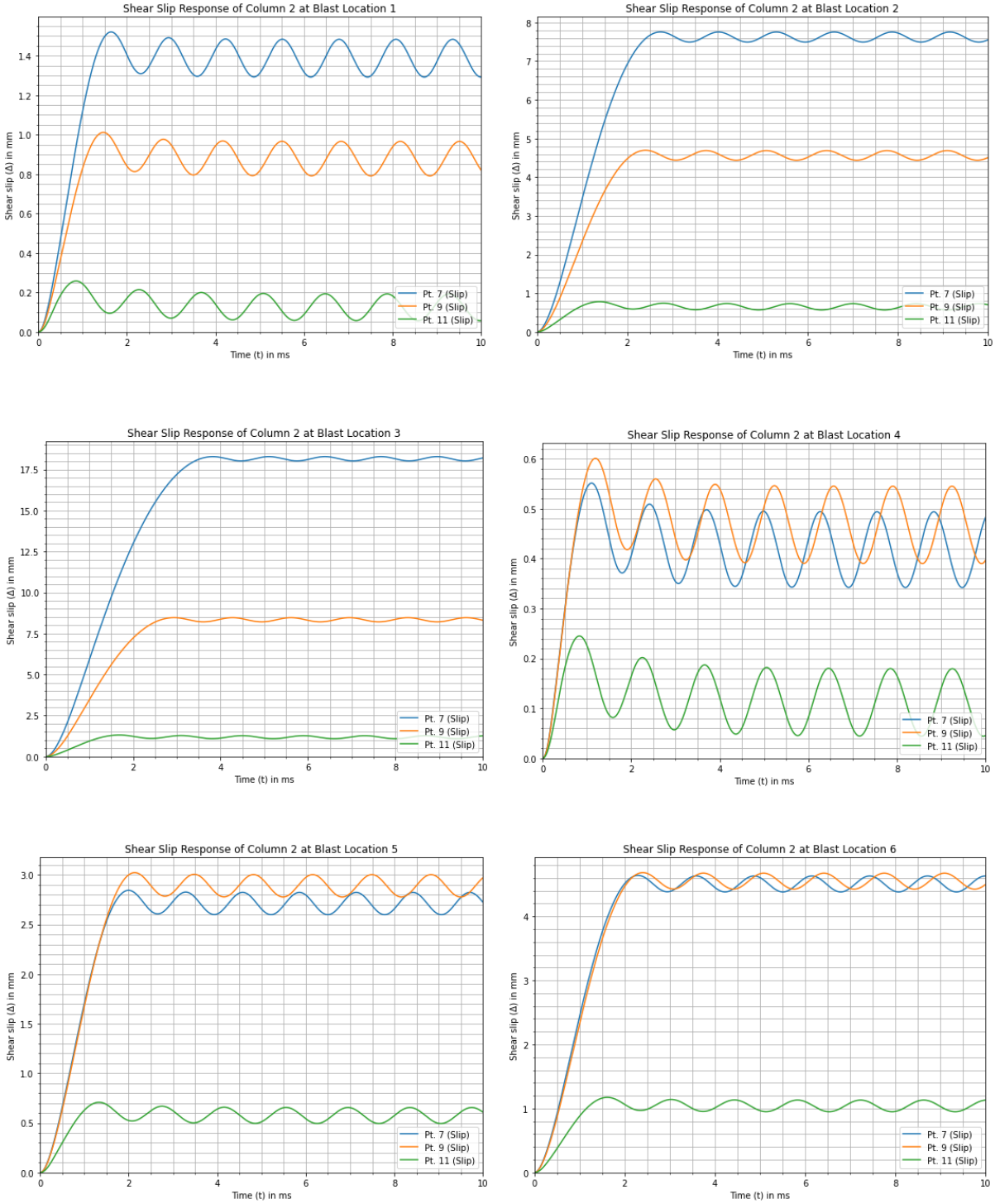

Figure 4-20: Direct shear response of column 2 at blast locations 1 to 6

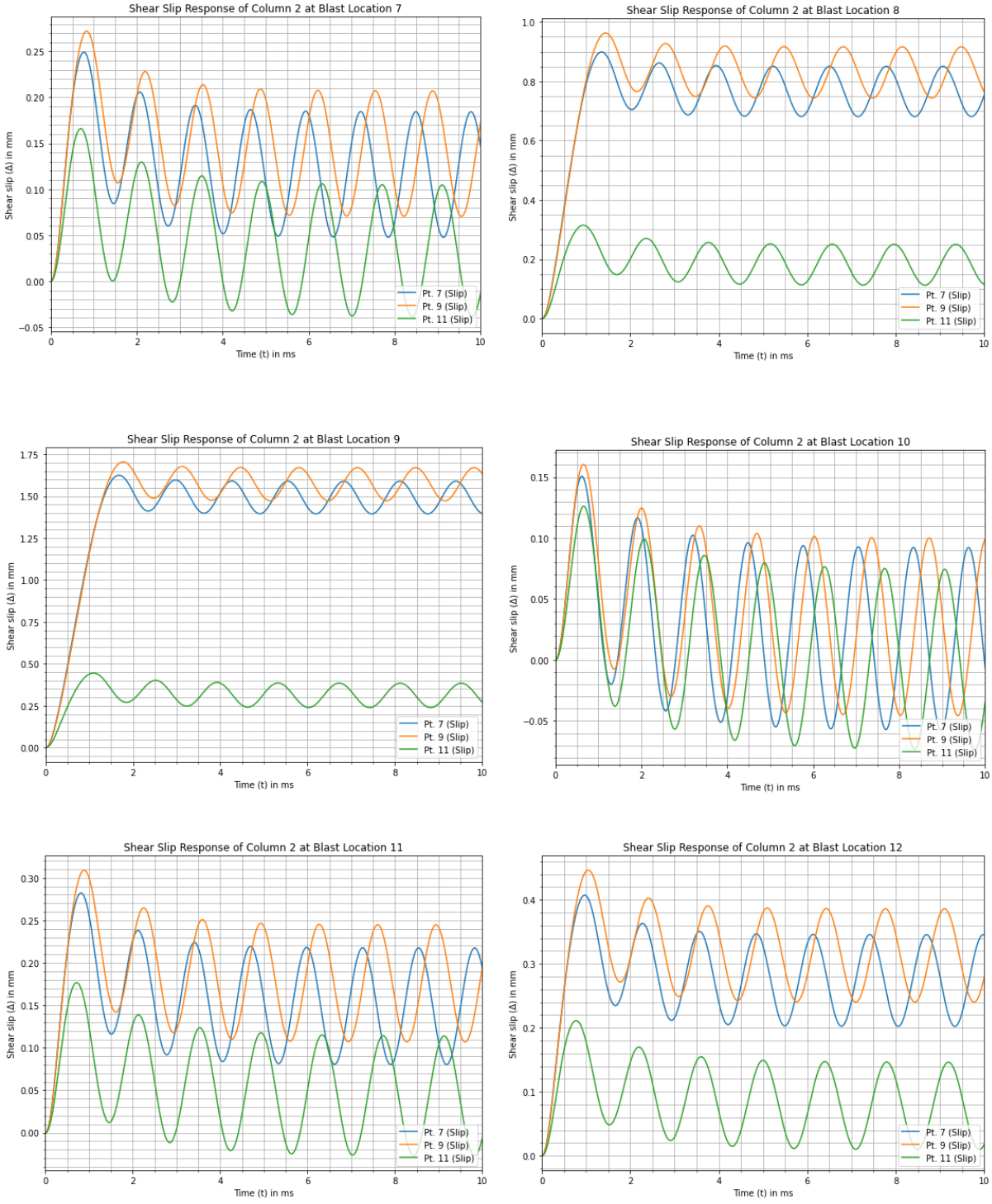

Figure 4-21: Direct shear response of column 2 at blast locations 7 to 12

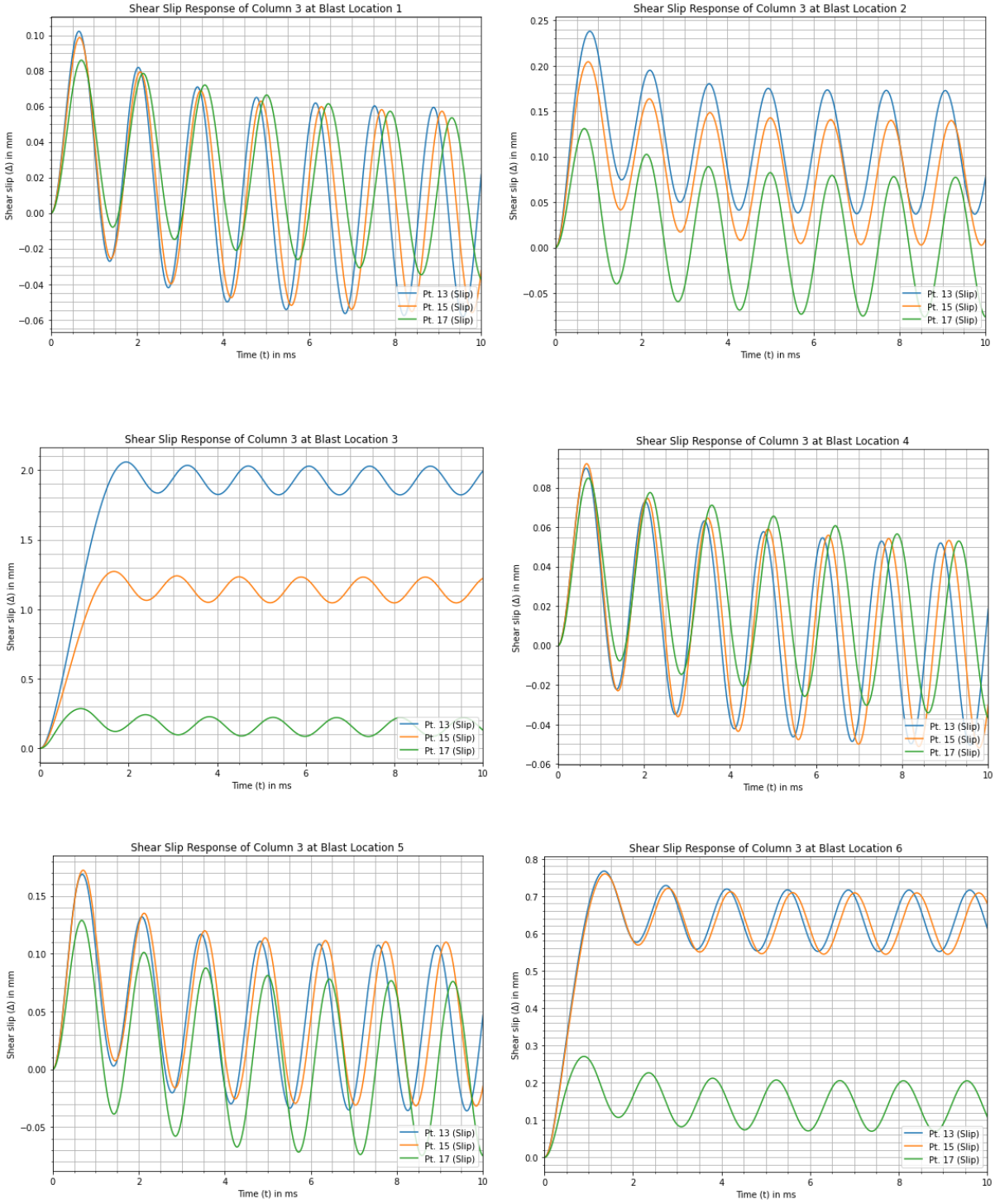

Figure 4-22: Direct shear response of column 3 at blast locations 1 to 6

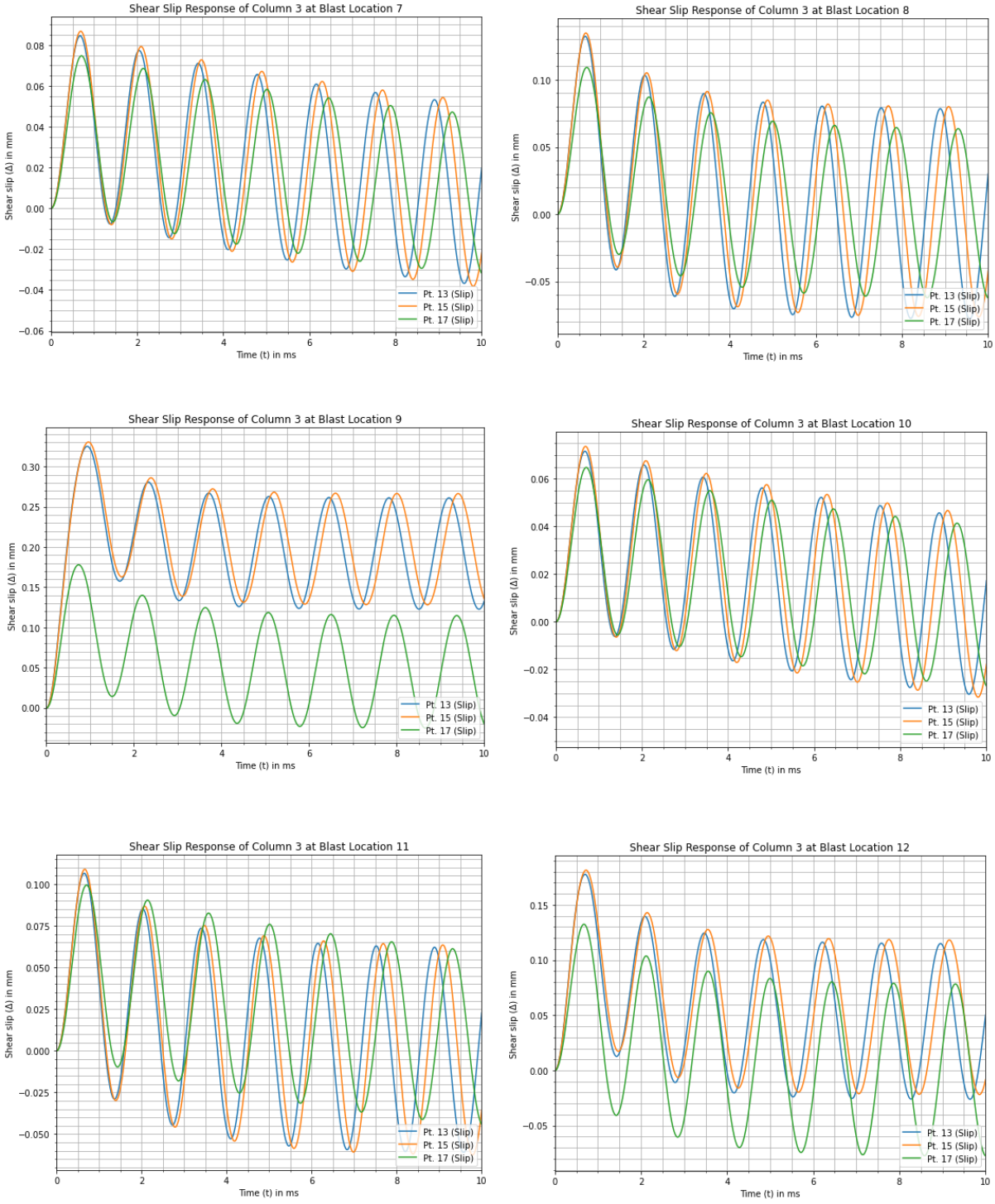

Figure 4-23: Direct shear response of column 3 at blast locations 7 to 12

The flexural and shear response levels and component damage based on the corresponding limits (table 4-2 to 4-4) are shown in tables 4-6 to 4-9. The flexural response

limits are selected considering the columns as compression seismic columns, hence, categorized based on ductility ratio.

Table 4-6: Flexural and shear response level and damage for the building columns (blast locations 1 to 3)

Blast location	Column	Flexure								Direct Shear			
		Point	Max. Displacement (mm)	Ductility ratio	Rotation (degree)	Damage Degree	Velocity (m/s)	Response level	Component Damage	Point	Max. Shear Slip (mm)	Average Shear Strain (%)	Component Damage
1	Axis 1-C	2	73.15	3.03	2.70	0.252	9.46	B4	Hazardous Damage	1	21.45	6.20	Severe Damage
		4	33.80	1.69	1.25	0.198	5.20	B3	Heavy Damage	3	9.65	2.79	Moderate Damage
		6	17.25	1.12	0.64	0.123	2.70	B3	Heavy Damage	5	1.48	0.43	Minor Damage
	Axis 2-C	7	27.24	0.74	1.01	0.000	4.30	B1	Superficial Damage	7	1.52	0.44	Minor Damage
		10	19.79	0.68	0.73	0.000	3.07	B1	Superficial Damage	9	1.01	0.29	Minor Damage
		12	14.39	0.70	0.53	0.000	2.20	B1	Superficial Damage	11	0.26	0.07	Minor Damage
	Axis 3-C	14	12.42	0.51	0.46	0.000	1.88	B1	Superficial Damage	13	0.10	0.03	Minor Damage
		16	22.48	1.13	0.83	0.000	2.72	B3	Heavy Damage	15	0.10	0.03	Minor Damage
		18	16.80	1.09	0.62	0.000	2.01	B3	Heavy Damage	18	0.09	0.02	Minor Damage
2	Axis 1-C	2	44.54	1.84	1.65	0.221	6.75	B3	Heavy Damage	1	9.35	2.70	Moderate Damage
		4	29.88	1.50	1.10	0.186	4.65	B3	Heavy Damage	3	5.47	1.58	Minor Damage
		6	16.22	1.05	0.60	0.116	2.51	B3	Heavy Damage	5	0.89	0.26	Minor Damage
	Axis 2-C	7	40.75	1.10	1.51	0.214	6.75	B3	Heavy Damage	7	7.76	2.24	Moderate Damage
		10	29.12	1.00	1.08	0.000	4.66	B2	Moderate Damage	9	4.70	1.36	Minor Damage
		12	16.45	0.80	0.61	0.000	2.51	B1	Superficial Damage	11	0.78	0.23	Minor Damage
	Axis 3-C	14	16.42	0.68	0.61	0.000	2.49	B1	Superficial Damage	13	0.24	0.07	Minor Damage
		16	14.58	0.73	0.54	0.000	2.23	B1	Superficial Damage	15	0.20	0.06	Minor Damage
		18	11.78	0.76	0.44	0.000	1.83	B1	Superficial Damage	18	0.13	0.04	Minor Damage
3	Axis 1-C	2	26.84	1.11	0.99	0.175	4.29	B3	Heavy Damage	1	2.06	0.59	Minor Damage
		4	19.50	0.98	0.72	0.000	3.07	B2	Moderate Damage	3	1.27	0.37	Minor Damage
		6	14.19	0.92	0.52	0.000	2.20	B2	Moderate Damage	5	0.29	0.08	Minor Damage
	Axis 2-C	7	61.47	1.66	2.27	0.243	9.47	B3	Heavy Damage	7	18.29	5.28	Severe Damage
		10	31.96	1.10	1.18	0.192	5.21	B3	Heavy Damage	9	8.47	2.45	Moderate Damage
		12	17.49	0.85	0.65	0.000	2.71	B1	Superficial Damage	11	1.31	0.38	Minor Damage
	Axis 3-C	14	26.84	1.11	0.99	0.175	4.29	B3	Heavy Damage	13	2.06	0.59	Minor Damage
		16	19.50	0.98	0.72	0.000	3.07	B2	Moderate Damage	15	1.27	0.37	Minor Damage
		18	14.19	0.92	0.52	0.000	2.20	B2	Moderate Damage	18	0.29	0.08	Minor Damage

Table 4-7: Flexural and shear response level and damage for the building columns (blast locations 4 to 6)

Blast location	Column	Flexure							Direct Shear			
		Point	Max. Displacement (mm)	Ductility ratio	Rotation (degree)	Damage Degree	Velocity (m/s)	Response level	Component Damage	Point	Max. Shear Slip (mm)	Average Shear Strain (%)	Component Damage
4	Axis 1-C	2	39.29	1.63	1.45	0.211	6.13	B3	Heavy Damage	1	5.74	1.66	Minor Damage
		4	32.01	1.60	1.18	0.193	4.93	B3	Heavy Damage	3	5.46	1.58	Minor Damage
		6	17.48	1.13	0.65	0.126	2.74	B3	Heavy Damage	5	1.33	0.38	Minor Damage
	Axis 2-C	7	22.43	0.61	0.83	0.000	3.50	B1	Superficial Damage	7	0.55	0.16	Minor Damage
		10	18.76	0.64	0.69	0.000	2.89	B1	Superficial Damage	9	0.60	0.17	Minor Damage
		12	14.50	0.71	0.54	0.000	2.21	B1	Superficial Damage	11	0.25	0.07	Minor Damage
	Axis 3-C	14	11.80	0.49	0.44	0.000	1.79	B1	Superficial Damage	13	0.09	0.03	Minor Damage
		16	21.73	1.09	0.80	0.152	2.69	B3	Heavy Damage	15	0.09	0.03	Minor Damage
		18	16.95	1.10	0.63	0.121	2.02	B3	Heavy Damage	18	0.08	0.02	Minor Damage
5	Axis 1-C	2	32.73	1.35	1.21	0.195	5.24	B3	Heavy Damage	1	3.66	1.06	Minor Damage
		4	26.76	1.34	0.99	0.175	4.23	B3	Heavy Damage	3	3.62	1.05	Minor Damage
		6	16.40	1.06	0.61	0.118	2.54	B3	Heavy Damage	5	0.81	0.23	Minor Damage
	Axis 2-C	7	32.42	0.88	1.20	0.000	5.25	B1	Superficial Damage	7	2.85	0.82	Minor Damage
		10	26.68	0.92	0.99	0.000	4.24	B2	Moderate Damage	9	3.02	0.87	Minor Damage
		12	16.63	0.81	0.61	0.000	2.55	B1	Superficial Damage	11	0.71	0.20	Minor Damage
	Axis 3-C	14	15.36	0.64	0.57	0.000	2.33	B1	Superficial Damage	13	0.17	0.05	Minor Damage
		16	14.24	0.71	0.53	0.000	2.18	B1	Superficial Damage	15	0.17	0.05	Minor Damage
		18	11.86	0.77	0.44	0.000	1.84	B1	Superficial Damage	18	0.13	0.04	Minor Damage
6	Axis 1-C	2	22.10	0.91	0.82	0.000	3.49	B2	Moderate Damage	1	0.77	0.22	Minor Damage
		4	18.48	0.93	0.68	0.000	2.89	B2	Moderate Damage	3	0.76	0.22	Minor Damage
		6	14.30	0.93	0.53	0.000	2.21	B2	Moderate Damage	5	0.27	0.08	Minor Damage
	Axis 2-C	7	37.25	1.01	1.38	0.206	6.14	B3	Heavy Damage	7	4.64	1.34	Minor Damage
		10	30.69	1.05	1.13	0.189	4.93	B3	Heavy Damage	9	4.68	1.35	Minor Damage
		12	17.73	0.87	0.66	0.000	2.75	B1	Superficial Damage	11	1.17	0.34	Minor Damage
	Axis 3-C	14	22.10	0.91	0.82	0.000	3.49	B2	Moderate Damage	13	0.77	0.22	Minor Damage
		16	18.48	0.93	0.68	0.000	2.89	B2	Moderate Damage	15	0.76	0.22	Minor Damage
		18	14.30	0.93	0.53	0.000	2.21	B2	Moderate Damage	18	0.27	0.08	Minor Damage

Table 4-8: Flexural and shear response level and damage for the building columns (blast locations 7 to 9)

Blast location		Flexure							Direct Shear			
	Column	Point	Max. Displacement (mm)	Ductility ratio	Rotation (degree)	Damage Degree	Velocity (m/s)	Response level	Component Damage	Point	Max. Shear Slip (mm)	Average Shear Strain (%)	Component Damage
7	Axis 1-C	2	28.89	1.20	1.07	0.183	4.65	B3	Heavy Damage	2	2.19	0.63	Minor Damage
		4	22.59	1.13	0.83	0.157	3.60	B3	Heavy Damage	4	2.11	0.61	Minor Damage
		6	15.51	1.01	0.57	0.110	2.40	B3	Heavy Damage	6	0.50	0.15	Minor Damage
	Axis 2-C	7	18.32	0.49	0.68	0.000	2.80	B1	Superficial Damage	7	0.25	0.07	Minor Damage
		10	16.39	0.56	0.61	0.000	2.47	B1	Superficial Damage	10	0.27	0.08	Minor Damage
		12	13.41	0.66	0.50	0.000	2.05	B1	Superficial Damage	12	0.17	0.05	Minor Damage
	Axis 3-C	14	21.47	0.89	0.79	0.000	3.26	B1	Superficial Damage	14	0.08	0.02	Minor Damage
		16	19.44	0.97	0.72	0.000	2.61	B2	Moderate Damage	16	0.09	0.03	Minor Damage
		18	15.45	1.00	0.57	0.000	1.93	B2	Moderate Damage	18	0.07	0.02	Minor Damage
8	Axis 1-C	2	24.99	1.03	0.92	0.167	3.98	B3	Heavy Damage	1	1.25	0.36	Minor Damage
		4	20.11	1.01	0.74	0.143	3.17	B3	Heavy Damage	3	1.21	0.35	Minor Damage
		6	14.83	0.96	0.55	0.000	2.30	B2	Moderate Damage	5	0.35	0.10	Minor Damage
	Axis 2-C	7	25.36	0.69	0.94	0.000	3.98	B1	Superficial Damage	7	0.90	0.26	Minor Damage
		10	20.41	0.70	0.75	0.000	3.18	B1	Superficial Damage	9	0.96	0.28	Minor Damage
		12	15.04	0.73	0.56	0.000	2.30	B1	Superficial Damage	11	0.31	0.09	Minor Damage
	Axis 3-C	14	14.14	0.59	0.52	0.000	2.14	B1	Superficial Damage	13	0.13	0.04	Minor Damage
		16	13.17	0.66	0.49	0.000	2.01	B1	Superficial Damage	15	0.13	0.04	Minor Damage
		18	22.43	1.46	0.83	0.000	2.65	B3	Heavy Damage	18	0.11	0.03	Minor Damage
9	Axis 1-C	2	18.05	0.75	0.67	0.000	2.79	B1	Superficial Damage	1	0.33	0.09	Minor Damage
		4	16.14	0.81	0.60	0.000	2.47	B1	Superficial Damage	3	0.33	0.10	Minor Damage
		6	13.21	0.86	0.49	0.000	2.05	B1	Superficial Damage	5	0.18	0.05	Minor Damage
	Axis 2-C	7	29.31	0.79	1.08	0.000	4.65	B1	Superficial Damage	7	1.63	0.47	Minor Damage
		10	22.93	0.79	0.85	0.000	3.61	B1	Superficial Damage	9	1.70	0.49	Minor Damage
		12	15.72	0.77	0.58	0.000	2.40	B1	Superficial Damage	11	0.44	0.13	Minor Damage
	Axis 3-C	14	18.05	0.75	0.67	0.000	2.79	B1	Superficial Damage	13	0.33	0.09	Minor Damage
		16	16.14	0.81	0.60	0.000	2.47	B1	Superficial Damage	15	0.33	0.10	Minor Damage
		18	13.21	0.86	0.49	0.000	2.05	B1	Superficial Damage	18	0.18	0.05	Minor Damage

Table 4-9: Flexural and shear response level and damage for the building columns (blast locations 10 to 12)

Blast location		Flexure							Direct Shear		
	Column	Point	Max. Displacement (mm)	Ductility ratio	Rotation (degree)	Damage Degree	Velocity (m/s)	Response level	Component Damage	Point	Max. Shear Slip (mm)	Average Shear Strain (%)	Component Damage
10	Axis 1-C	2	20.48	0.85	0.76	0.000	3.21	B1	Superficial Damage	1	0.56	0.16	Minor Damage
		4	17.57	0.88	0.65	0.000	2.73	B1	Superficial Damage	3	0.56	0.16	Minor Damage
		6	13.93	0.90	0.51	0.000	2.16	B1	Superficial Damage	5	0.23	0.07	Minor Damage
		7	15.82	0.43	0.58	0.000	2.36	B1	Superficial Damage	7	0.15	0.04	Minor Damage
	Axis 2-C	10	14.65	0.50	0.54	0.000	2.20	B1	Superficial Damage	9	0.16	0.05	Minor Damage
		12	12.19	0.60	0.45	0.000	1.86	B1	Superficial Damage	11	0.13	0.04	Minor Damage
		14	18.76	0.78	0.69	0.000	3.22	B1	Superficial Damage	13	0.07	0.02	Minor Damage
	Axis 3-C	16	17.14	0.86	0.63	0.000	2.57	B1	Superficial Damage	15	0.07	0.02	Minor Damage
		18	13.93	0.90	0.51	0.000	1.96	B1	Superficial Damage	18	0.06	0.02	Minor Damage
11	Axis 1-C	2	18.65	0.77	0.69	0.000	2.90	B1	Superficial Damage	1	0.37	0.11	Minor Damage
		4	16.51	0.83	0.61	0.000	2.53	B1	Superficial Damage	3	0.38	0.11	Minor Damage
		6	13.42	0.87	0.50	0.000	2.08	B1	Superficial Damage	5	0.19	0.05	Minor Damage
		7	18.93	0.51	0.70	0.000	2.90	B1	Superficial Damage	7	0.28	0.08	Minor Damage
	Axis 2-C	10	16.76	0.58	0.62	0.000	2.54	B1	Superficial Damage	9	0.31	0.09	Minor Damage
		12	13.61	0.66	0.50	0.000	2.08	B1	Superficial Damage	11	0.18	0.05	Minor Damage
		14	12.85	0.53	0.47	0.000	1.95	B1	Superficial Damage	13	0.11	0.03	Minor Damage
	Axis 3-C	16	11.98	0.60	0.44	0.000	1.83	B1	Superficial Damage	15	0.11	0.03	Minor Damage
		18	19.00	1.23	0.70	0.136	2.29	B3	Heavy Damage	18	0.10	0.03	Minor Damage
12	Axis 1-C	2	15.59	0.65	0.58	0.000	2.36	B1	Superficial Damage	1	0.18	0.05	Minor Damage
		4	14.42	0.72	0.53	0.000	2.20	B1	Superficial Damage	3	0.18	0.05	Minor Damage
		6	12.01	0.78	0.44	0.000	1.86	B1	Superficial Damage	5	0.13	0.04	Minor Damage
		7	20.78	0.56	0.77	0.000	3.22	B1	Superficial Damage	7	0.41	0.12	Minor Damage
	Axis 2-C	10	17.84	0.61	0.66	0.000	2.73	B1	Superficial Damage	9	0.45	0.13	Minor Damage
		12	14.13	0.69	0.52	0.000	2.16	B1	Superficial Damage	11	0.21	0.06	Minor Damage
		14	15.59	0.65	0.58	0.000	2.36	B1	Superficial Damage	13	0.18	0.05	Minor Damage
	Axis 3-C	16	14.42	0.72	0.53	0.000	2.20	B1	Superficial Damage	15	0.18	0.05	Minor Damage
		18	12.01	0.78	0.44	0.000	1.86	B1	Superficial Damage	18	0.13	0.04	Minor Damage

CHAPTER 5 FINITE ELEMENT ANALYSIS WITH LS-DYNA

The finite element analysis is conducted using LS-Dyna of Livermore Software Technology (LST) software. LS-DYNA is a powerful and versatile software used for explicit finite element analysis (FEA) and simulations involving complex physics. It shines in the field of blast analysis, allowing engineers and researchers to predict the behavior of structures and materials under the influence of explosive loads.

LS-DYNA offers several unique features for blast analysis:

- **Multiple blast loading methods**: It provides various options for defining the blast load, including empirical models, particle blast methods, and 3D Arbitrary Lagrangian-Eulerian (ALE) formulations. This allows for accurate representation of different blast scenarios, from simple explosions to complex interactions with surrounding structures.

- **Material modeling capabilities**: LS-DYNA boasts a wide range of material models that can capture the non-linear and dynamic behavior of materials subjected to blast loading. This includes materials like concrete, steel, and explosives themselves, allowing for realistic simulations of real-world structures and their response to explosive events.

These features, combined with its robust capabilities in handling non-linearity, large deformations, and fluid-structure interaction, make LS-DYNA a valuable tool for engineers and researchers in fields ranging from civil and defense applications to mining and automotive safety.

5.1 Blast loading

There are basically three methods in LS-Dyna to account blast loading on structures: Load_Blast_Enhanced, Arbitrary Lagrangian-Eulerian (ALE) and direct pressure-time history. Load_Blast_Enhanced uses empirical equations (based on the work of Kingery-Bulmash) to solve for the blast pressure and applies directly to faces defined. It defines a function to calculate the pressure generated by an air blast from a conventional explosive detonation [45]. The function is based on the model presented by Randers-Pehrson and

Bannister in their 1997 report. Arbitrary Lagrangian-Eulerian is a Computational Fluid Dynamics (CFD) method, where both the explosive and the surrounding air are modeled in detail resulting in relatively accurate result. The pressure wave generated by the explosion travels through the air (represented by the ALE domain) and interacts with the structure (represented by the Lagrangian structure) through a process called Fluid-Structure Interaction (FSI) [46]. This method however has large drawback, significant computational cost. The last method is the pressure-time history, in this case the pressure at each instant time is initially calculated by the user and applied directly to the defined faces of the structure.

In this research Load_Blast_Enhanced is considered on account of simplicity and proven analysis method that provides a more practical solution for resource-limited scenarios, compared to the ALE method and experimental data.

5.2 Material modeling

5.2.1 Concrete Material Model

Two widely used methods for modeling concrete are Mat_Concrete_Damage_REL3 and MAT_CSCM. The former model type is based on Karagozian and Case (K&C) concrete model. It is a three-invariant model, has three shear failure surfaces, includes damage and strain-rate effects [47]. This model has the ability for parameter generation based on solely the unconfined compression strength. The latter model type MAT_CSCM (Continuous Surface Cap Model) has a continuous and smooth intersection formulation between the failure surface and hardening cap [48]. The following features are included in this model; isotropic constitutive equations, three stress invariant yield surface with translations for pre-peak hardening, a hardening cap that expands and contracts, damage-based softening with erosion and modulus reduction and rate effects for increasing in high-strain rate applications.

The best suited for blast analysis (capturing both the flexural and direct shear failure) is the concrete constitutive model Mat_Concrete_Damage_REL3. This is mainly because the K&C Concrete Model's default settings are based on a specific type of concrete that has been extensively tested. In which the testing involved applying various forces (uniaxial, biaxial, and triaxial) in both pulling (tension) and pushing (compression)

directions, and measuring the material's response under different strain conditions (isotropic and uniaxial) [49]. Additionally, the model incorporates well-established relationships between the concrete's tensile and compressive properties, like how tensile strength is related to compressive strength. The solid element is modelled as a single 8-noded element (cube unit) using one-point integration.

In order to account failure of concrete, an erosion method is applied to eliminate certain elements of the concrete material after failure (based on strain). The failure criteria considered are principal strain and shear strain, when the plastic strain exceeds 15% and/or the shear strain exceeds 90%, the concrete element is eroded. This value is concluded based on the experimental data from Zhang et al. [32], Farouk [9], work done by Shi et al. [11] and Warakorn et al [50]. It's important to note that the erosion technique is a numerical tool, not based on fundamental physical principles, to address the issue of excessive mesh distortion in simulations [11], nevertheless, it can represent various physical phenomena leading to material loss or discontinuity, such as erosion, shear, cratering, spalling, and fracture. While strain-based erosion criteria are basic, they offer a clearer connection to the physical damage observed in concrete under explosive and high-impact forces [51].

5.2.2 Rebar Material Model

Similar to the concrete models, there are two models typically suited for reinforced concrete (RC) structural members; MAT_PIECEWISE_LINEAR_PLASTICITY and MAT_PLASTIC_KINEMATIC. MAT_PIECEWISE_LINEAR_PLASTICITY exhibits both elastic and plastic behavior. Its stress response depends not only on the amount of deformation (strain) but also on the rate at which that deformation occurs (strain rate). Both the stress-strain relationship and the strain rate dependency can be described by arbitrary functions [47]. MAT_PLASTIC_KINEMATIC model is versatile and can account for both isotropic and kinematic hardening, as well as the influence of deformation speed (rate effects) if needed [47]. It's practically efficient and can be used with various element types, including beams, shells, and solids.

MAT_PIECEWISE_LINEAR_PLASTICITY is selected as the beam element of the structural element in lieu of MAT_PLASTIC_KINEMATIC because it enables to define arbitrary stress-strain curve.

A paramount concept in modelling both rebar and concrete as independent elements is to consider the bond. There are basically two approaches to this problem; mesh the rebar and the concrete at the same node (unrealistic) or provide constraints between the nodes of the rebar and concrete. The latter approach can be performed in two basic ways; CONSTRAINED_BEAM_IN_SOLID or CONSTRAINED_LAGRANGE_IN_SOLID. Both cases resulted in similar outcomes but depends on the concrete model. As the concrete model considered is Mat_Concrete_Damage_REL3, the constraint utilized is CONSTRAINED_LAGRANGE_IN_SOLID.

5.3 Finite Element Analysis Validation

Similar to verification of the SDOF method, the finite element analysis is compared with the experimental results. In addition to the response of the structure to blast loading, the erosion technique is also substantiated. For Zhang et al. [32] B2-4 is selected to showcase both the response and scabbing of concrete cover. The displacement-history is shown in figure 5-1. The maximum displacement of the experiment is 40mm whereas the maximum displacement according to LS-Dyna is 44.1mm and 41.43mm in SDOF. Consequently, the errors are 10.25% and 6.05% compared to the experiment and SDOF analysis, respectively.

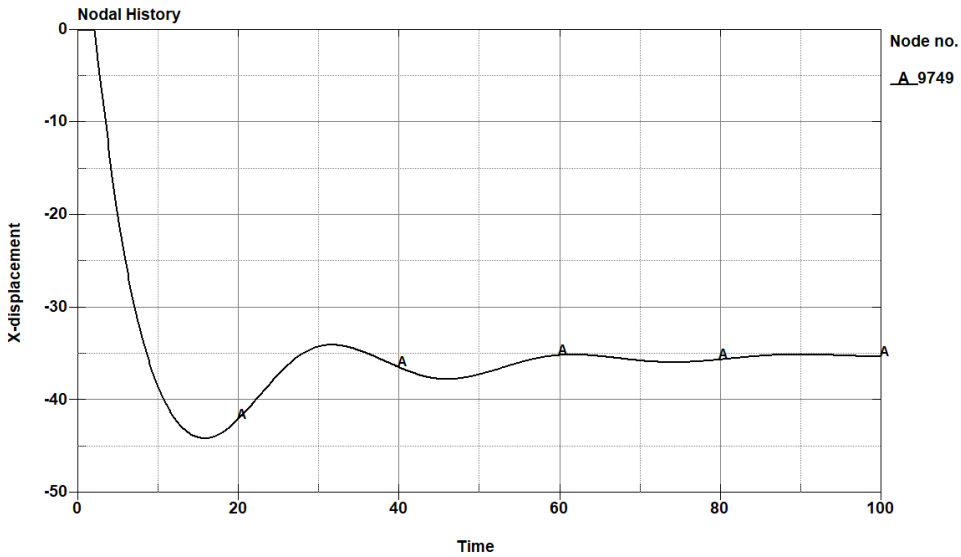

Figure 5-1: Displacement history of Zhang et al. experiment in LS-Dyna

The faces of beam B2-4 after the end of the loading are shown in figures 5-2 and 5-3. These figures show that the erosion method and the value of the principal strain

considered is justified. Similarly, LS-Dyan output of Farouk's experiment [9] and the actual results are nearly similar as shown in figure 5-6. Zhang et al. [32] experiment showed a flexure prevailing failure mode and Farouk's showed shear failure mode.

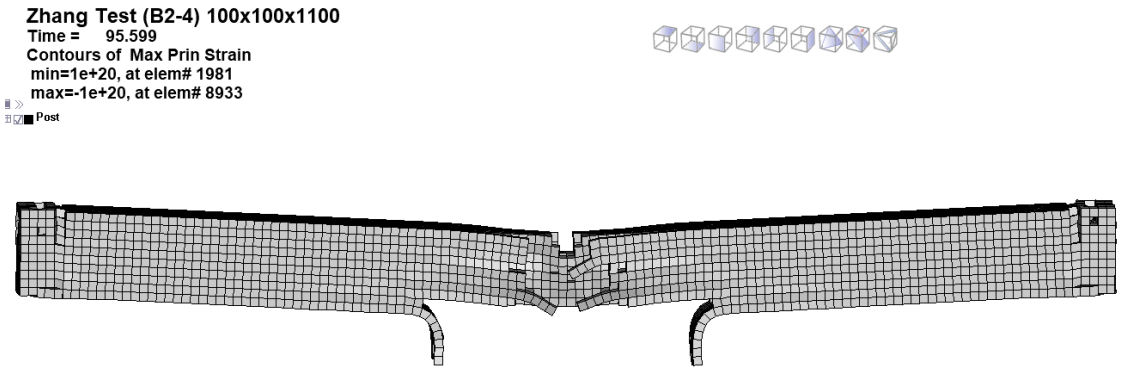

Figure 5-2: Side Face deflection of beam B2-4 in LS-Dyna

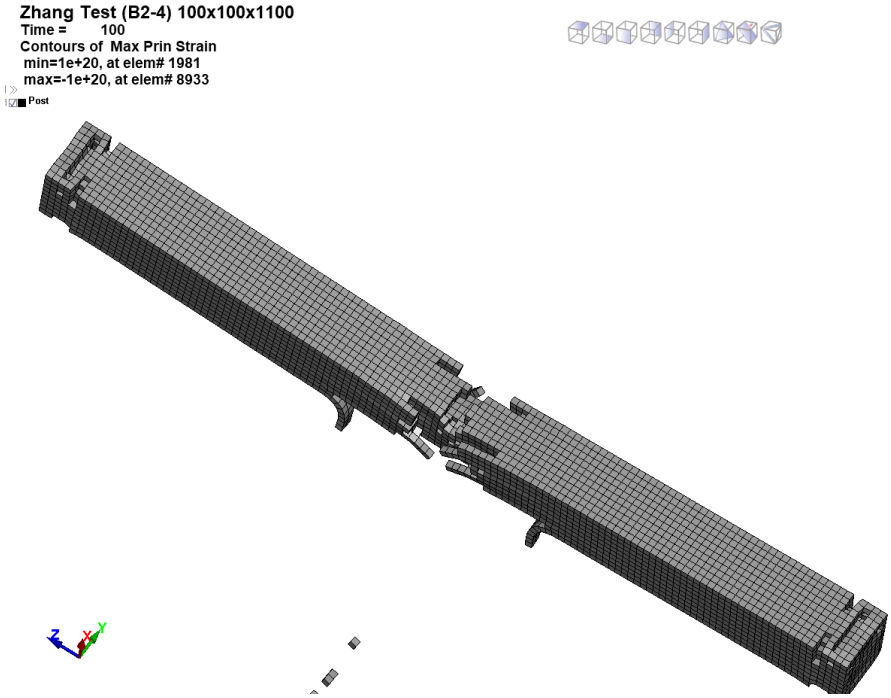

Figure 5-3: Isometric view deflection of beam B2-4 in LS-Dyna

The combination of FEA and the erosion method effectively predicted the damage observed in the experiments. As shown in Figures 5-2 and 5-3, this approach successfully captured both concrete scabbing and residual beam deflection. Similarly, Figure 5-6 demonstrates the ability to predict the shear failure mode and crack pattern. These results strongly suggest that FEA, when coupled with an appropriate damage model (like the erosion method in this case), is a valuable tool for predicting the response and damage of structural members subjected to blast loading.

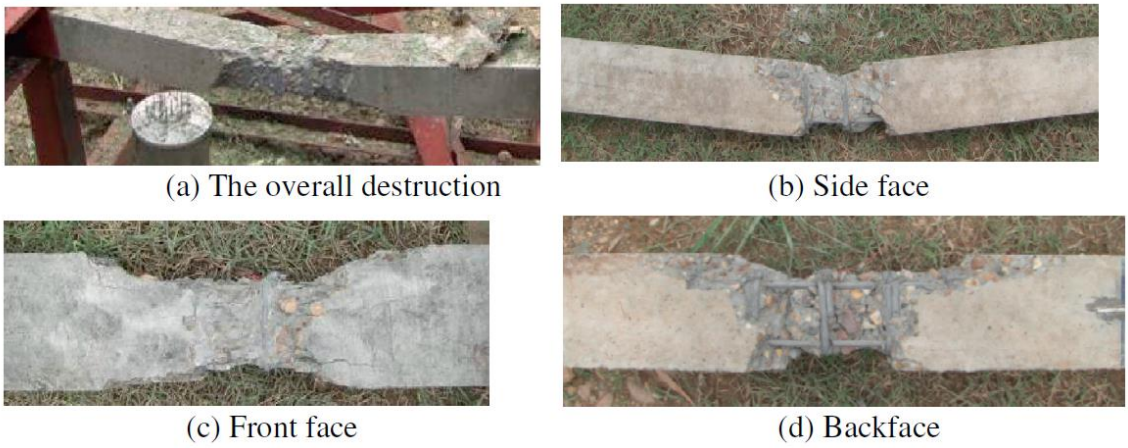

Figure 5-4: Test result destruction of beam B2-4 [32]

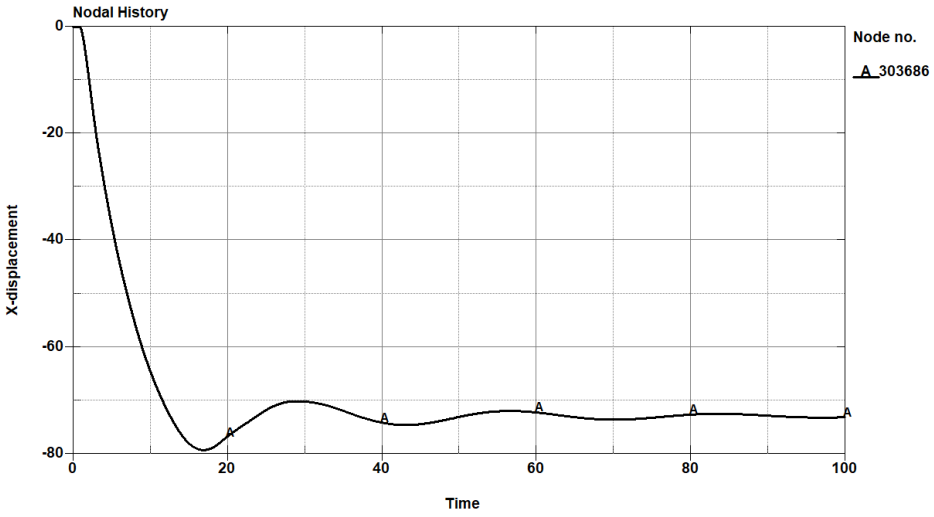

Figure 5-5: Displacement history of Farouk's experiment in LS-Dyna

Before proceeding to progressive collapse analysis, response of the structural element of this building is compared between the SDOF and LS-Dyna analysis. 1st story column on axis C-1 is selected at two blast locations; 1 and 4. At blast location 1, the column fails under direct shear in both results. Hence, the column will be removed from progressive collapse analysis. Whereas, at blast location 4, the maximum deflection according to SDOF analysis (without axial load) is 51.51mm and 49.60mm as per LS-Dyna, in both cases the concrete neither failed in flexure nor shear (see table 4-7 and figure 5-8). Similarly, the displacement is shown in figure 5-11. Even though at blast location 1, the column has failed, the displacement history is shown in figure 5-10 and the corresponding displacement in figure 5-12.

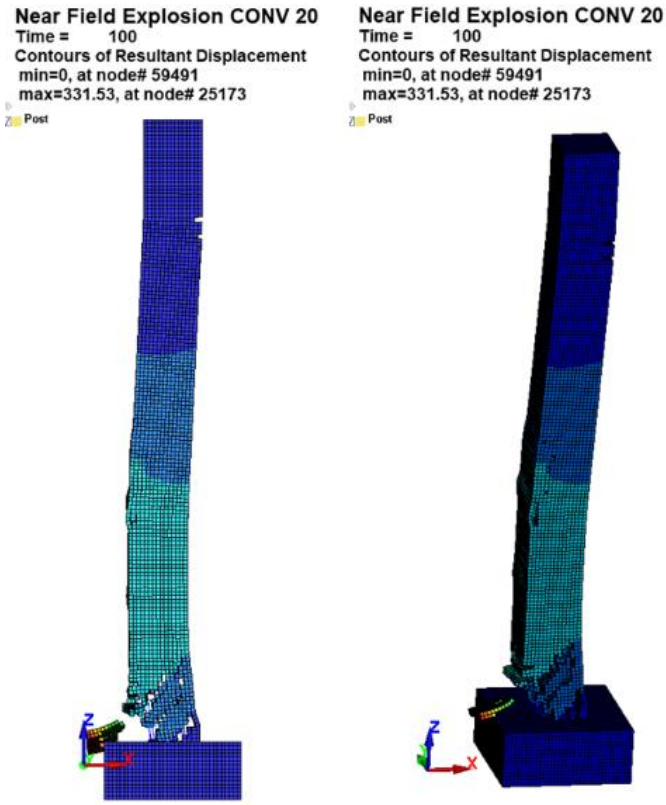

Figure 5-6: Side face and isometric view deflection of Farouk's column in LS-Dyna

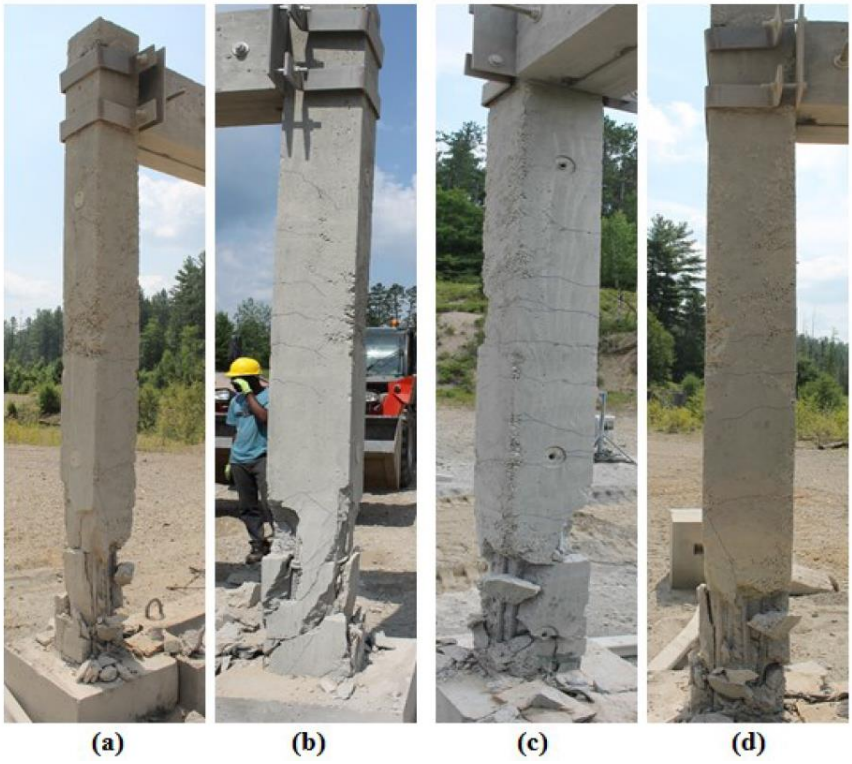

Figure 5-7: Farouk's Column (Conv20): (a) Front face, (b) Side face (right), (c) Back face and (d) Side face (left) [9]

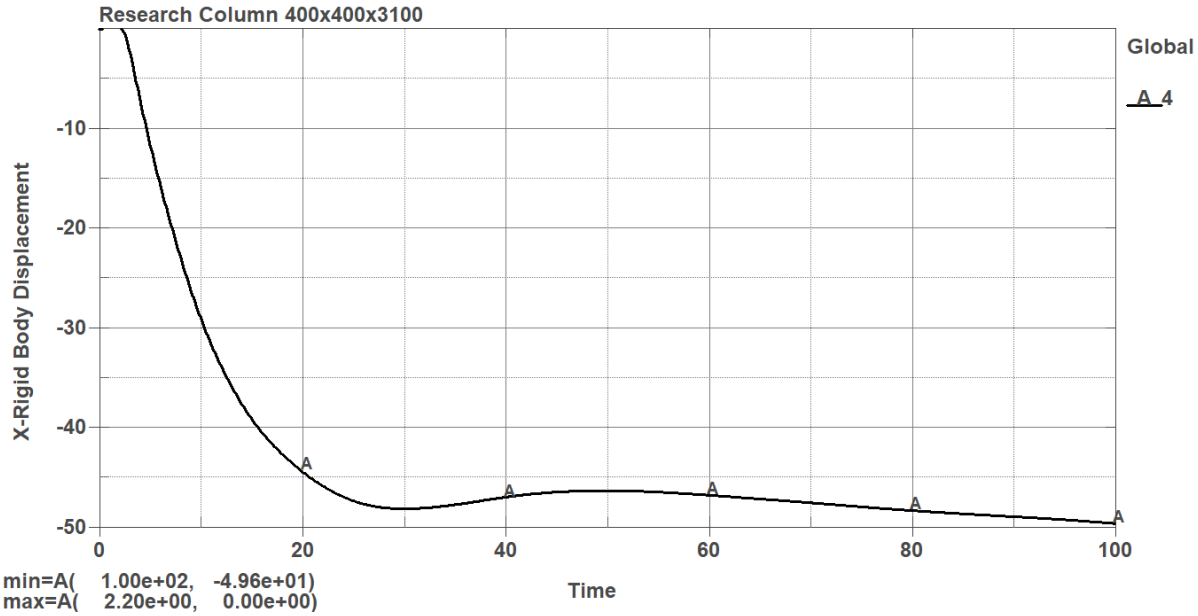

Figure 5-8: Displacement history of 1st story column on axis 1-C under blast location 4 as per LS-Dyna

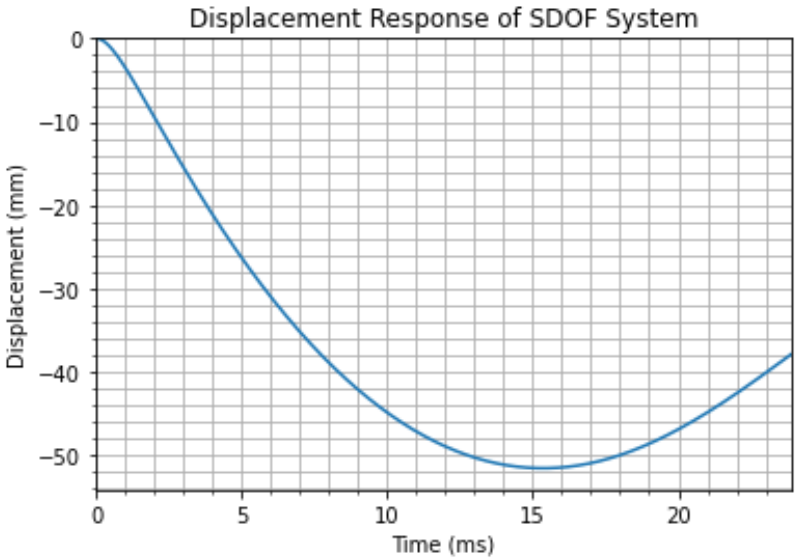

Figure 5-9: Displacement history of 1st story column on axis 1-C under blast location 4 as per SDOF

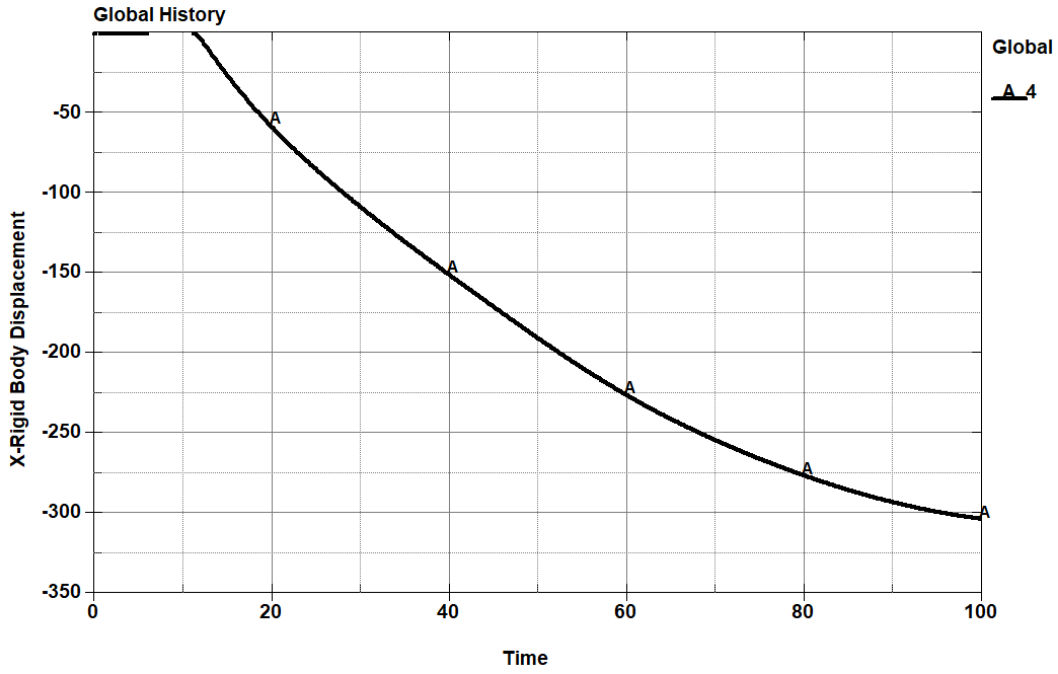

Figure 5-10: Displacement history of 1st story column on axis 1-C under blast location 1 as per LS-Dyna

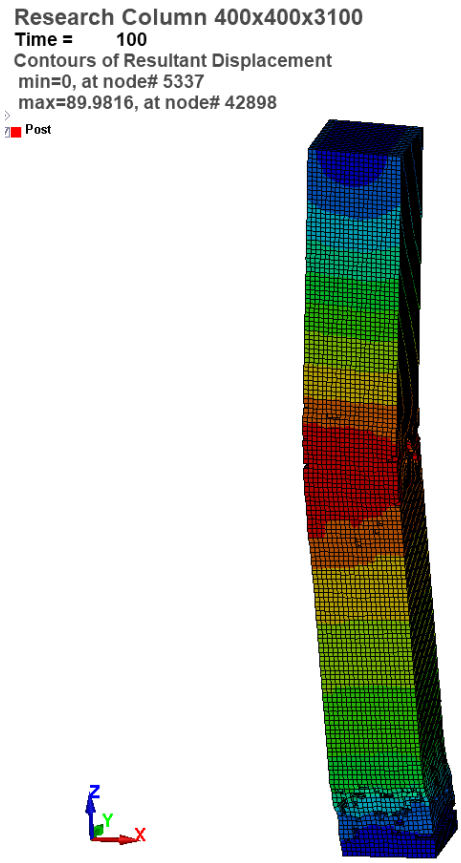

Figure 5-11: Lateral displacement of 1st story column on axis 1-C under blast location 4 as per LS-Dyna

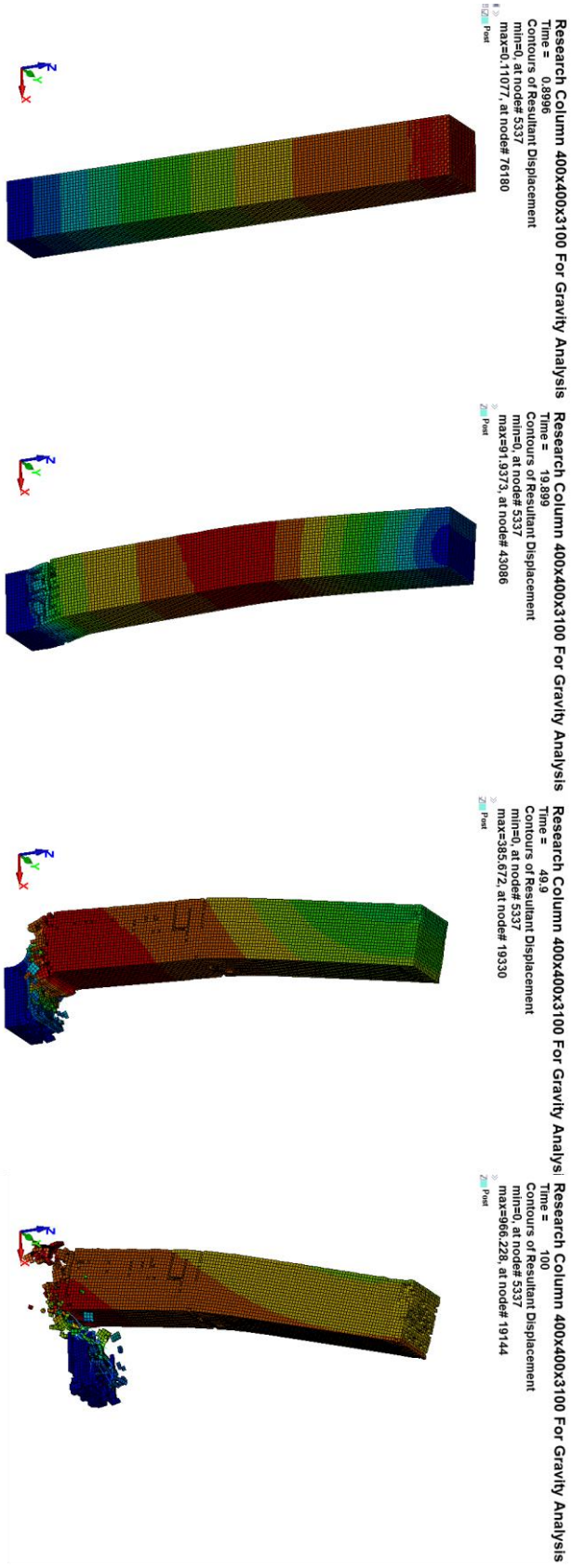

Figure 5-12: Lateral displacement of 1st story column on axis 1-C under blast location 1 as per LS-Dyna

CHAPTER 6 PROGRESSIVE COLLAPSE ANALYSIS

Progressive collapse manifests when the failure of a single structural element triggers the failure of adjacent elements, propagating through the entire structure and potentially causing partial or complete collapse. Utilized as a design aid, progressive collapse analysis evaluates the likelihood of such a scenario transpiring. A collapse analysis serves primarily as a design aid. Its aim isn't to offer a precise replica of structural collapse but rather to furnish designers with valuable insights for evaluating the structure's performance and making informed safety-related decisions [52].

When a structural element undergoes yielding, the focus shifts from the forces within the member to its deformations. The most sensible design strategy involves assessing deformation demands and capacities, and consequently, the ratios of deformation demand to capacity. Achieving this necessitates nonlinear analysis. In this paper a two-stage progressive collapse analysis is taken into account: removing the critically damaged columns accounting the initial velocity and damage of the non-critical columns (see section 4.5) and finally checking the collapse potential of the building under sustained gravity loading. This method differs from the APM method as it accounts the non-zero condition of the neighboring columns.

Three analyses are carried out for each blast location; APM method, APM plus initial condition and blast-structure interaction. Based on these three methods the potential for collapse is assessed. The measuring parameters are; vertical displacement, transverse displacement and vertical velocity. Vertical displacement dictates the displacement history under gravity loading, lateral displacement shows the transverse displacement parallel to blast location and finally, the vertical velocity indicates the rate of collapse. The velocity for second method is obtained from the SDOF analysis and applied as an initial condition in LS-DYNA.

6.1 Verification of initial condition

The initial condition (velocity) for the non-critical columns obtained from SDOF analysis is assigned as preload for progressive collapse analysis using the keyword INITIAL_VELOCITY_NODE. This is checked by applying initial velocity and damage

as input in LS-DYNA and the response is verified with Load_Blast_Enhanced (figures 6-1 to 6-4) for 1st story column on axis 1 and 2 under blast location 1 and 6, respectively.

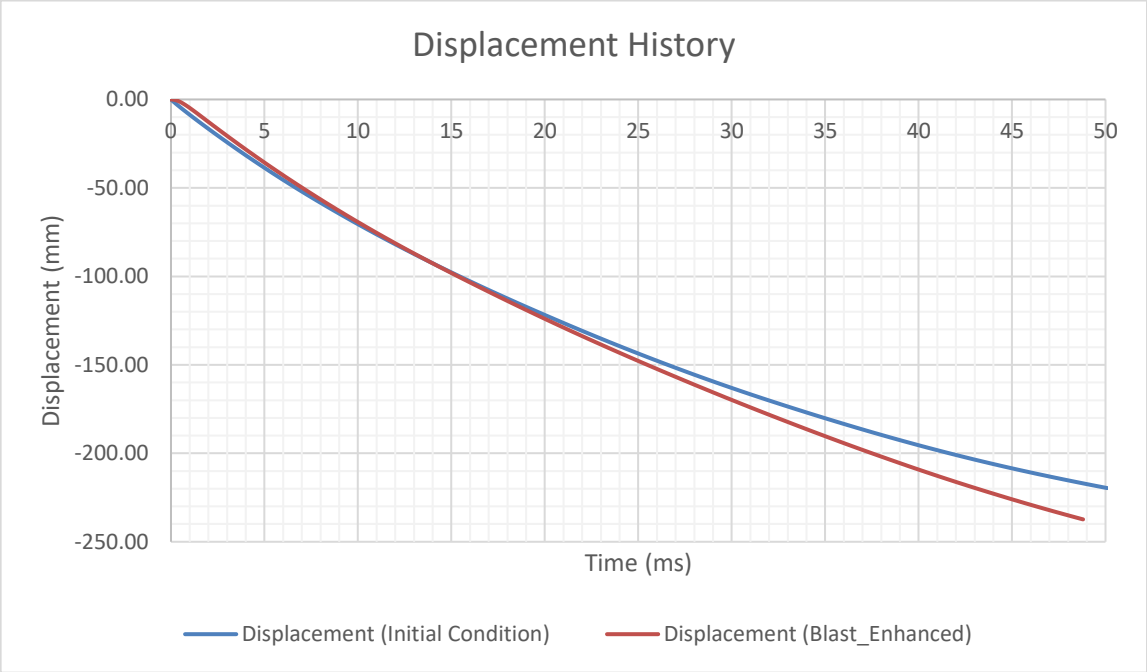

Figure 6-1: Displacement history based on Initial_Velocity and Blast_Enhanced under blast location 1

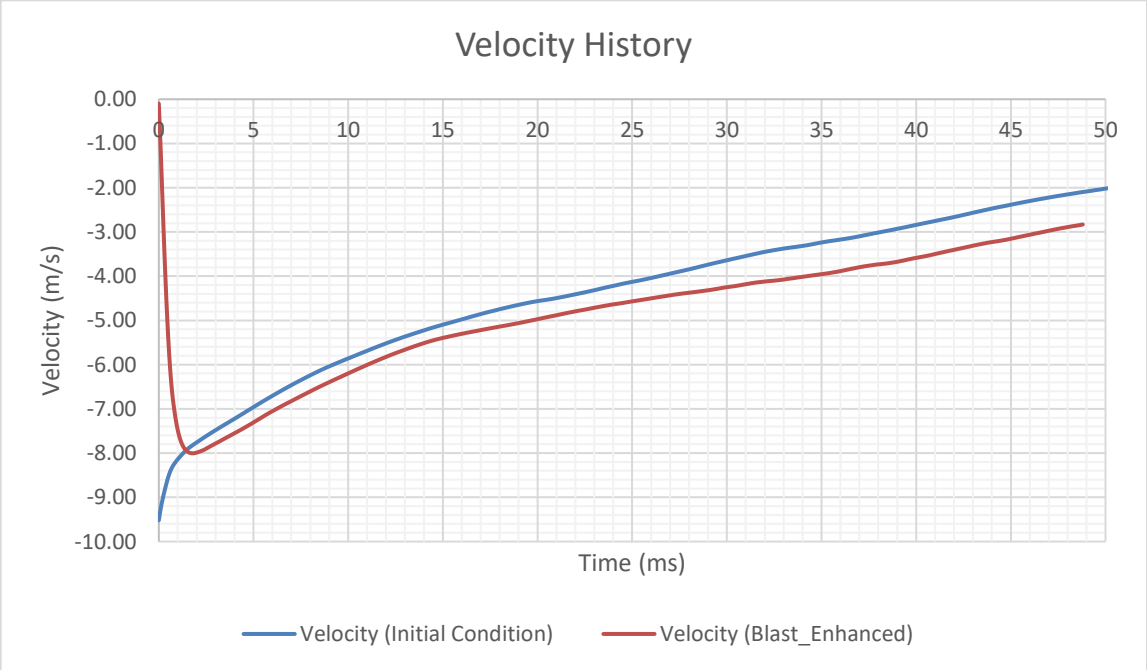

Figure 6-2: Velocity history based on Initial_Velocity and Blast_Enhanced under blast location 1

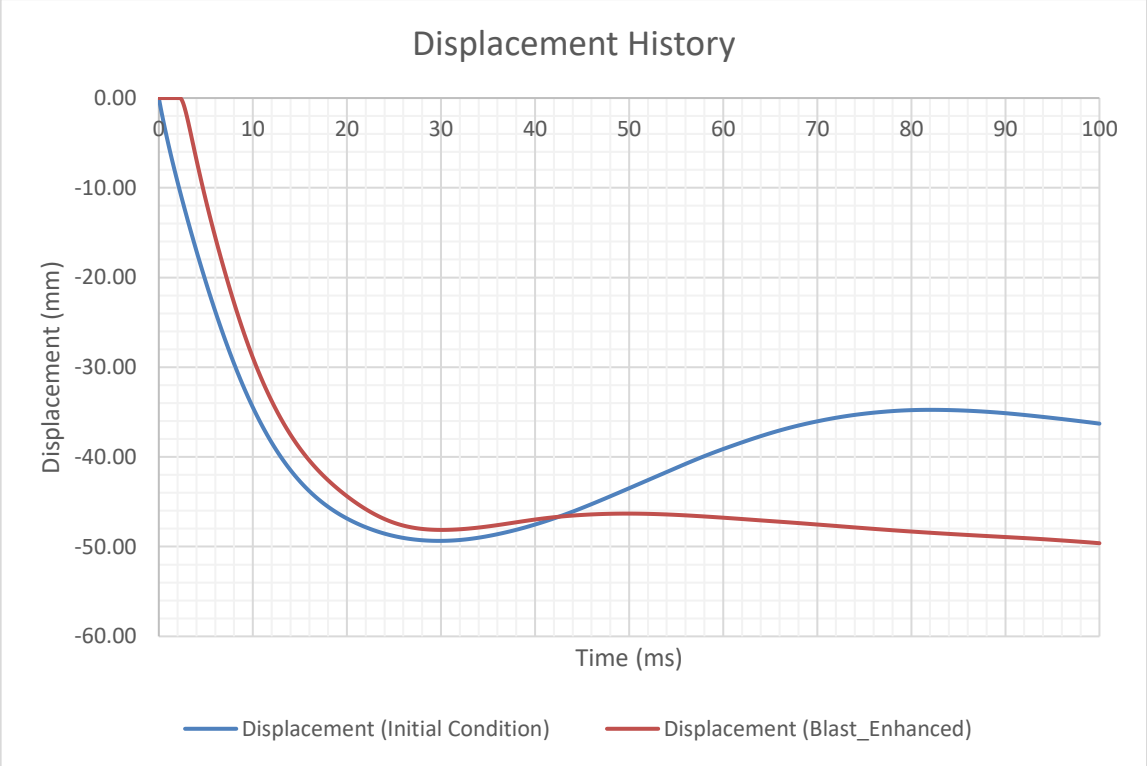

Figure 6-3: Displacement history based on Initial_Velocity and Blast_Enhanced under blast location 6

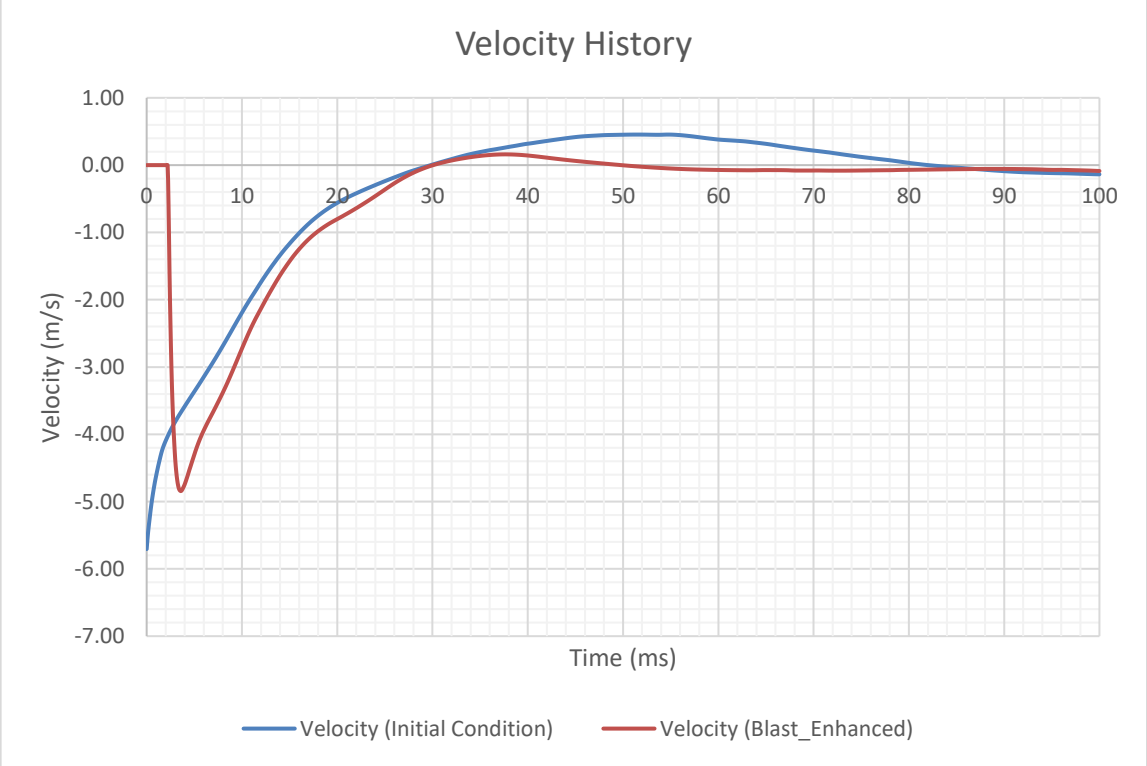

Figure 6-4: Velocity history based on Initial_Velocity and Blast_Enhanced under blast location 6

6.2 Participation of vertical elements

For the APM and APM with non-zero initial condition, the number of columns removed is obtained prior to collapse analysis based on the level of protection (response limit) discussed in section 4.5 (tables 4-6 to 4-9). Subsequently, columns designated as "Hazardous" in flexure are removed from participating in bearing gravity load. Similarly, columns designated as "Severe Damage" in shear are also removed from collapse analysis. 1st story column on axis 1 and 2 are removed from participating in collapse analysis under blast location 1 and 3, respectively. The remaining columns on axis 1 are then subjected to the non-zero initial condition based on the blast location.

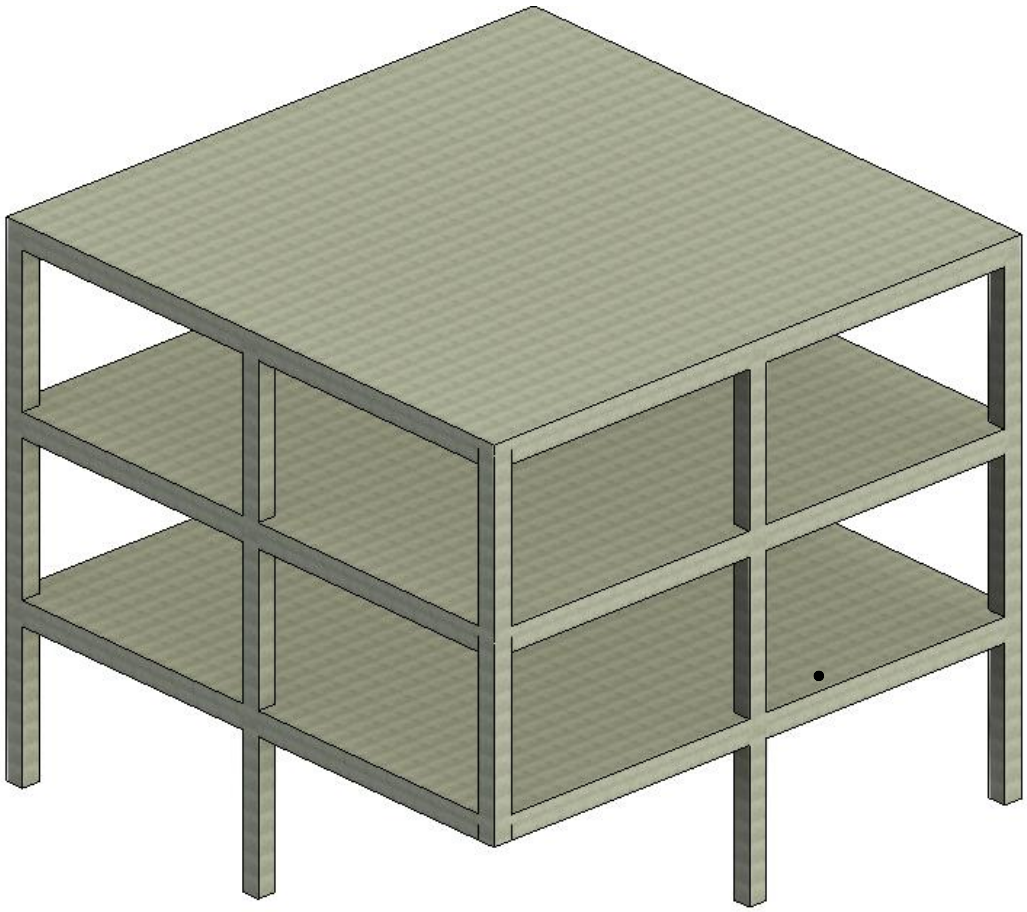

Figure 6-5: Structural framing for collapse analysis under blast location 1

For the remaining blast locations, none of the columns have failed based on the response level and hence all the vertical elements are considered for collapse analysis.

However, initial damage and velocity are considered for all blast locations based on tables 4-6 to 4-9.

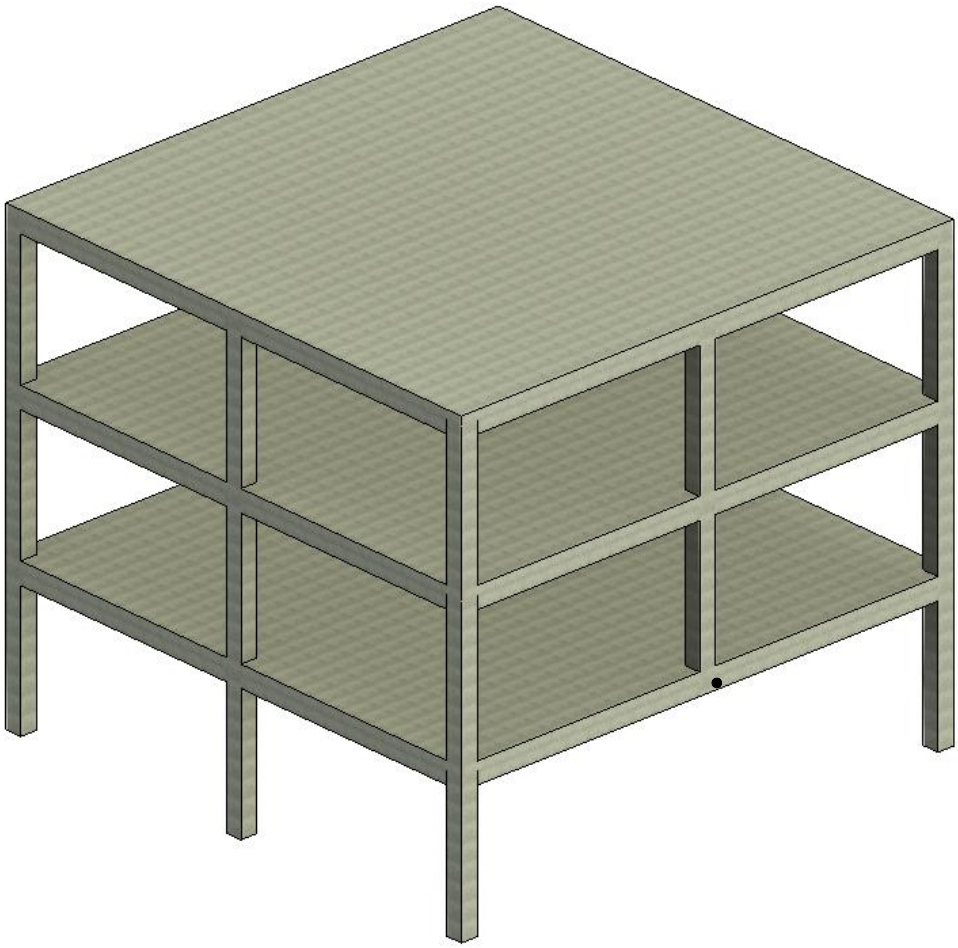

Figure 6-6: Structural framing for collapse analysis under blast location 3

Based on the three method of analysis, progressive collapse is compared. This entails whether total collapse or partial collapse occurs and the output (vertical displacement, transverse (Y-direction) displacement and vertical velocity) is compared. For the outputs the nodal location for computing the displacement and velocity is on axis C-2 at 1st story level (shown by the black dot in figures 6-5 and 6-6).

Under blast location 1, according to Blast_Enhanced method, the progressive collapse begins by direct shear failure of 1st story column on axis 1, followed by plastic hinge formation at the ends of first story beams on axis C (1-2), accompanied by failure of column on axis 2 and finally formation of plastic hinges at the ends of first story beams on axis C (2-3) and pullout of this beam from axis B. Based on this method, partial collapse is observed between axis B-C and 1-3.

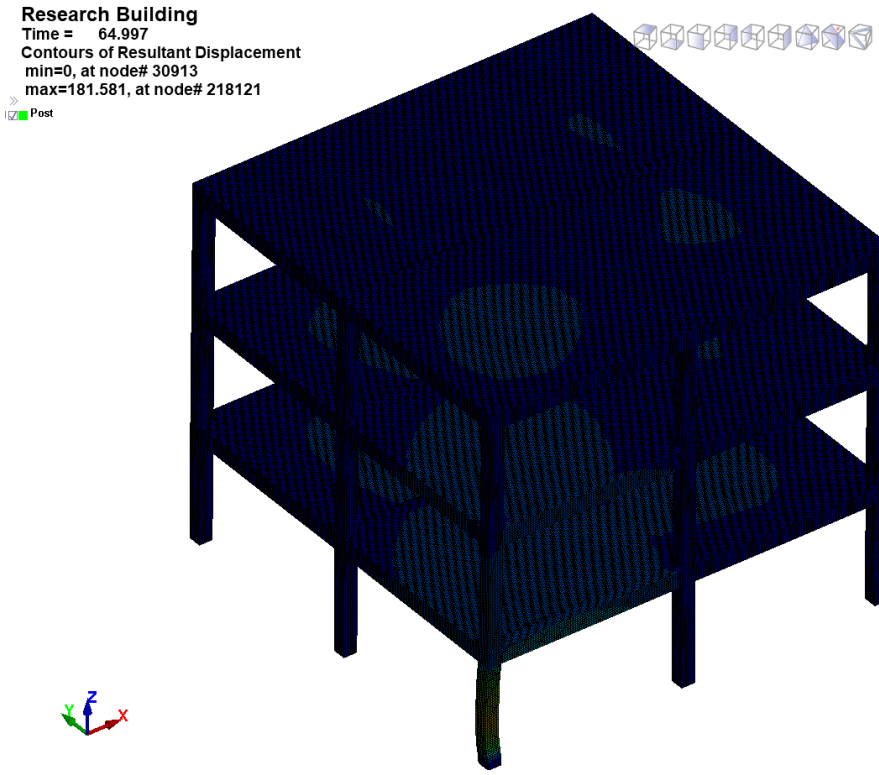

Figure 6-7: Blast_Enhanced method of analysis after blast propagates (blast location 1)

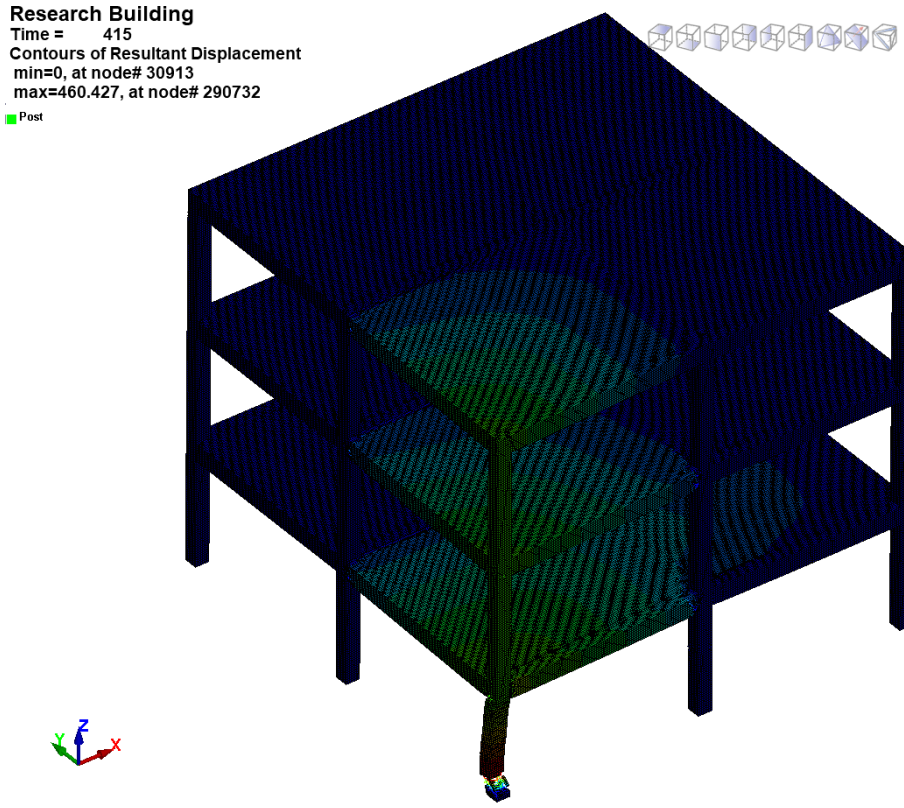

Figure 6-8: Blast_Enhanced method of analysis at column failure on axis C-1 (blast location 1)

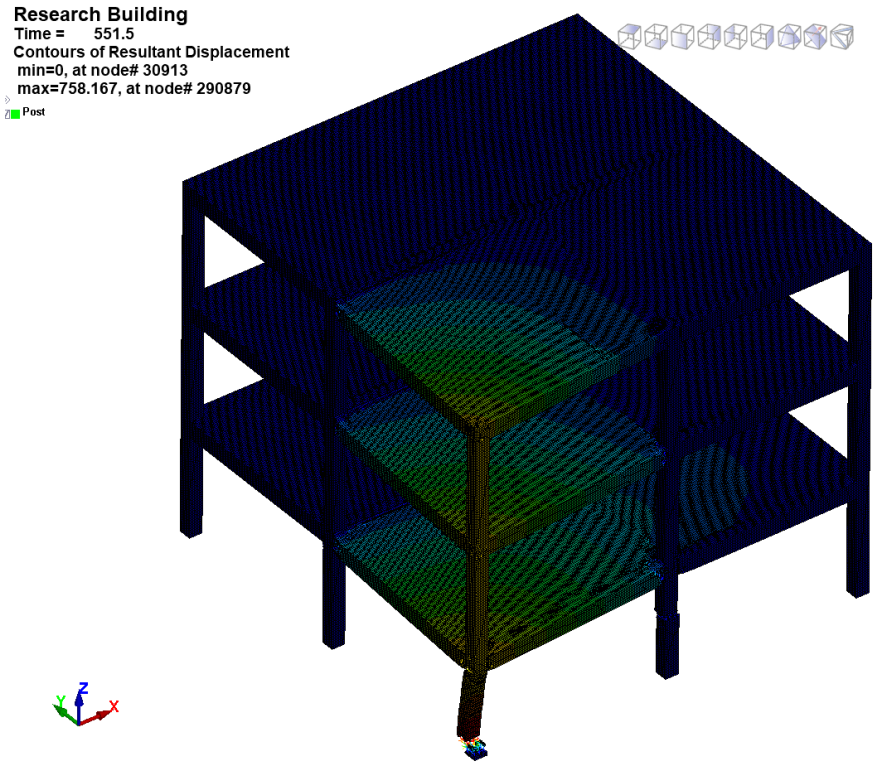

Figure 6-9: Blast_Enhanced method of analysis at initiation of column failure on axis C-2 (blast location 1)

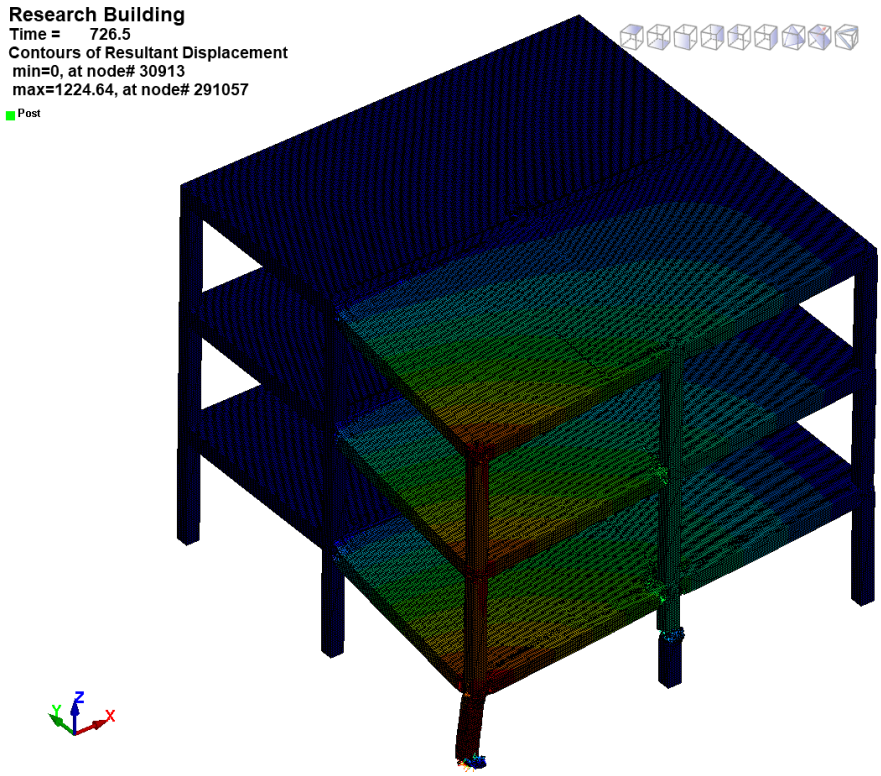

Figure 6-10: Blast_Enhanced method of analysis at column failure on axis C-2 (blast location 1)

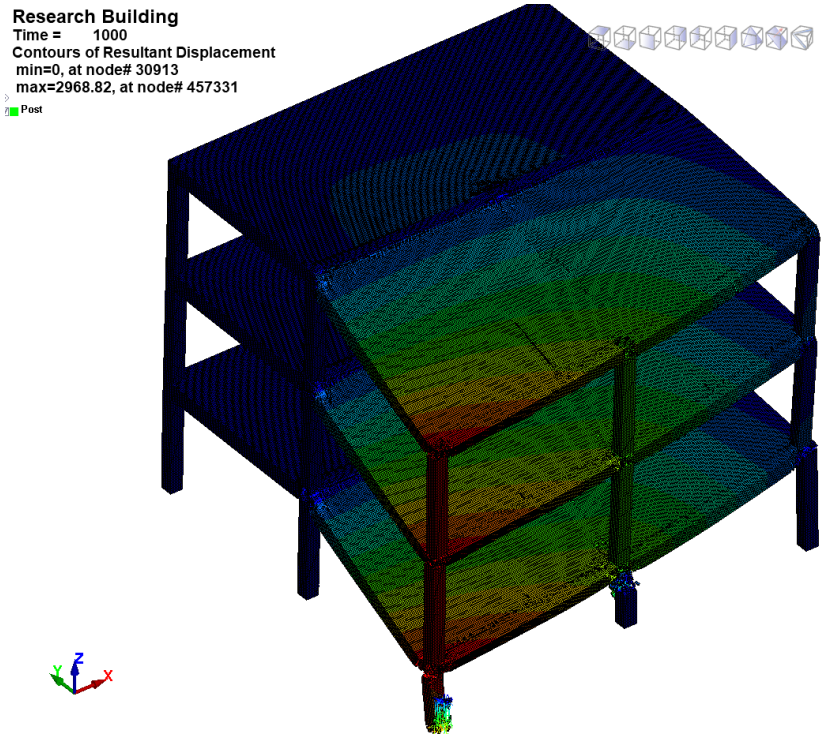

Figure 6-11: Blast_Enhanced method of analysis at partial collapse of axis B1-C3 (blast location 1)

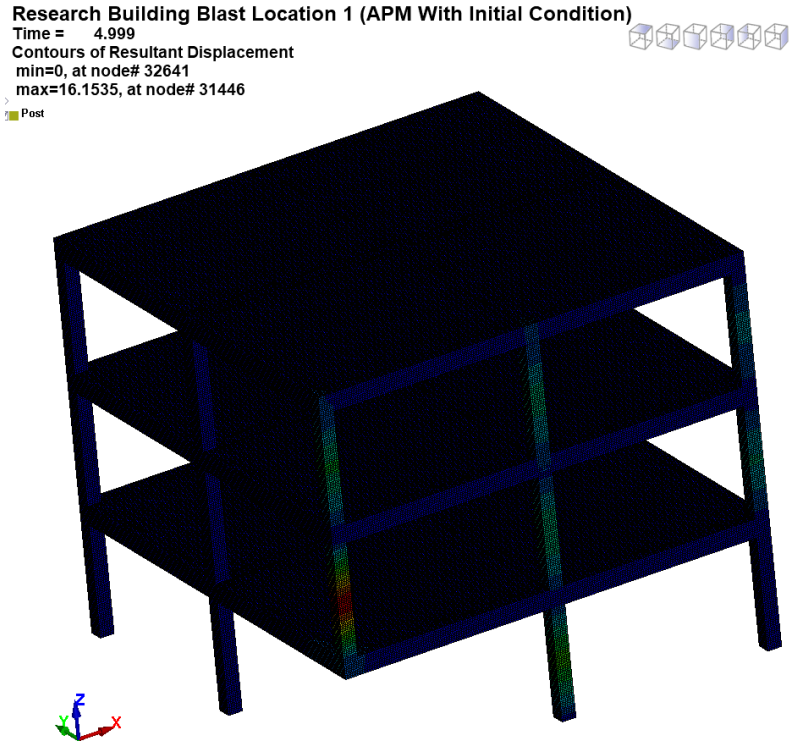

Figure 6-12: APM with initial condition method at initial velocity stage (blast location 1)

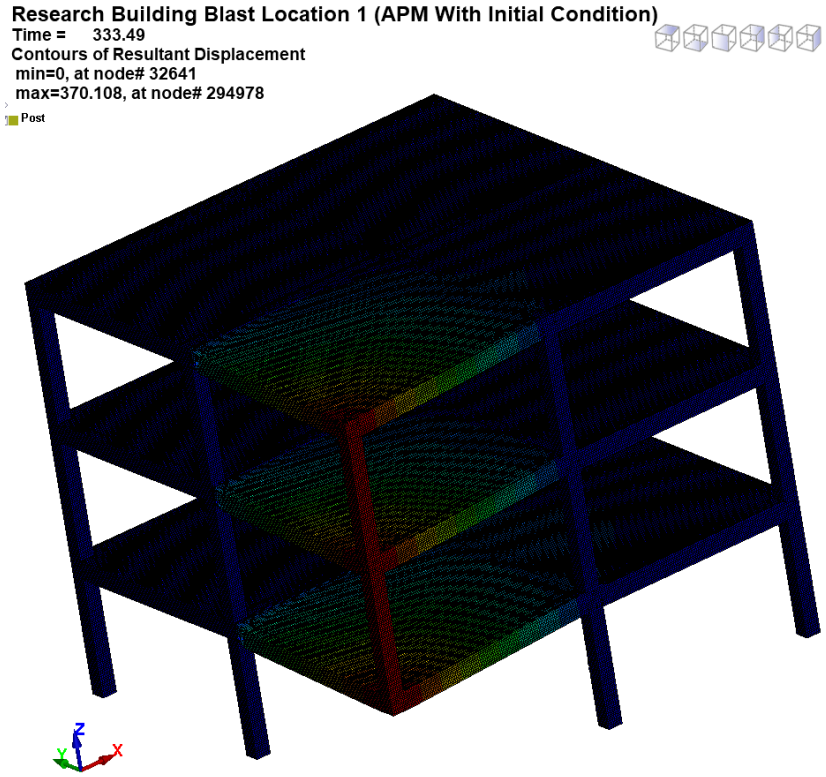

Figure 6-13: APM with initial condition method at formation of plastic hinge on axis B-1 & C-2 (blast location 1)

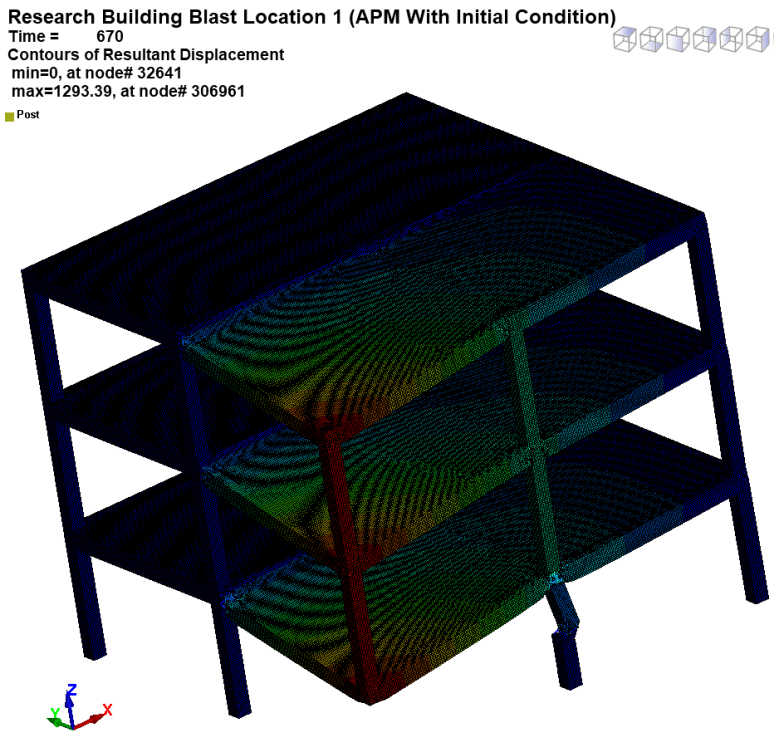

Figure 6-14: APM with initial condition method at failure of 1st story column on axis C-2 (blast location 1)

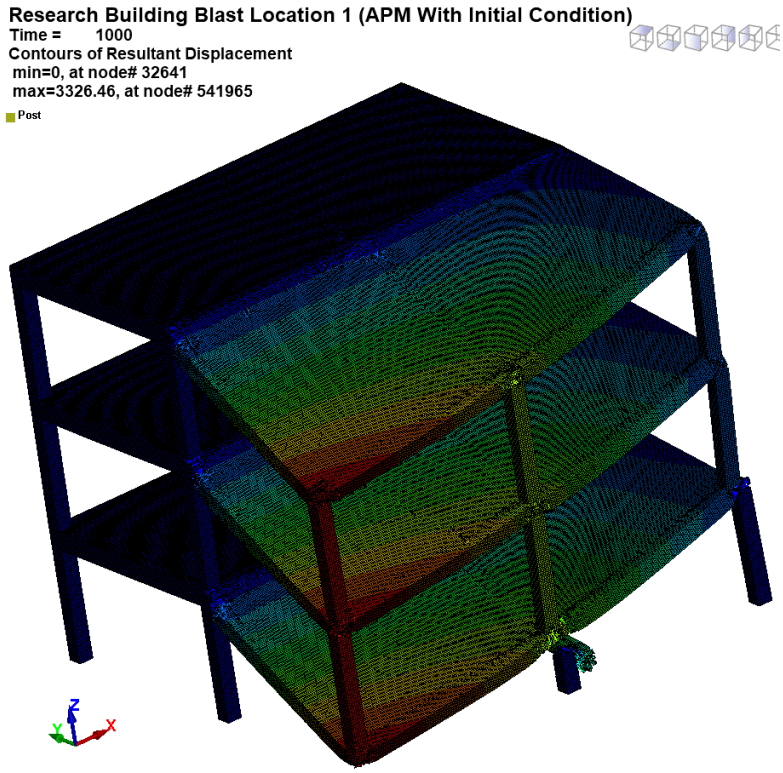

Figure 6-15: APM with initial condition method at partial collapse of axis B1-C3 (blast location 1)

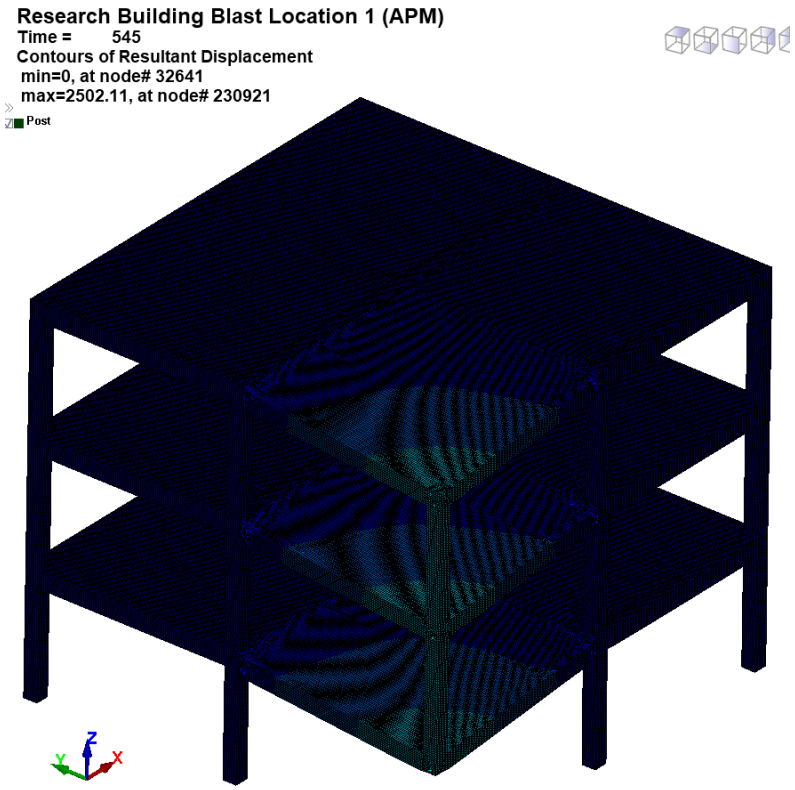

Figure 6-16: APM method at formation of plastic hinge on axis B-1 & C-2 (blast location 1)

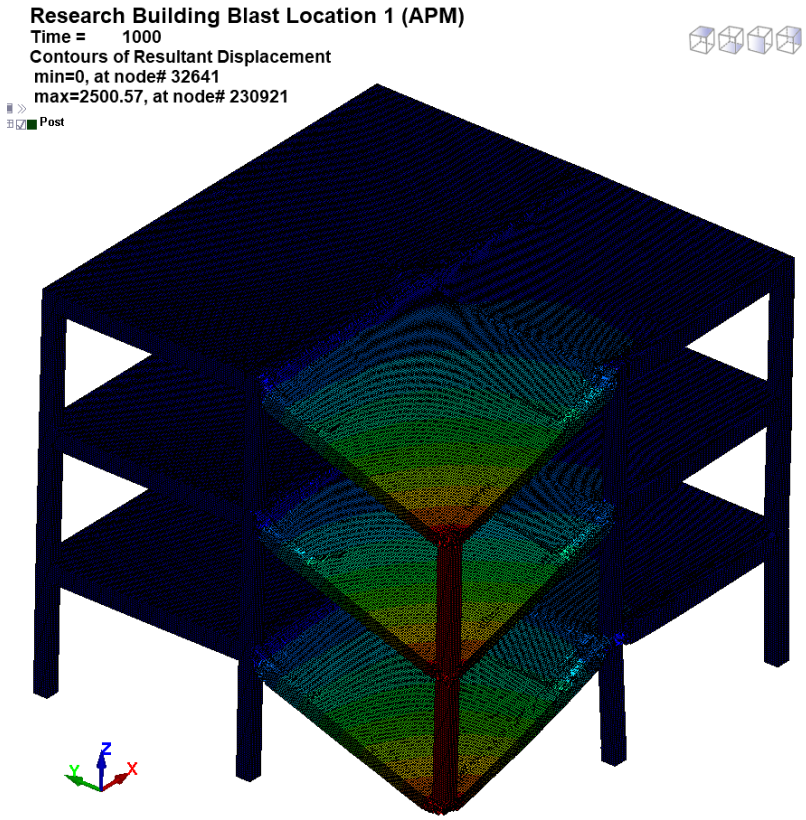

Figure 6-17: APM method at partial collapse of grid B-C and 1-2 (blast location 1)

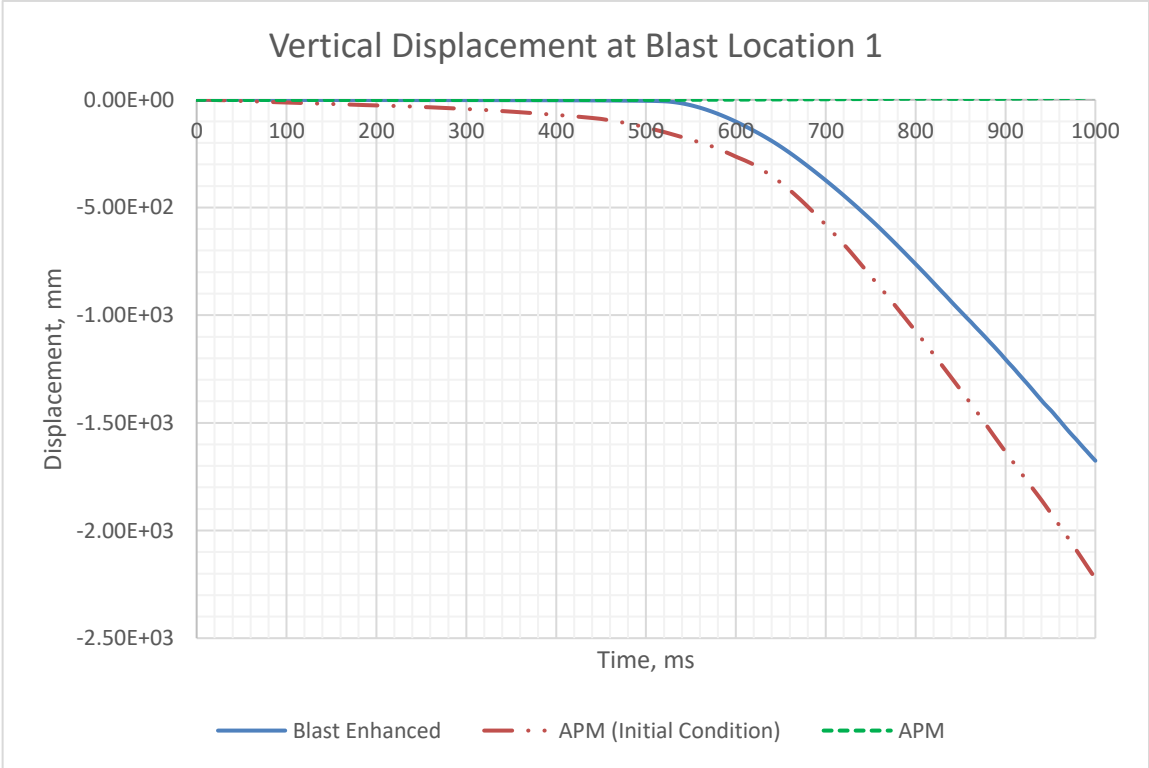

Figure 6-18: Nodal vertical displacement comparison at blast location 1

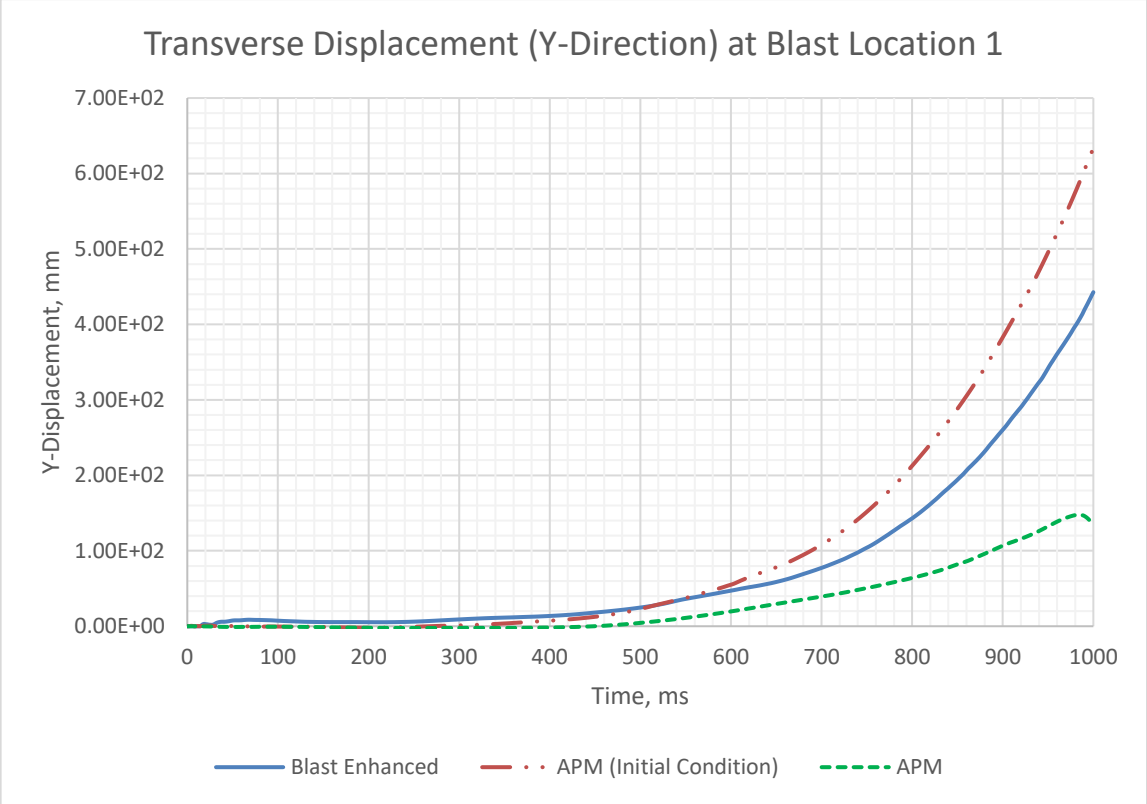

Figure 6-19: Nodal lateral displacement (Y-direction) comparison at blast location 1

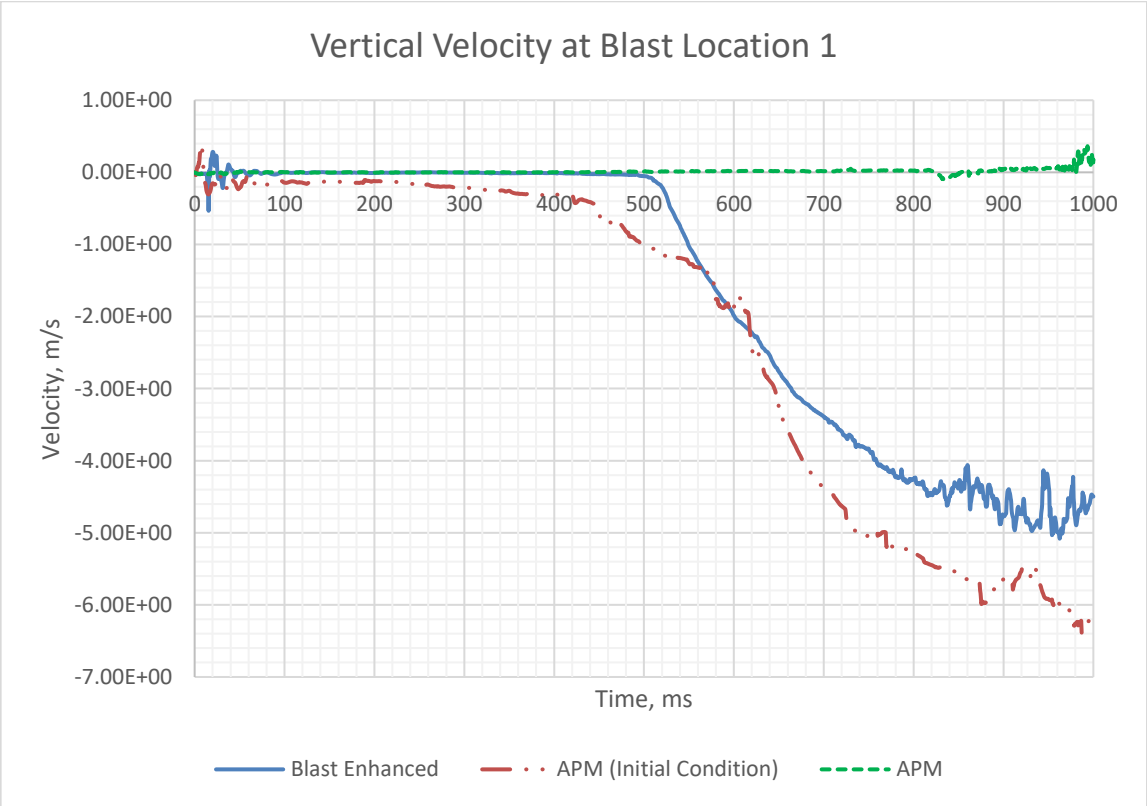

Figure 6-20: Nodal vertical velocity comparison at blast location 1

Based on APM with initial condition, 1st story column on axis 1 is removed prior to collapse analysis. Similar to Blast_Enhanced method, collapse begin by the formation of hinges at beams on axis B&C followed by failure of 1st story column on axis 2 and hinge formation of 1st story beams on axis 3-C and finally pullout of this beams from column on axis 3. However, based on APM method collapse begins by formation of plastic hinges at 1st story beams on axis B&C, but this terminates at 1st story column on axis 2. Subsequently, partial collapse is observed on grids 1-2 and B-C only (figures 6-16 and 6-17). Whereas, under APM with initial condition and Blast_Enhanced method, partial collapse is observed in grids 1-3 and B-C (figures 6-7 to 6-15).

As shown in figure 6-18, the nodal displacement at 1st story column on axis 2 shows that this column under APM method is still a load bearer, unlike APM with initial condition and Blast_Enhanced method. Similar to figure 6-18, figures 6-19 and 6-20 shows the nodal lateral displacement and vertical velocity, respectively. The time gap between the APM with initial and Blast_Enhanced method is owing to the time it takes for the first story column on axis 1 to reach failure (unable to bear load) and arrival time of blast loading, in contrast the APM with initial condition commences with an already removed column.

At blast location 2, as indicated by SDOF analysis and later verified by LS-DYNA none of the columns failed directly from the blast load. Nonetheless, initial damage and velocity is calculated which later is used to run progressive collapse analysis. However, after 1000ms run time there were no eminent collapse, only plastic hinges are formed at 1st floor beams on axis C. Subsequently, this blast location is not further discussed.

At blast location 3, column on axis C-2 is overwhelmed by direct shear and succumbed to this failure (confirmed by both SDOF and LS-DYNA analysis). Based on Blast_Enhanced method of analysis, column on axis C-2 failed first due to direct blast loading, followed by plastic hinge formation on axes C-1 and C-3 caused by the distribution of load to the neighboring columns above the first floor. Finally, this joints pulled-out of the beam-column connection resulting in the partial collapse of the structure from axis B-1 and B-3 to C-1 and C-3. Similar trend in failure and response is obtained by both APM and APM with initial conditions.

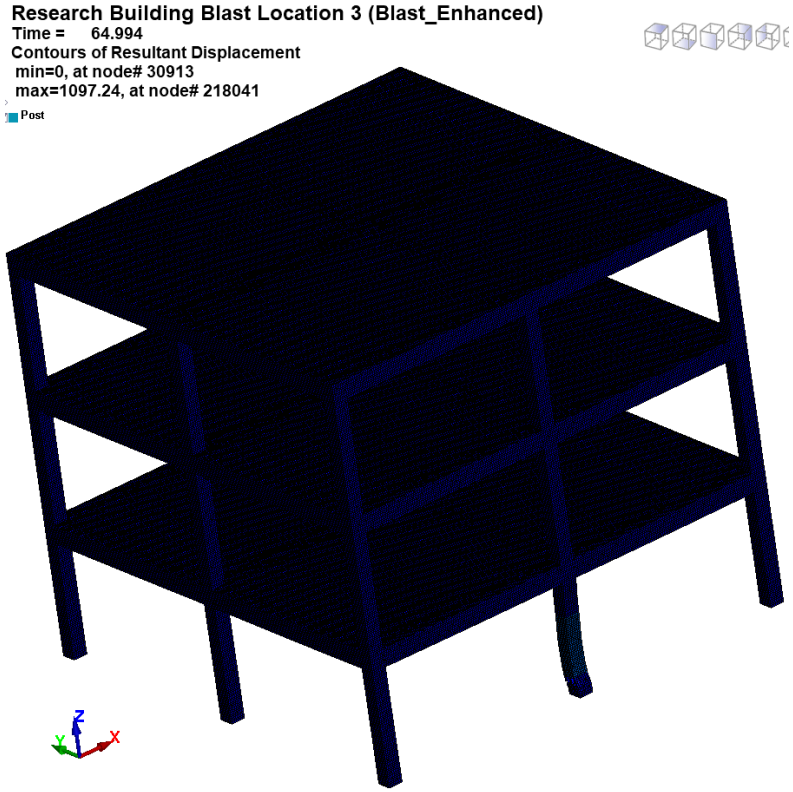

Figure 6-21: Blast_Enhanced method of analysis after blast propagates (blast location 3)

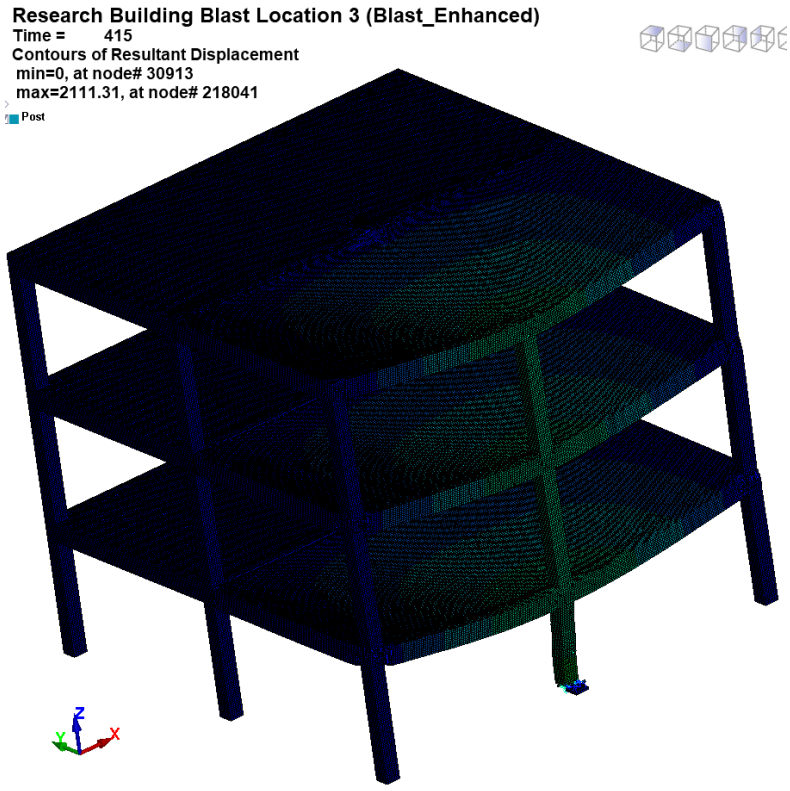

Figure 6-22: Blast_Enhanced method of analysis at column failure on axis 2 (blast location 3)

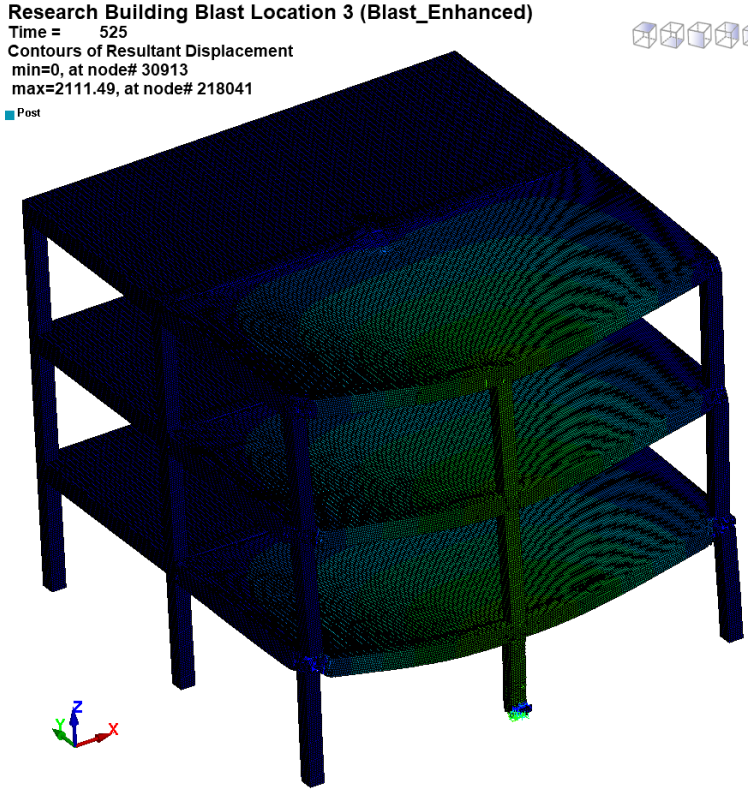

Figure 6-23: Blast_Enhanced method of analysis at initiation of plastic hinge on axis C-1 and C-3 (blast location 3)

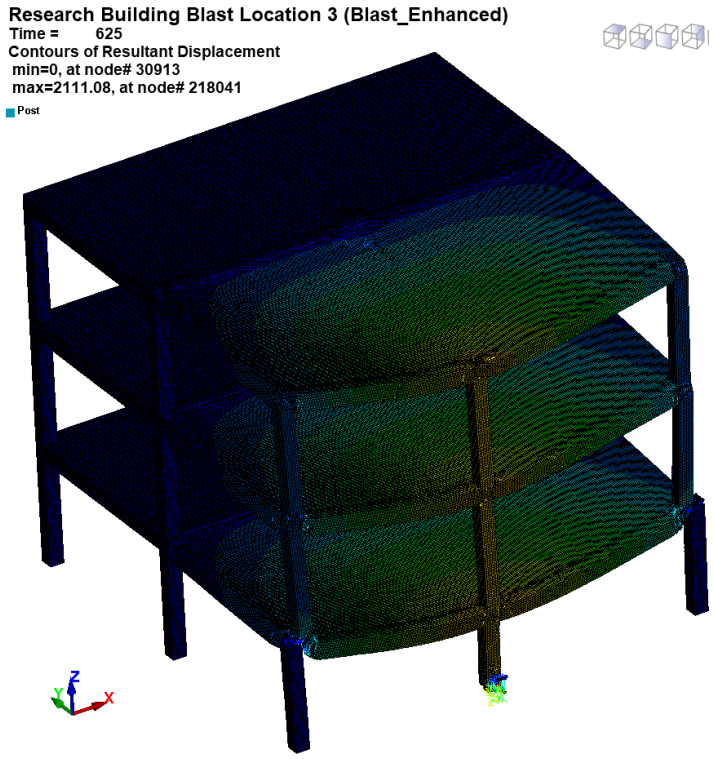

Figure 6-24: Blast_Enhanced method of analysis at beam-column failure on axis C-1 and C-3 (blast location 3)

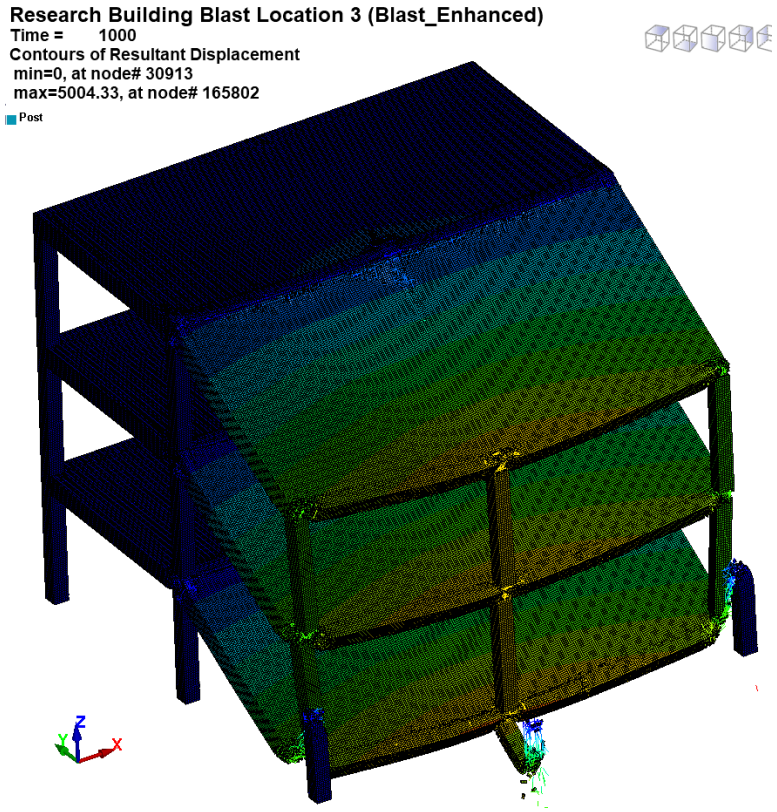

Figure 6-25: Blast_Enhanced method of analysis at partial collapse (blast location 3)

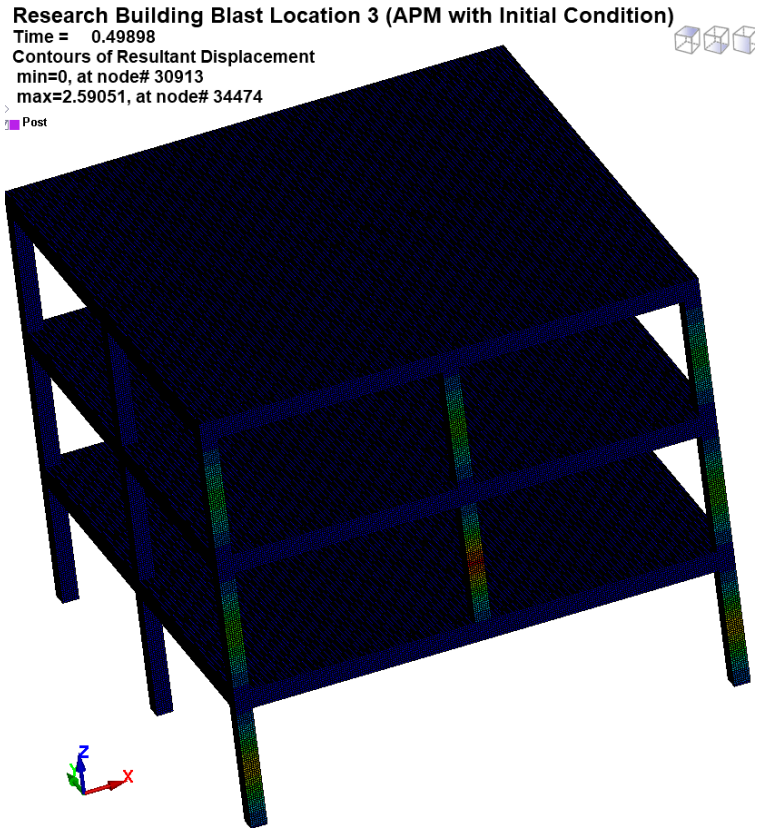

Figure 6-26: APM with initial condition method at initial velocity stage (blast location 3)

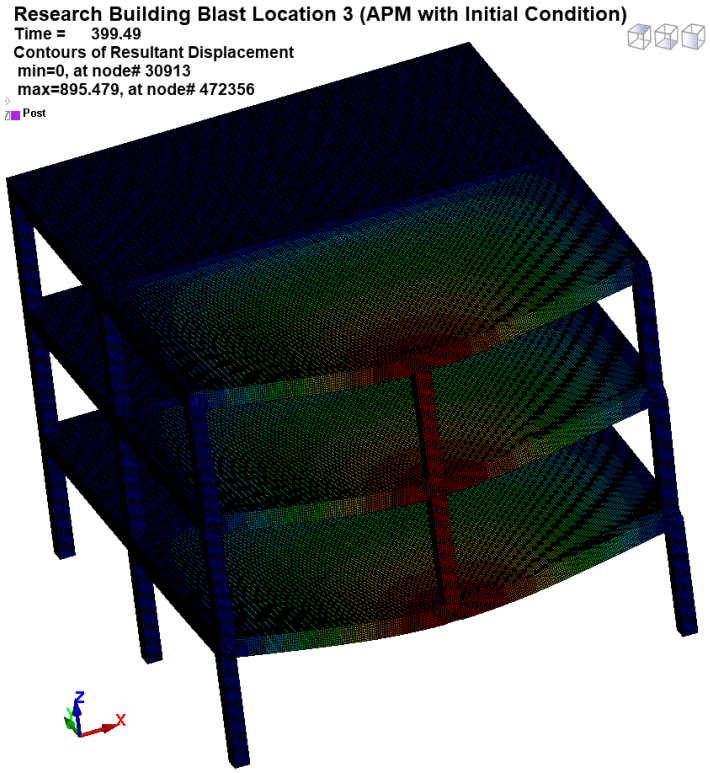

Figure 6-27: APM with initial condition method of analysis at the formation of plastic hinge on axis C-1 & C-3 (blast location 3)

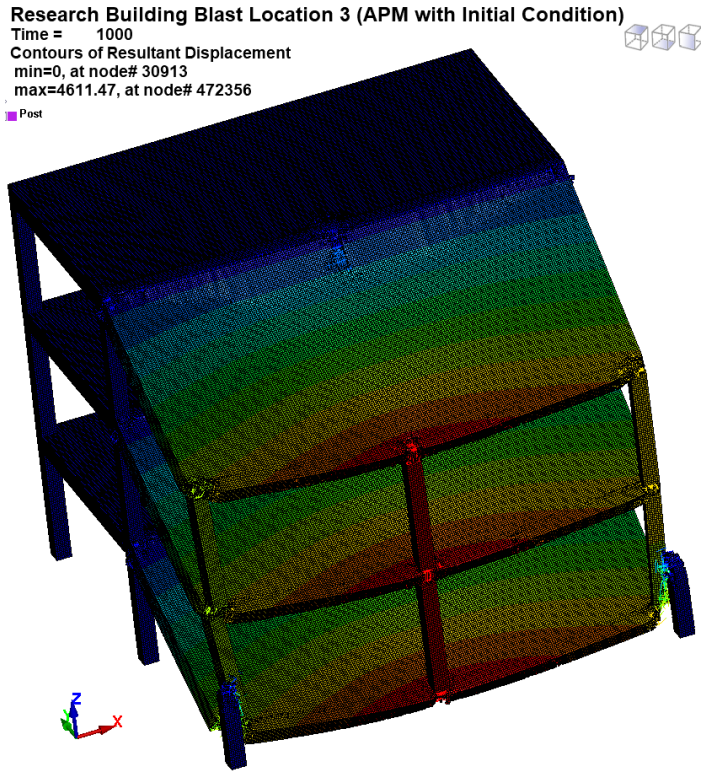

Figure 6-28: APM with initial condition method of analysis at partial collapse (blast location 3)

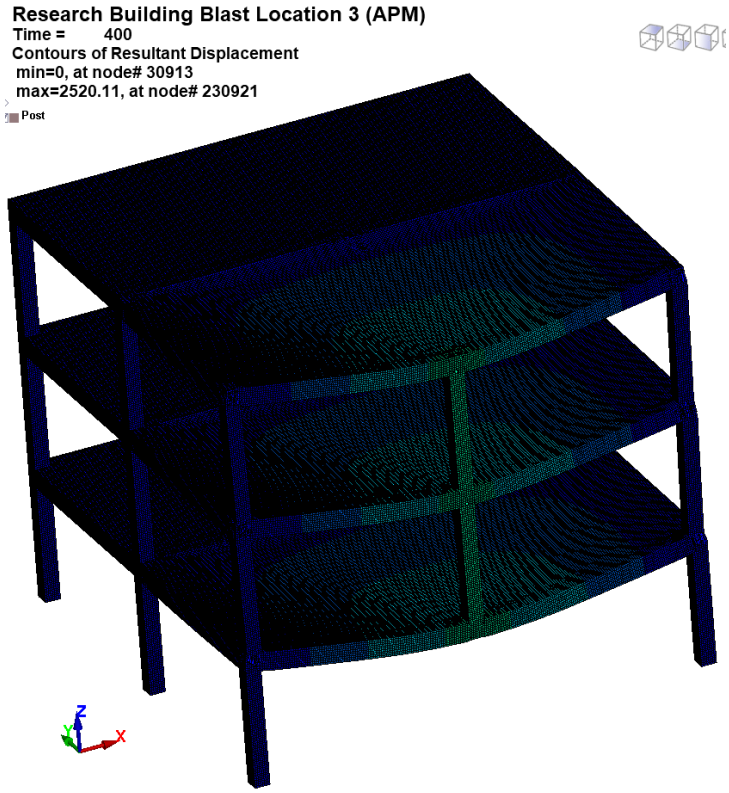

Figure 6-29: APM method of analysis at the formation of plastic hinge on axis C-1 & C-3 (blast location 3)

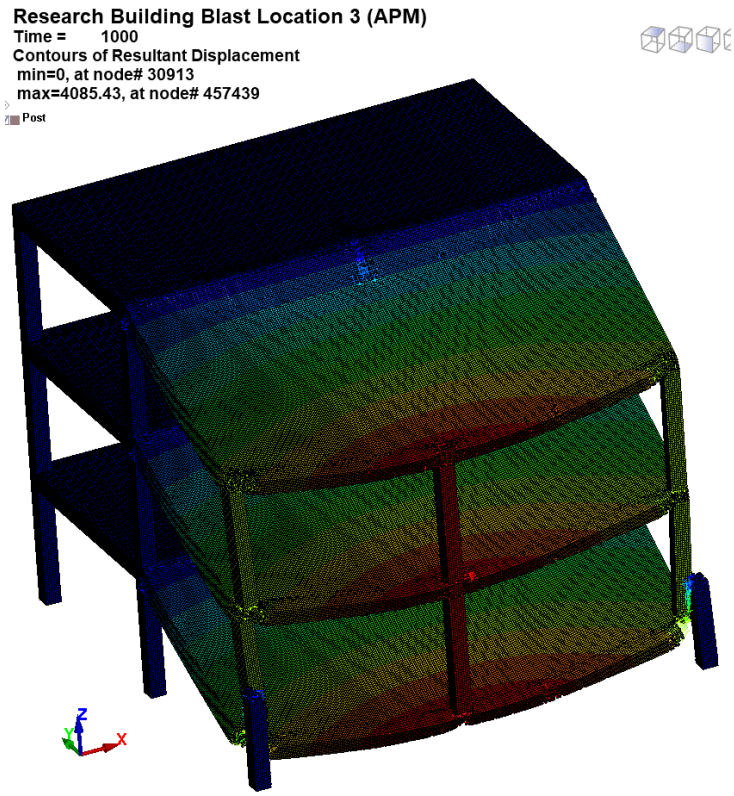

Figure 6-30: APM method of analysis at partial collapse (blast location 3)

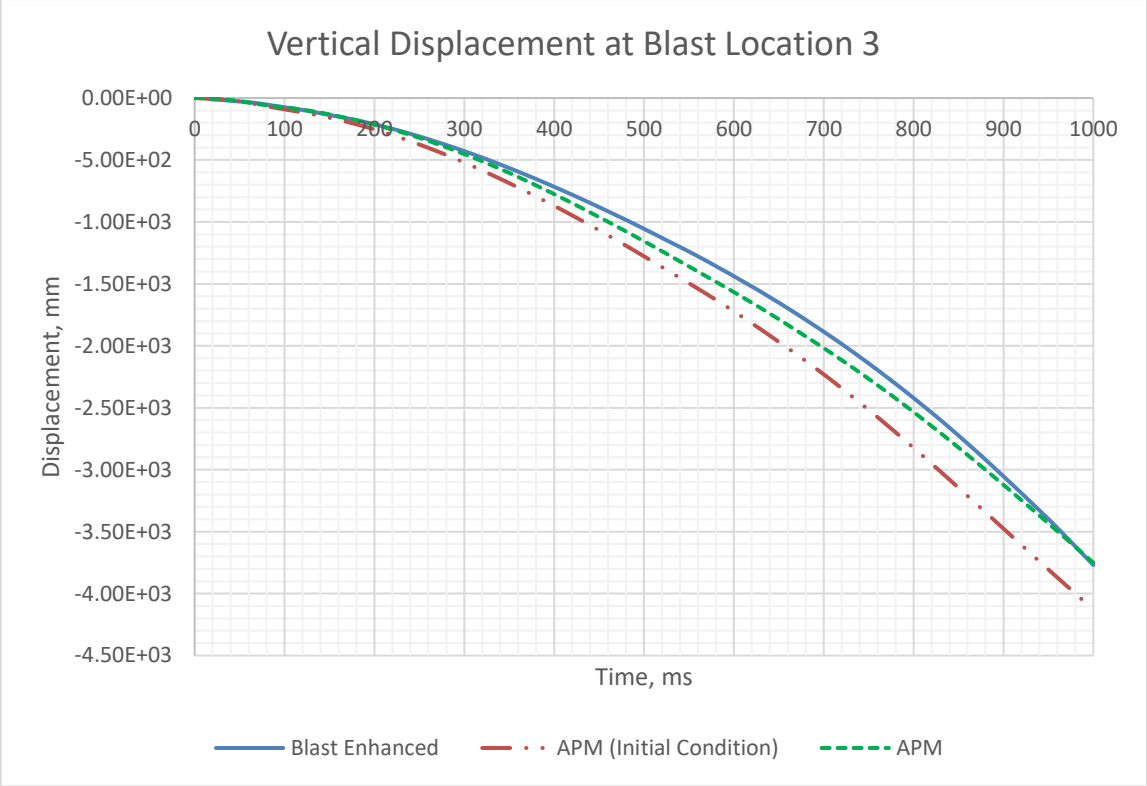

Figure 6-31: Nodal vertical displacement comparison at blast location 3

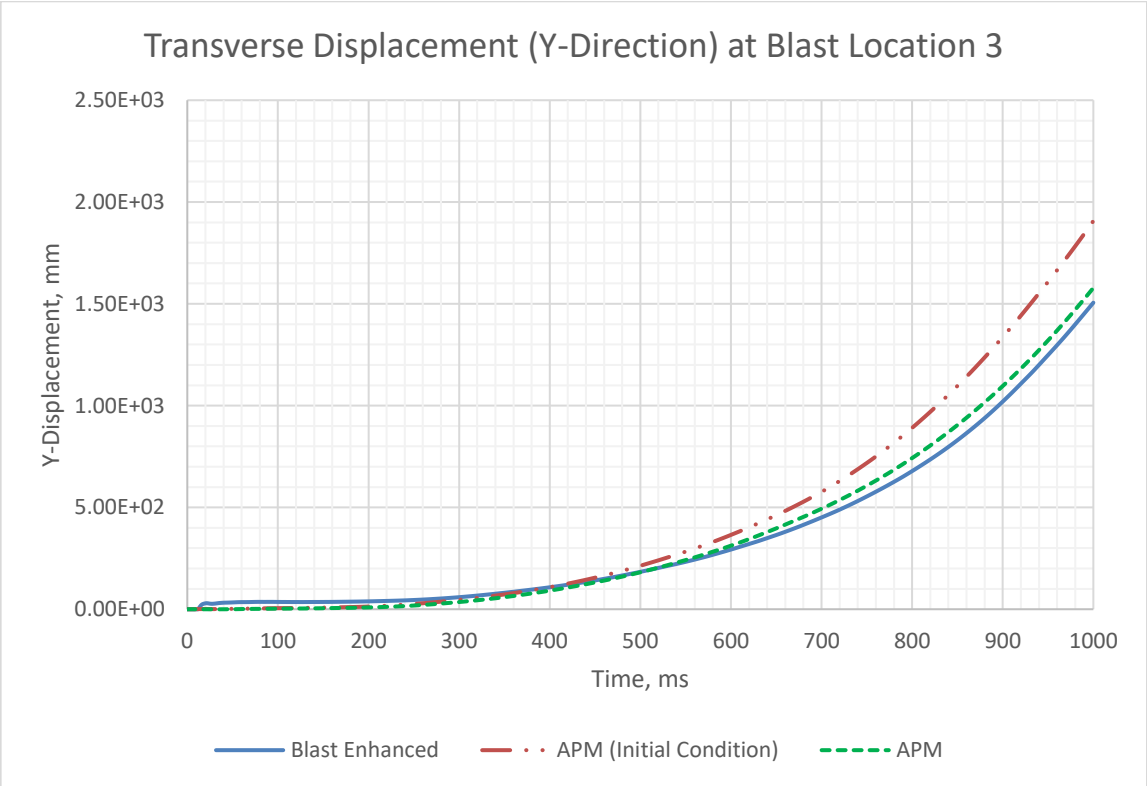

Figure 6-32: Nodal lateral displacement (Y-direction) comparison at blast location 3

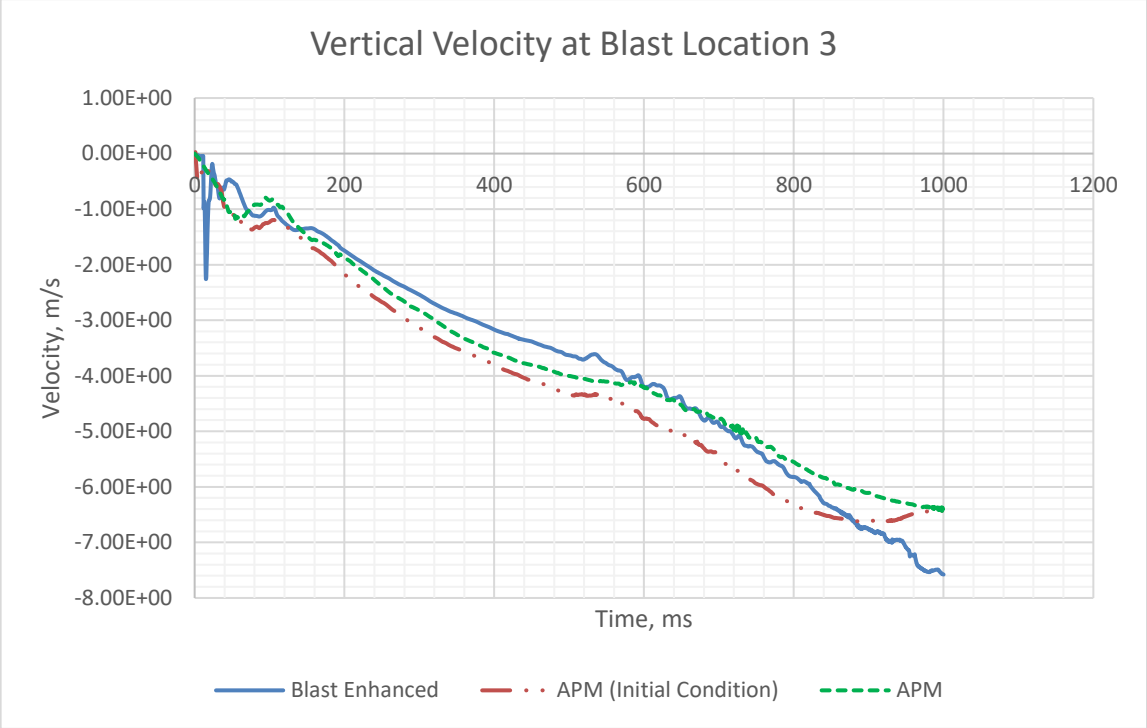

Figure 6-33: Nodal vertical velocity comparison at blast location 3

The main differentiating aspect between APM and both Blast_Enhanced and APM with initial condition is what happens when none of the columns fail under direct blast loading. This is clearly seen by blast location 6. In addition to blast location 1, this case shows that APM overestimates the capacity of the structure to potential collapse. Under Blast_Enhanced method, at blast location 6, 1st story column on axis C2 under direct blast loading is exposed to permanent deflection (figure 5-12 and table 4-7), but still remains load bearing member. After some time (after blast loading duration) this column is succumbed to the large deflection leading to failure. Similar to blast location 3, due to failure of column on axis 2, column 1 and 3 is subjected to large axial load and moment, subsequently, failure of these columns is triggered. Prior to failure of column 2, multiple hinges appeared at axis 1, 2 and 3. Likewise, according to APM with initial condition, similar failure is obtained, however, the duration of failure of column on axis C-2 is longer (figure 6-43) and also the failure mechanism compared to the Blast_Enhanced method is different. The column failed at the mid span and at the beam-column joint for Blast_Enahnced method and APM with initial condition, respectively. This is clearly shown in figure 6-44, the lateral displacement between the two method widens as time progressed. Nevertheless, after 1250ms, initiation of progressive collapse of axis B-C and 1-3 commenced following the formation of multiple plastic hinges at grid C from 1 to 3.

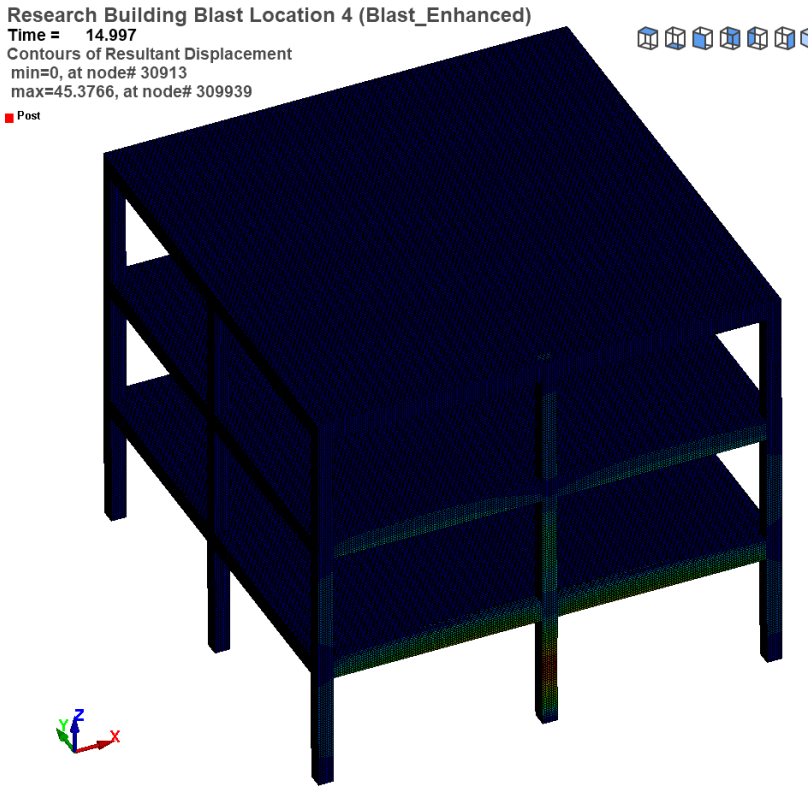

Figure 6-34: Blast_Enhanced method of analysis after blast propagates (blast location 6)

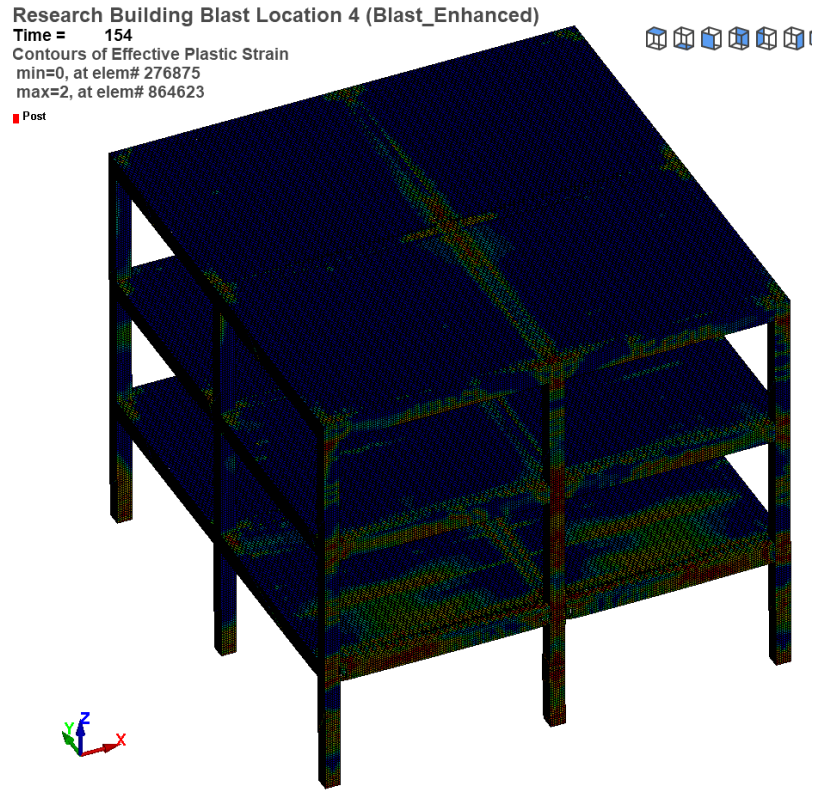

Figure 6-35: Blast_Enhanced method of analysis at initiation of plastic hinge on axis 1, 2 and 3 (blast location 6)

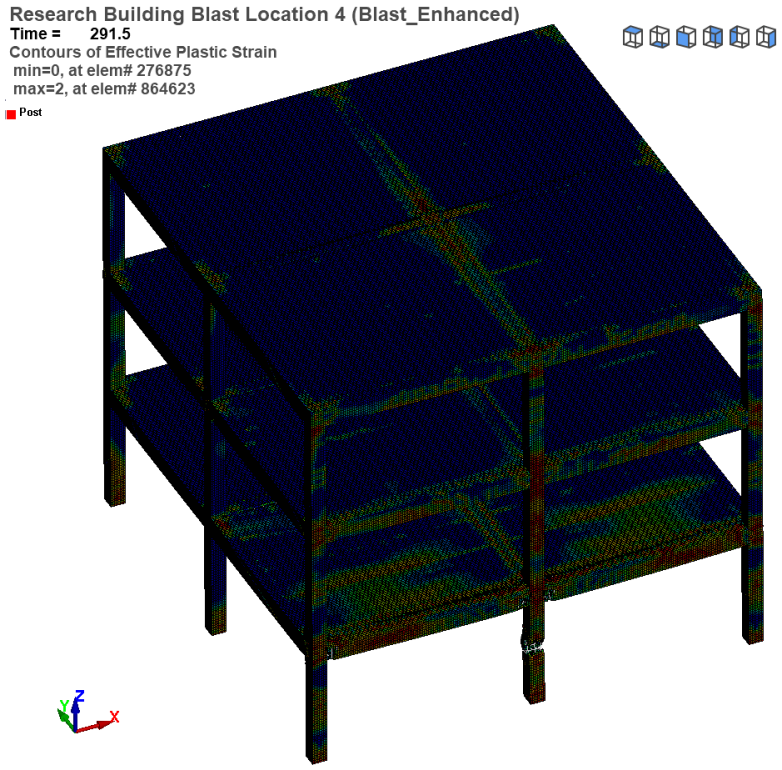

Figure 6-36: Blast_Enhanced method of analysis at column failure on axis 2 (blast location 6)

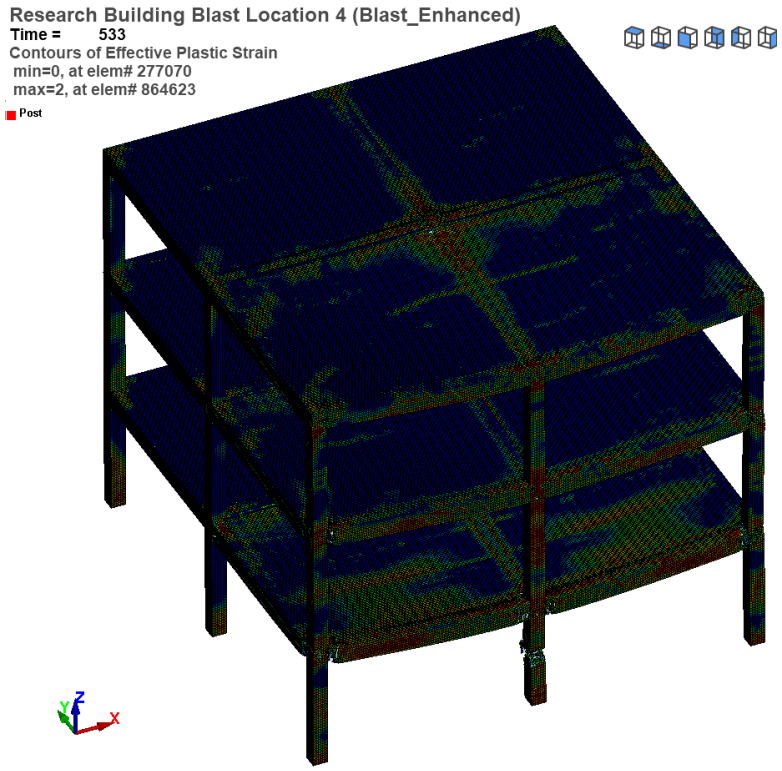

Figure 6-37: Blast_Enhanced method of analysis at multiple plastic hinge formation on axis C (blast location 6)

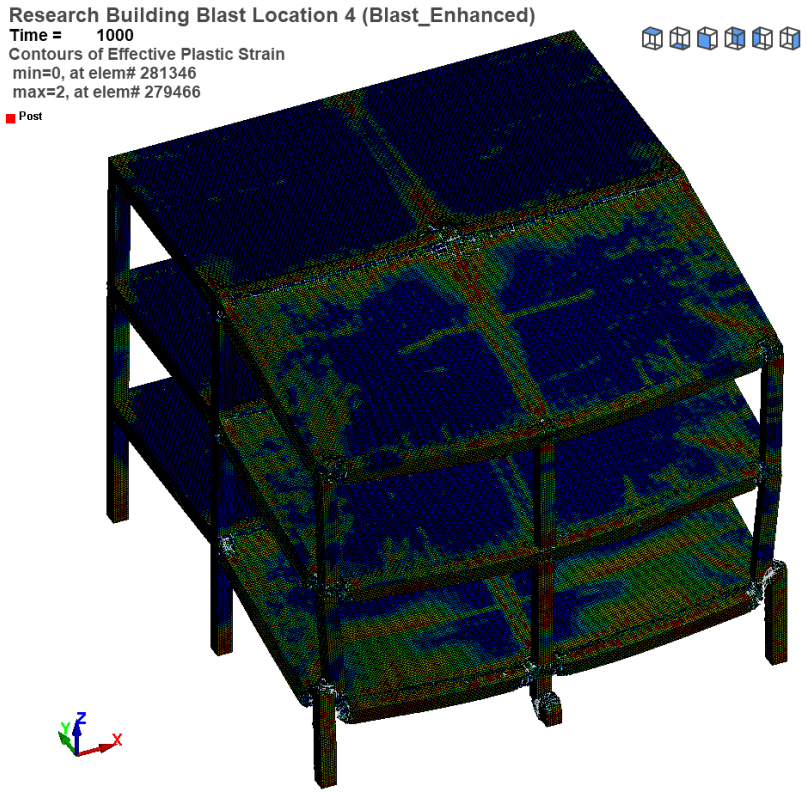

Figure 6-38: Blast_Enhanced method of analysis at partial collapse of grid B-C and 1-3 (blast location 6)

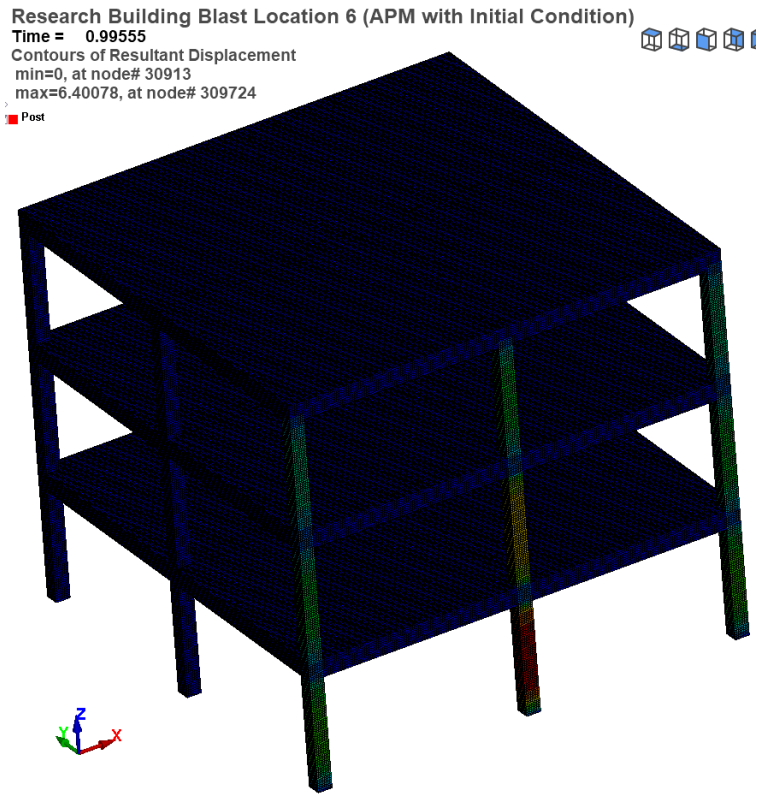

Figure 6-39: APM with initial condition method at initial velocity stage (blast location 6)

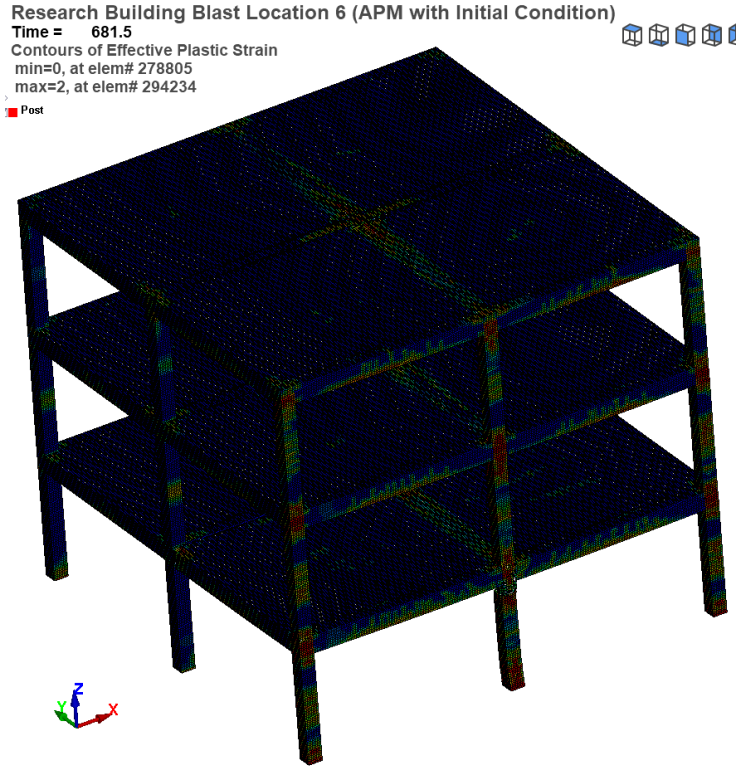

Figure 6-40: APM with initial condition method at initiation of column failure on axis C-2 (blast location 6)

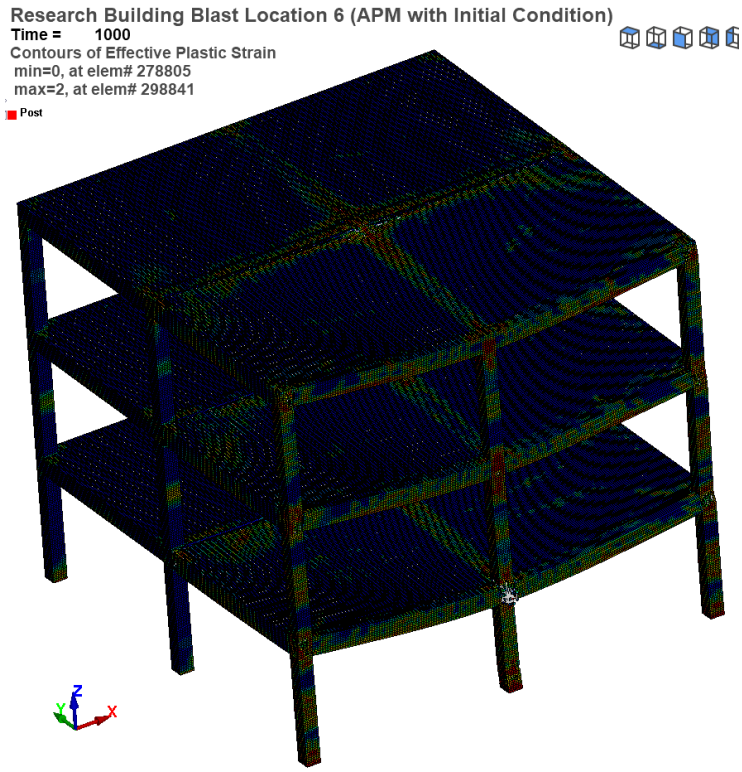

Figure 6-41: APM with initial condition method at multiple plastic hinge formation on axis C (blast location 6)

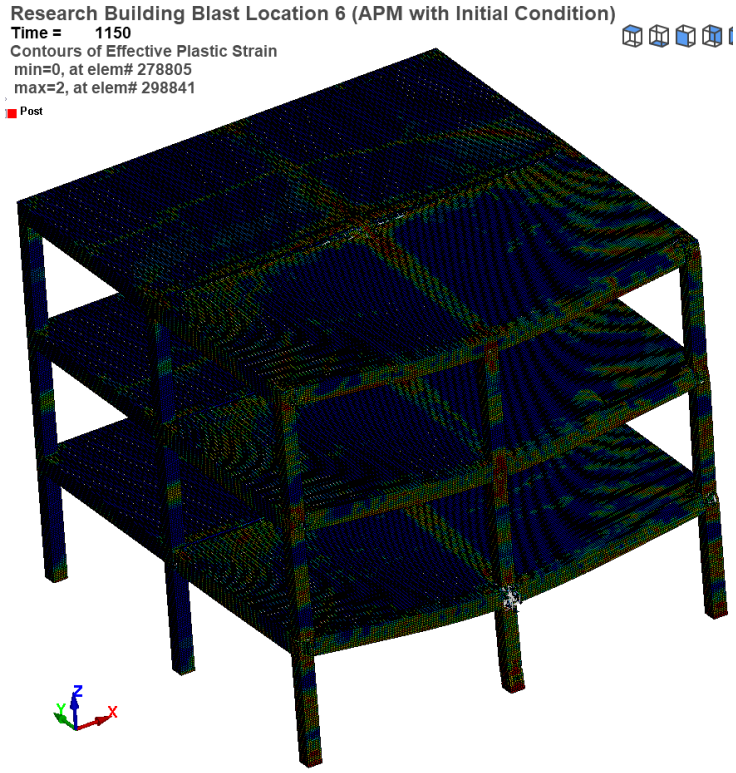

Figure 6-42: APM with initial condition method of analysis at commencement of partial collapse of grid B-C and 1-3 (blast location 6)

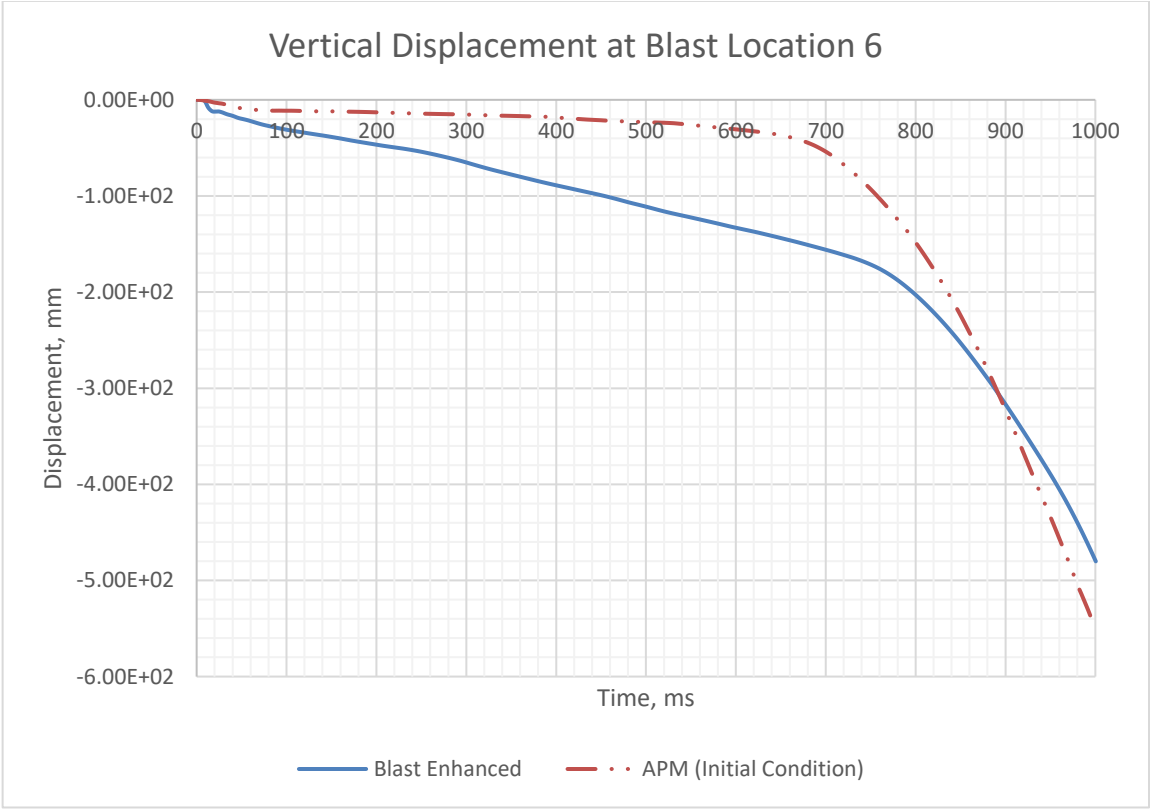

Figure 6-43: Nodal vertical displacement comparison at blast location 6

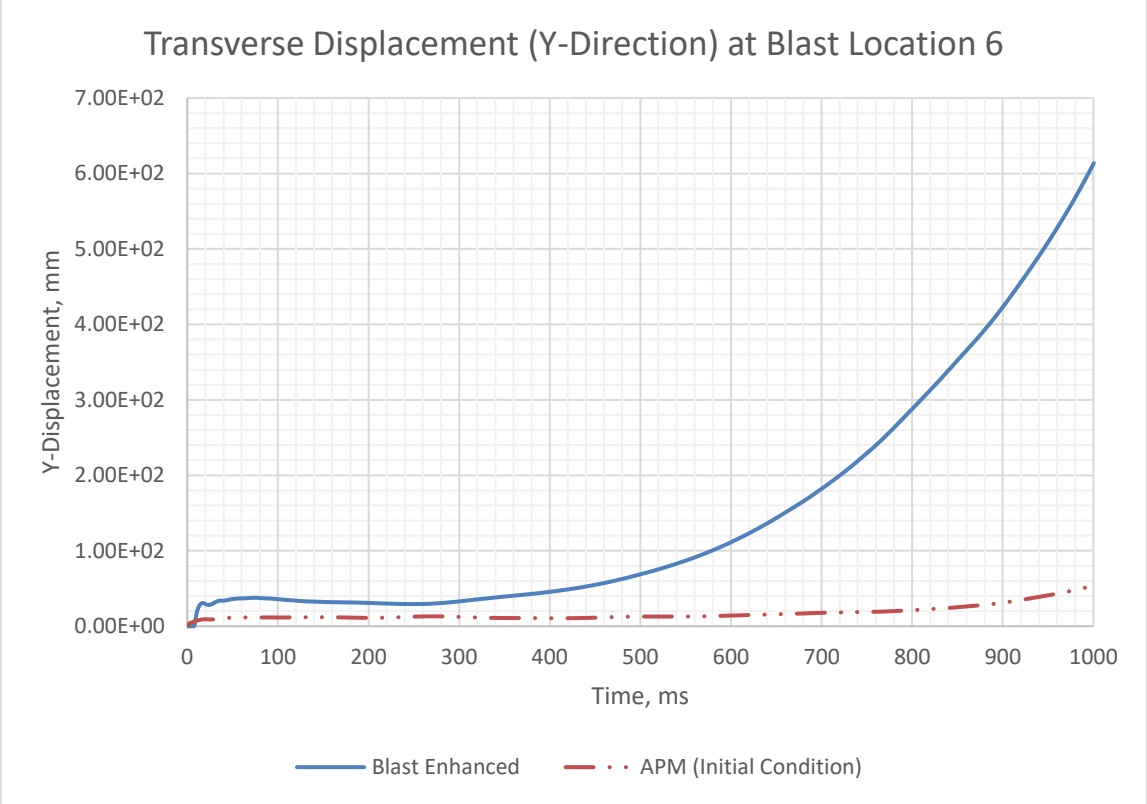

Figure 6-44: Nodal lateral displacement (Y-direction) comparison at blast location 6

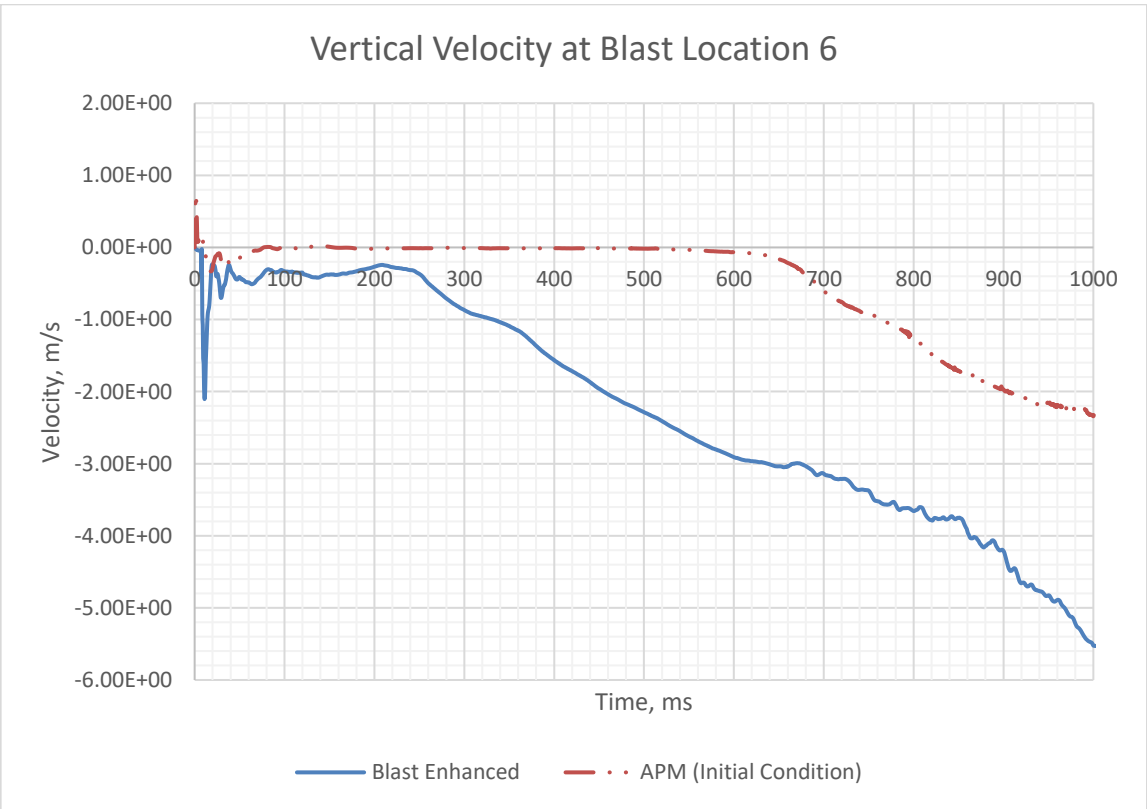

Figure 6-45: Nodal vertical velocity comparison at blast location 6

CHAPTER 7 CONCLUSION AND RECOMMENDATION

7.1 Conclusion

The research tried to investigate the overestimation of APM method to progressive collapse under different blast location scenarios with the provision of modified method proposed by Shi et al. [11] Prior to computing blast analysis, the building is designed for gravity, lateral loads (wind and earthquake) following ES EN 2015. According to the conventional design, 12 blast locations are selected considering access points and potential for different failures. Several iterations were performed to select a single charge weight that would cause column failure at multiple blast locations. Based on this charge weight and standoff distance blast analysis is carried out, several methods exist for computing blast load parameters (incident pressure, reflected pressure, positive time duration, arrival time, and wave decay coefficient). The Kingery-Bulmash's empirical equation provides a relatively better prediction for these parameters. Based on the output of the pressure-time history, SDOF analysis is utilized to determine the response of structural members. SDOF method is a powerful analysis that can predict the response of column subjected to blast loading considering axial load and non-linear behavior of members.

Reinforced concrete structural members (both concrete and rebar) have larger strength under high strain-rate. This is evident when conducting blast response analysis. Under direct blast loading, structural columns fail in three major modes; breach, flexure and direct shear. It is highly unlikely that columns fail in breach as the requirement for seismic demand usually leads to a higher column size. Under blast location close to the ground and close contact, columns are subjected to direct shear failure mode rather than flexural failure mode. Similarly, at spherical blasts (above ground floor) and large standoff distance, the prevailing failure mode is flexure. After subjecting columns to blast loading it is imperative to determine the residual axial load carrying capacity. A simplified approach is provided here by obtaining the maximum strain in the concrete and determining the crushed concrete and calculating the buckling or plastic capacity of the rebar. Together (concrete and rebar) the residual axial load carrying capacity can easily be obtained. From the SDOF analysis and residual axial-load carrying capacity, the initial velocity and damage, respectively, are used to determine the potential for progressive collapse.

Three methods are compared for estimating the potential for progressive collapse; APM, APM with initial condition and blast-structure (bench mark) method. APM gave reliable result for blast location 3, however, at blast locations 1 and 6, it failed short of predicting the actual collapse scenario. However, APM with initial condition provided a better and close result with the bench mark analysis in all the three blast locations. However, at blast location 6 (where none of the columns failed under direct blast loading) collapse initiated later than the bench mark analysis, furthermore, the lateral displacement showed large deviation. Nevertheless, it gave a good approximation to the bench mark analysis.

7.2 Recommendation

This research investigated the overestimation of APM method on the potential for progressive collapse and provided a method based on Shi et al. for accounting the missed parameters (initial condition and damage) of APM. The findings revealed that after blast duration columns are not in static equilibrium and undamaged. However, the study was limited to moment resisting frame and single charge weight.

Based on these results, the following recommendations are proposed:

Integration into other software: LS-DYNA is a powerful tool but comes with a cost, computational time and large memory requirement (For instance, analyzing a single blast location for progressive collapse can require approximately 23 hours in LS-DYNA for a laptop with 6 cores (Intel(R) Core (TM) i7-10750H CPU@2.60GHz and 64Gb RAM). Therefore, considering the promising results, other researches are encouraged to pilot this method (APM with initial conditions and damage) in another software where the run time and memory usage is minimal (e.g. LS-DYNA modelling where columns and beams are modelled as beam elements and slabs as shell elements instead of solid elements or other software modelling in similar way).

Further Research on the effect of ground shock: Ground shock, a compression wave that propagates through the ground upon detonation, can have significant structural implications. It can cause soil liquefaction, which reduces the soil's load-bearing capacity, and can also induce vibrations that can resonate with and damage structures.

Investigating the effect of post-blast thermal loading: The effect of temperature from heat after blast is another potential for inducing progressive collapse (for example, the World Trade Center towers). When an explosion occurs, the intense heat and pressure can rupture gas lines, ignite flammable materials, and create sparks that can initiate fires. These fires can engulf nearby structures, leading to further structural damage, the release of hazardous materials, and the potential for additional explosions. The exclusion of thermal loading from the study's scope may underestimate the overall impact of the blast event. A more comprehensive assessment would involve analyzing the combined effects of the blast and the subsequent fire to accurately evaluate the structure's resilience and identify potential mitigation strategies.

Investigating the impact of non-structural components: Non-structural elements, such as interior walls, partitions, and exterior cladding, can provide additional support and redundancy to the structural frame. In the event of a localized failure, non-structural elements can help redistribute loads and prevent the collapse from propagating throughout the structure. Neglecting the influence of non-structural elements in the analysis may lead to an underestimation of the structure's ability to withstand progressive collapse.

Further research on the effect of blast waves in confined spaces: confined spaces drastically increase the reflected pressure as the blast wave bounce form one surface to another. Reflected blast waves can cause more damage to structures than incident blast waves because they can concentrate the energy of the blast wave in a smaller area. This can cause the structure to collapse or to be severely damaged. Additionally, reflected blast waves can be more difficult to predict than incident blast waves because they can be affected by the shape and size of the reflecting structure. This can make it difficult to design structures that can withstand reflected blast waves.

Further research using ALE formulations: ALE allows for simulating the complex interaction between the blast wave (often modeled as a fluid) and the impacted structure. Which is leaps ahead of the empirical formulas (yet powerful) used in the current research. Furthermore, ALE can handle a wide range of materials, including fluids, solids, and even mixtures, making it suitable for various blast scenarios.

REFERENCES

[1] DoD, Design of Buildings to Resist Progressive Collapse, Department of Defense (United State of America), 2016.

[2] Z. LI and Y. SHI, "Methods for Progressive Collapse Analysis of Building Structures Under Blast and Impact Loads," *Tianjin University and Springer -Verlag,* p. 11, 2008.

[3] Y. Al-Salloum, T. Almusallam, T. Ngo, H. Elsanadedy, H. Abbas and P. Mendis, "Progressive Collapse Analysis of Medium-Rise Circular RC Building Against Blast Loads," in *Ocean, Offshore and Arctic Engineering*, Busan, 2016.

[4] I. M. H. Alshaikh, A. A. Abadel, K. Sennah, M. L. Nehdi, R. Tuladhar and M. Alamri, "Progressive Collapse Resistance of RC Beam–Slab Substructures Made with Rubberized Concrete," *Buildings,* vol. 12, no. 1724, p. 33, 2022.

[5] W. Baker, P. Cox, P. Westine, J. Kulesz and R. Strehlow, Explosive Hazards and Evaluation, Amesterdam: ELSEVIER, 1983.

[6] D. M. V. A. d. Carvalho, "Simplified analysis of RC beam and beam-column elements under blast loading," Nova School of Science and Technology, Lisbon, 2021.

[7] M. D. Chiranjeevi and J. Simon, "Analysis of Reinforced Concrete 3d Frame under Blast Loading and Check for Progressive Collapse," *Indian Journal of Science and Technology,* vol. 9, no. 30, p. 6, 2016.

[8] M. A. Galal, M. Bandyopadhyay and A. K. Banik, "Progressive Collapse Analysis of Three-Dimensional Steel–Concrete Composite Building due to Extreme Blast Load," *Journal of Performance of Constructed Facilities,* vol. 3, no. 34, p. 14, 2020.

[9] F. Siba, "Near-Field Explosion Effects on Reinforced Concrete Columns: An Experimental Investigation," Carleton University, Ontario, 2014.

[10] H. C. Engineers, General Services Administration Alternate Path Analysis & Design Guidelines for Progresive Collapse Resistance, Washington DC: GSA Office of Design and Construction, 2016.

[11] S. Yanchao, L. Zhong-Xian and H. Hong, "A new method for progressive collapse analysis of RC frames under blast loading," *Engineering Structures*, p. 13, 2010.

[12] G. J. Matthew, F. T. Corey, E. Q. Spencer and Q. E. Spencer, "Blast-Induced Damage Mapping Framework for Use in Threat-Dependent Progressive Collapse Assessment of Building Frames," *American Society of Civil Engineers*, p. 16, 2016.

[13] A.-S. Y.A., A. H., A. T.H., N. T. and M. P., "Progressive collapse analysis of a typical RC high-rise tower," *Journal of King Saud University - Engineering Science*, p. 8, 2017.

[14] A. Kassahun, "Blast Loading And Blast Effects On Rc Frame Buildings," Addis Ababa Institute Of Technology School, Addis Ababa, 2011.

[15] Department of Defence, "Unified Facilities Criteria - Structures to Resist the Effects of Accidental Explosions," Department of Defence, Washington DC, 2008.

[16] U.S. Army Corps of Engineers, "User's Guide for the Single-Degree-of-Freedom Blast Effects Design Spreadsheets (SBEDS)," U.S. Army Corps of Engineers, 2008.

[17] K. A. Marchand and F. Alfawakhiri, "Blast and Progressive Collapse," *American Institute of Steel Construction INC.*, p. 67, 2004.

[18] J. Munshi, "State-of-the-art vs. State-of-the-practice in Blast and Progressive Collapse Design of Reinforced Concrete Structures," American Society of Civil Engineers (ASCE), Illinois, 2004.

[19] X. Jun-Xiang and L. Xi-la, "A Two-step Approach to Progressive Collapse Analysis of Building Structures under Blast Loading," J. Shanghai Jiaotong University, Shanghai, 2009.

[20] J. R. McConnell and H. Brown, "Evaluation of progressive collapse alternate load path analyses in designing for blast resistance of steel columns," ELSEVIER, Delaware, 2011.

[21] M. Sasani, A. Shukla, Y. D. Rajapakse and M. E. Hynes, "Progressive Collapse Resistance of Reinforced Concrete Structures," in *Blast Mitigation: Experimental and Numerical Studies*, Boston, Springer, 2015, pp. 331-350.

[22] S. Jeyarajan, J. Y. R. Liew and C. G. Koh, "Analysis of Steel-Concrete Composite Buildings for Blast Induced Progressive Collapse," *International Journal of Protective Structures*, vol. 6, no. 3, p. 29, 2015.

[23] M. F. El-Shahat, *Progressive collapse analysis of RC building frames with different seismic design levels*, Cairo: American University in Cairo, 2013.

[24] H.-S. Kim, J.-G. Ahn and H.-S. Ahn, "Numerical Simulation of Progressive Collapse for a Reinforced Concrete Building," *World Academy of Science, Engineering and Technology International Journal of Civil and Environmental Engineering*, vol. 7, no. 4, p. 4, 2013.

[25] D. Cormie, G. Mays and P. Smith, Blast Effects on Buildings, London: ICE Publishing, 2009.

[26] V. Karlos and G. Solomos, "Calculation of Blast Loads for Application to Structural Components," European Commission: Luxemberg, Italy, 2013.

[27] M. M. and S. Jr., "Simplified Kingery Airblast Calculations," Indian Head Division/Naval Surface Warfare Center, New Hampshire, 1994.

[28] G. F. Kinney and K. J. Graham, Explosive Shocks in Air, New york: Springer, 1985.

[29] J. Henrych, "The dynamics of explosion and its use," Elsevier, Amsterdam, 1979.

[30] M. Sadovskiy, "Mechanical effects of air shockwaves from explosions according to experiments," Nauka Press, Moscow, 2004.

[31] V. Karlos, G. Solomos and M. Larcher, "Analysis of the blast wave decay coefficicent using the Kingery-Bulmash data," *International Journal of Protective Structures,* vol. 7, no. 3, p. 21, 2016.

[32] D. Zhang, S. Yao, F. Lu, X. Chen, G. Lin, W. Wang and Y. Lin, "Experimental Study on Scaling of RC Beams Under Close-in Blast Loading," *ELSEVIER,* vol. 33, p. 8, 2013.

[33] Y. Liu, J. Yan, Z. Li and F. Huang, "Improved SDOF and Numerical Approach to Study the Dynamic Response of Reinforced Concrete Columns Subjected to Close-in Blast Loading," *ELSEVIER,* no. 22, p. 25, 2019.

[34] S. Yasseri, "Iso-Damage Diagram for Blast Resistant Design," *Research and Development,* no. 42, p. 10, 2015.

[35] A. K. Chopra, Dynamics of Structures Theory and Applications to Earthquake Engineering, Harlow: Pearson Education Limited, 2020.

[36] C. Kyei, "Effects of blast loading on Seismically Detailed Reinforced Concrete Columns," Carelton University, Ottawa, 2014.

[37] T. Krauthammer, N. Bazeos and T. J. Holmquist, "Modified SDOF Analysis of RC Box-Type Structures," *Journal of Structural Engineering,* vol. 112, no. 20502, p. 19, 1986.

[38] L. Cui, X. Zhang and H. Hao, "Improved analysis method for structural members subjected to blast loads considering strain hardening and softening effects," *Advances in Structural Engineering,* vol. 10, no. 1177, p. 15, 2021.

[39] Y. Shi, H. Hao and Z.-X. L. Li, "Numerical Derivation of Pressure-Impulse Diagrams for Prediciton of RC Column Damage to Blast Loads," *ELSEVIER*, vol. 35, pp. 1213-1227, 2007.

[40] G. Warn and M. Unal, "Estimating the Residual Axial Load Capacity of Flexure-dominated Reinforced Concrete Bridge Columns," The Pennsylvania State University, Pennsylvania, 2014.

[41] M. N. Priestley, Seismic design and retrofit of bridges, New York: John Wiley & Sons, Inc., 1996.

[42] M. Berry and M. Eberhard, "Performance Models for Flexural Damage in Reinforced Concrete Columns," Pacific Earthquake Engineering Research Center, California, 2003.

[43] Structural Engineering Institute (SEI), Blast Protection of Buildings, Virginia: American Society of Civil Engineers (ASCE), 2011.

[44] Y. Temash, A. Jahami, J. Khatib and M. Sonebi, "Numerical Analysis of a Reinforced Concrete Beam Under Blast Loading," *MATEC Web of conferences*, vol. 149, p. 5, 2018.

[45] L. S. t. (LST), LS-DYNA Keyword User's Manual Volumne I, Michigan: Livermore Software Technology Corporation, 2021.

[46] T. P. Slavik, "A Coupling of Empirical Explosive Blast Loads to ALE Air Domains in LS-DYNA," in *Materials Science and Engineering*, California, 2010.

[47] L. S. T. (LST), LS-DYNA Keyword User's Manual Volume II, Michigan: Livermore Software Technology Corporation, 2021.

[48] Y. D. Murray, A. Abu-Odeh and R. Bligh, "Evaluation of LS-Dyna Concrete Material Model 159," U.S. Department of Transportation, Colorado Springs, 2007.

[49] L. E. Schwer and J. L. Malvar, "Simplified Concrete Modelling With Mat_Concrete_Damage_REL3," JRI LS-Dyna, 2005.

[50] W. Tantrapongsaton, C. Hansapinyo, P. Wongmatar and T. Chaisomphob, "Flexural Reinforced Concrete Members With Minimum Reinforcement Under Low-Velocity Impact Load," *International Journal of GEOMATE,* vol. 14, no. 46, p. 8, 2018.

[51] B. Luccioni and G. Araoz, "Erosion Criteria For Frictional Materials Under Blast Load," *Asociación Argentina de Mecánica Computacional,* vol. XXX, p. 23, 2011.

[52] G. Powell, "Collapse Analysis Made Easy (More or Less)," University of California at Berkely, California, 2004.

[53] A. R. I. A. El-Gamal, "Reducing Progressive Collapse In Reinforced Concrete Building Structures," Benha University, Benha, Egypt, 2018.

[54] A. C. Jacinto, R. D. Ambrosini and R. F. Danesi, "Experimental and computational analysis of plates under air blast loading," *Impact Engineering,* no. 25, p. 21, 2001.

[55] M. L J and R. C A, "Review of Strain Rate Effects for Concrete in Tension," *American Concrete Institute (ACI),* vol. 95, no. 6, p. 5, 1998.

[56] A. K. Pandey, R. Kumar, D. K. Paul and D. N. Trikha, "Strain Rate Model for Dynamic Analysis of Reinforced Concrete Structures," *Journal of Structural Engineering,* vol. 132, no. 9, p. 9, 2006.

[57] L. Malvar, "Review of Static and Dynamic Properties of Steel Reinforcing Bars," *American Concrete Institute (ACI),* vol. 95, no. 5, p. 9, 1998.

APPENDIX A

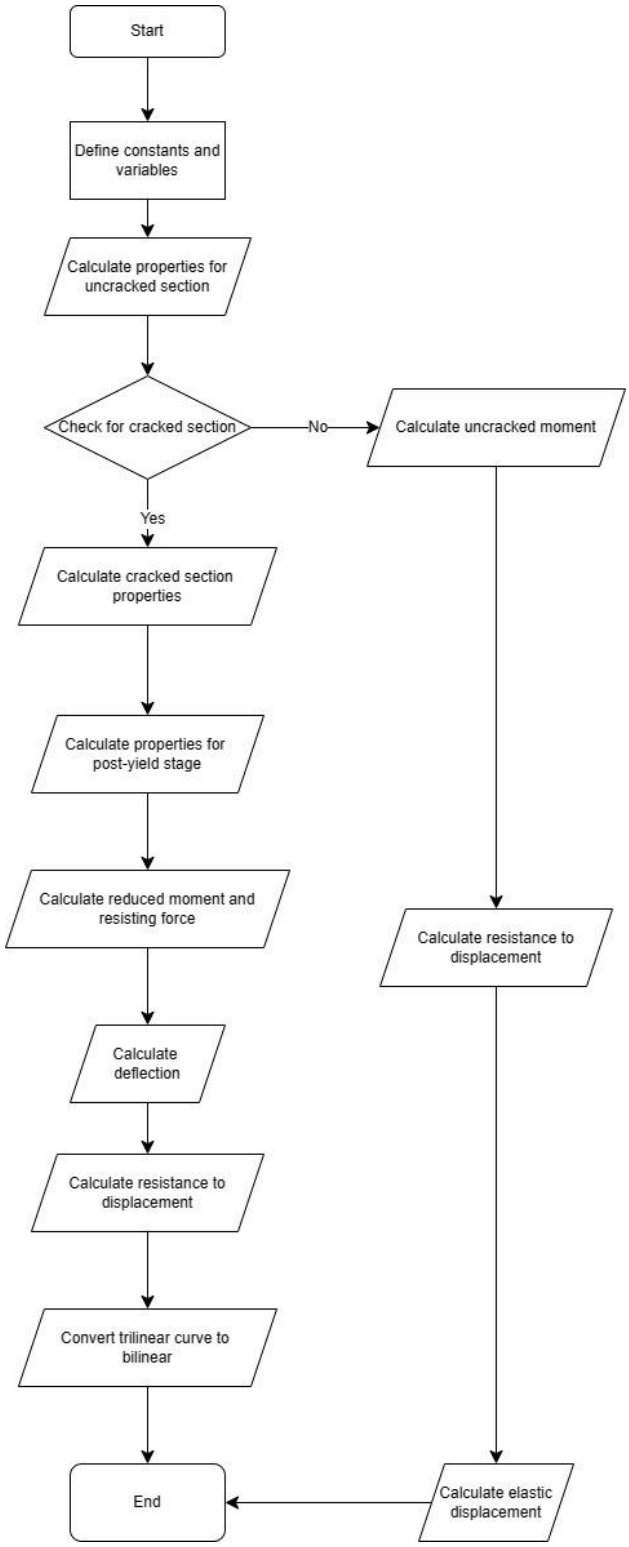

Figure 7-1: Code framework for computing flexural stiffness and displacement

This flow chart shows the code framework for calculating the restoring force and displacements (elastic, elasto-plastic and maximum) for flexure.

APPENDIX B

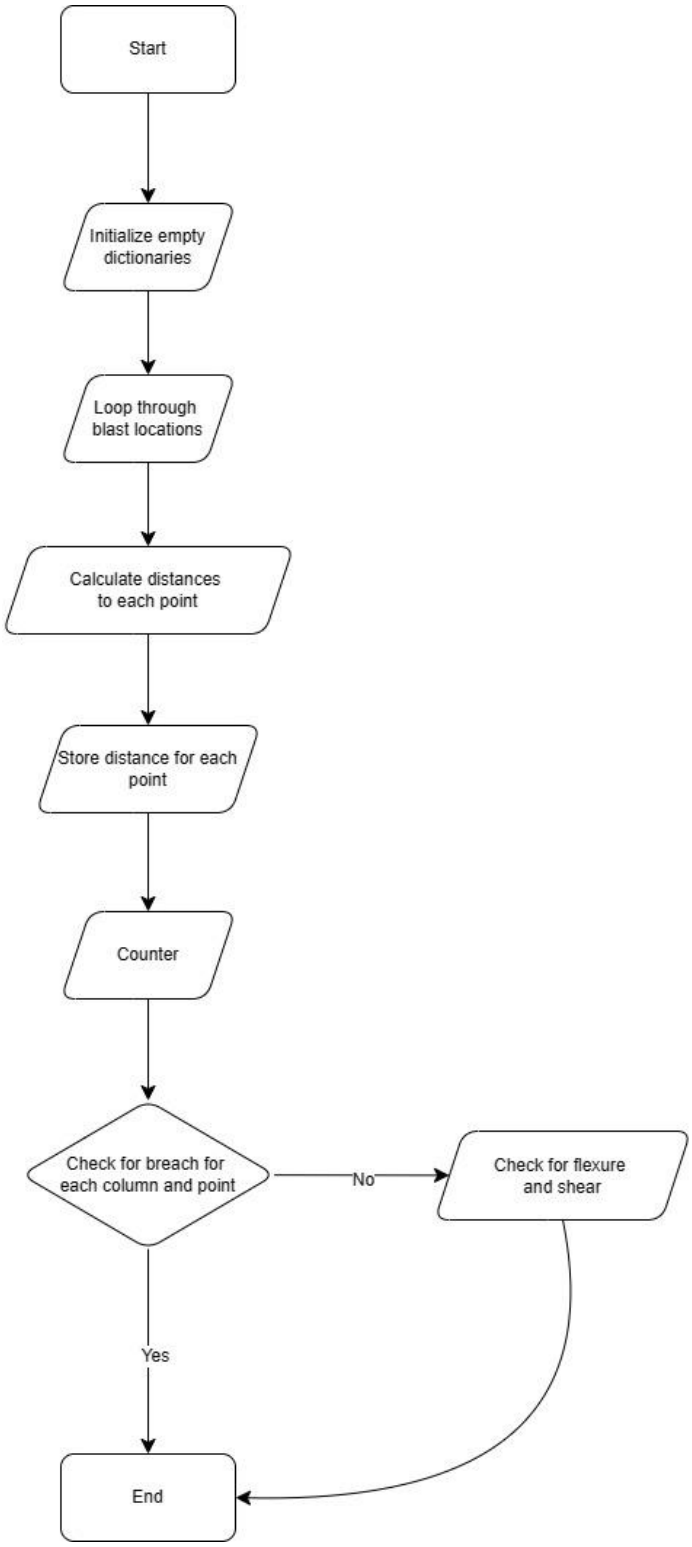

Figure 7-2: Code framework for computing breach response

Figure 7-2 shows the framework for verifying breach failure prior to flexural and direct shear failure.

APPENDIX C

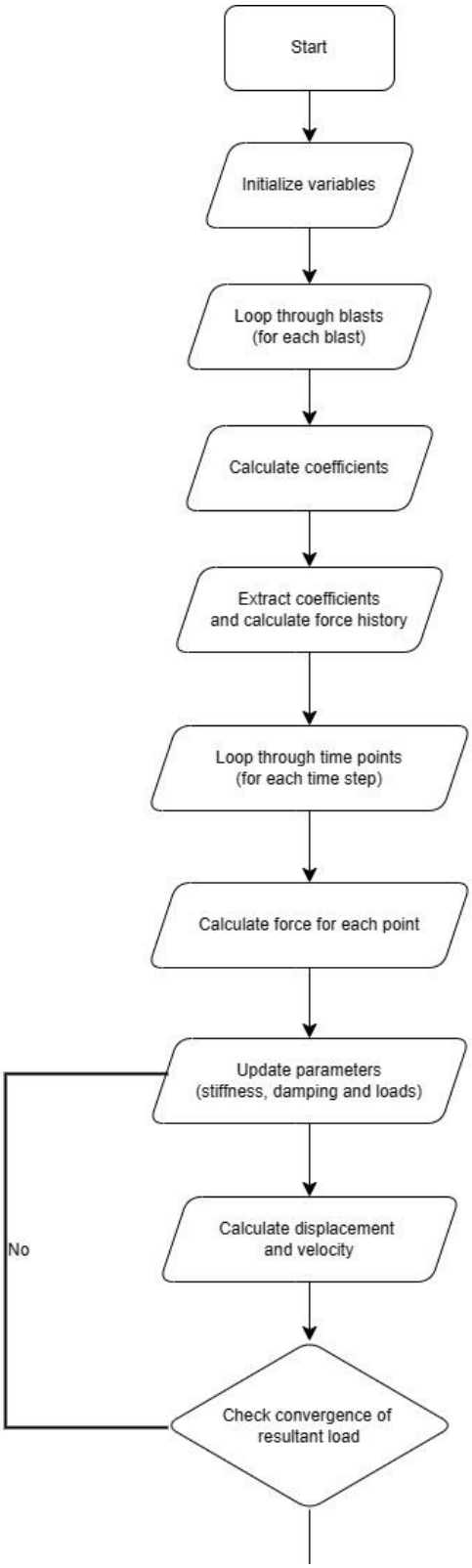

Figure 7-3: Code framework for computing flexural response part 1

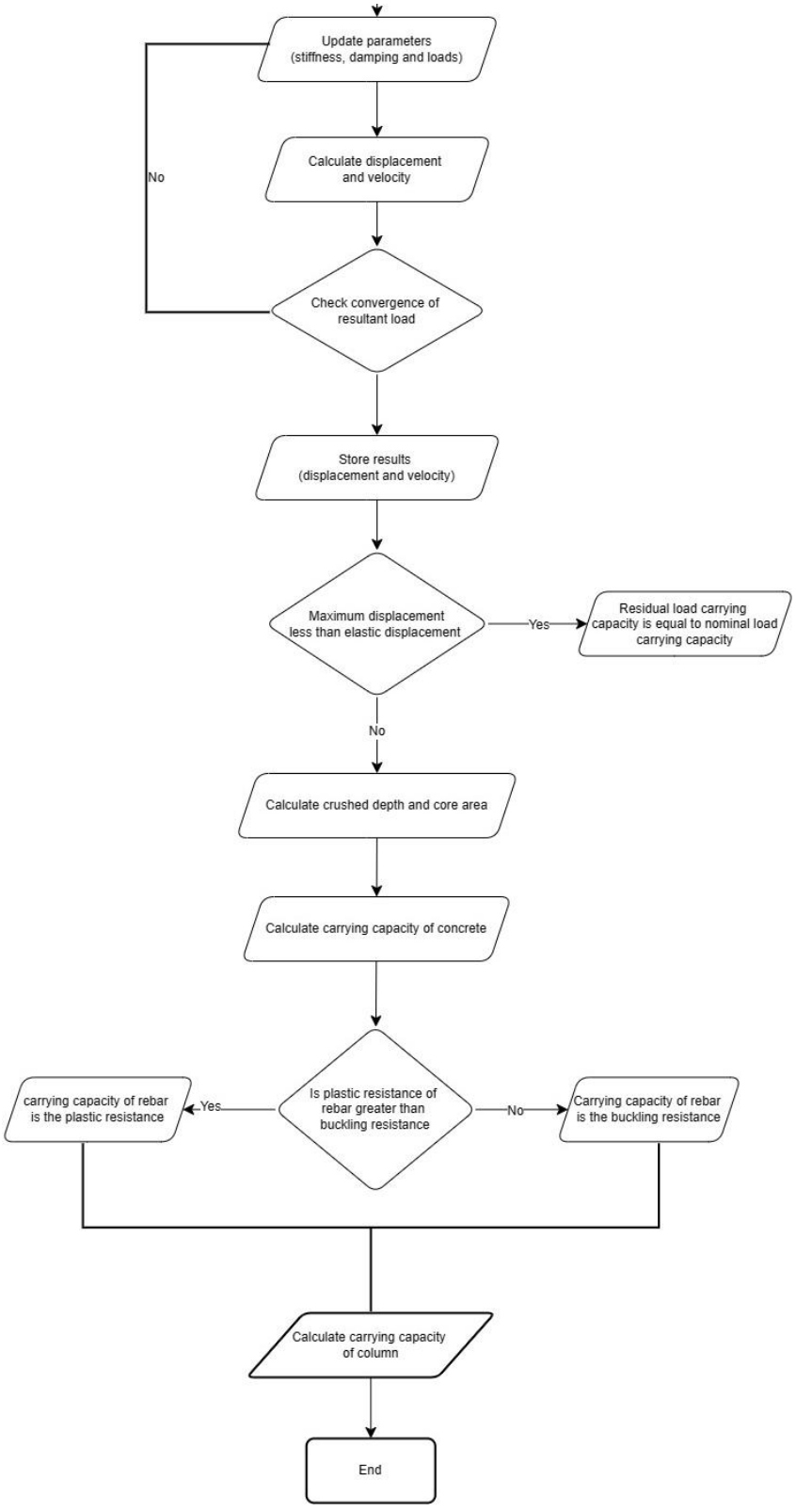

Figure 7-4: Code framework for computing flexural response part 2

Figures 7-3 and 7-4 demonstrate the python code for obtaining flexural response based on Newmark's Beta method.

APPENDIX D

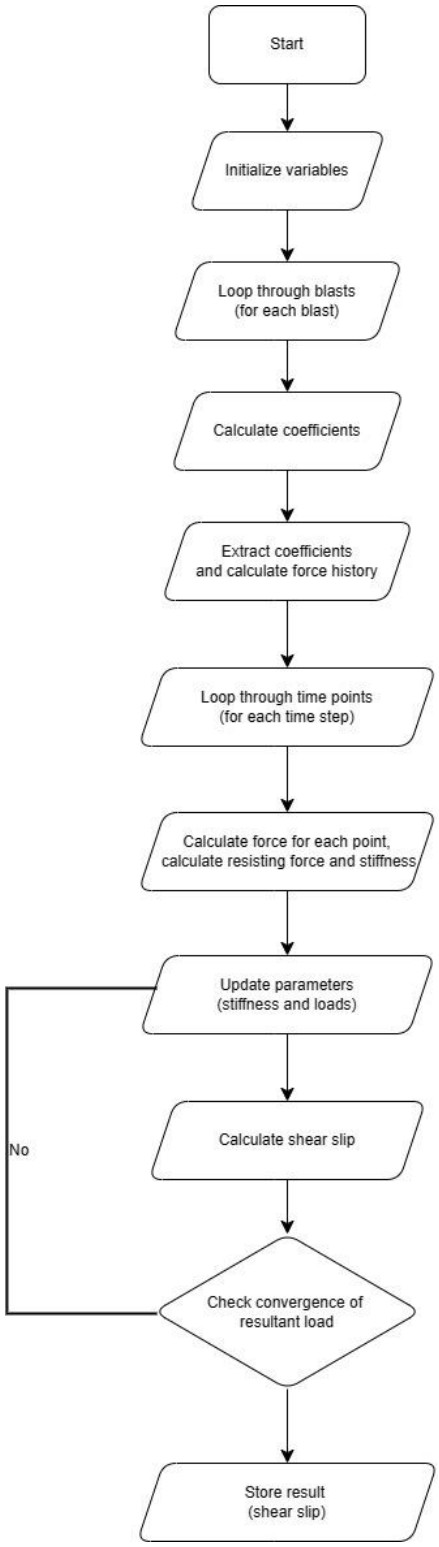

Figure 7-5: Code framework for computing direct shear response

Figure 7-5 shows the flowchart for calculating the direct shear response (shear slip).